# CONTACT ELEMENT ANALYSIS OF FRP REINFORCED RC BEAMS

**A DISSERTATION**

*Submitted in partial fulfillment of the*

*requirements for the award of the degree*

*of*

**MASTER OF TECHNOLOGY**

*in*

**EARTHQUAKE ENGINEERING**

(With specialization in Structural Dynamics)

*by*

**GIRISH NARAYAN PRAJAPATI**


**DEPARTMENT OF EARTHQUAKE ENGINEERING**
**INDIAN INSTITUTE OF TECHNOLOGY ROORKEE**
**ROORKEE – 247667, UTTARAKHAND, INDIA**
**JUNE, 2016**

## CANDIDATE'S DECLARATION

I hereby declare that the work carried out in this Dissertation report entitled, "**CONTACT ELEMENT ANALYSIS OF FRP REINFORCED RC BEAMS",** submitted to the Department of Earthquake Engineering, Indian Institute of Technology, Roorkee in partial fulfillment of the requirements for the award of degree of "Master of Technology" in Earthquake Engineering with specialization in Structural Dynamics, under the supervision of **Mr. Ashok D. Pandey**, Assistant Professor, Department of Earthquake Engineering, I.I.T., Roorkee.

I have not submitted the record embodied in this report for the award of any other degree or diploma.

Date: Girish Narayan Prajapati

Place: Roorkee (14526011)

## CERTIFICATE

This is to certify that the above statement made by the candidate is correct to the best of my knowledge and belief.

Mr. Ashok D. Pandey

Assistant Professor

Date: Department of Earthquake Engineering

Place: Roorkee Indian Institute of Technology Roorkee

# ACKNOWLEDGEMENT

I wish to express my deep sense of gratitude and indebtedness to my elite guide & mentor **Mr. Ashok D. Pandey**, Assistant Professor, Department of Earthquake Engineering, IIT Roorkee, for being helpful and a great source of inspiration. I am thankful to him for his persistent interest, constant encouragement, vigilant supervision and critical evaluation. His encouraging attitude has always been a source of inspiration for me. His helping nature, invaluable suggestions and scholastic guidance are culminated in the form of the present work.

I am highly appreciative to all faculty members, research scholars and all other mentors in our department for their valuable suggestions, encouragement and facilities extended throughout the dissertation work.

I am thankful to Mr. M. J. Mahesh, research scholar, Department of Earthquake Engineering, IIT Roorkee, for their valuable suggestion and guidance.

I find myself fortunate to express my gratitude to my parents, who have forever been a source of inspiration and strength to me. I would also thankful to my fellow mates Mr. Aalok, Mr. T. Brahma Reddy, Mr. Nihir Boro, Mr. Aakash Khatri, Mr. Devendra Shrimal and Mr. Subhajit De for their enthusiastic help, continuous support and constant discussion throughout the report.

Date: Girish Narayan Prajapati

Place: Roorkee (14526011)

# ABSTRACT

The use of the Fibre Reinforced Polymer (FRP) for the strengthening and rehabilitation of the reinforced concrete member is increasing in the past decades due to its anti-corrosion, high strength to weight ratio, ease transportation, high strength and high elastic modulus. Due to change in the seismic codes, the existing structure may not fulfill modern design requirements. Thus, it is required to strengthen the structures in order to gain strength and ductility as required by the seismic codes. In present study, literature review of FRP confined concrete models (design oriented and analysis oriented) and reinforced concrete (RC) beam strengthened with FRP in shear and flexure has been conferred. The mechanical and material property of the different FRP (BFRP, CFRP, GFRP) types are studied by simulating the plain concrete cylinder, prism and prism with groove to understand its compression, flexural and fracture behavior respectively using finite element (FE) tool ANSYS 14.0. 20 RC beams (2 control and 18 reinforced externally with FRP in different pattern) are model analytically for understanding its behaviour in shear and flexure with two different grades of concrete. RC portal which was design in SAP2000 for gravity load is modeled analytically in ANSYS 14.0 to predict its behaviour during lateral load.

The results obtained from the finite element analysis (FEA) for plain concrete member and RC beams are compared with previous research. The axial stress-strain plot of the concrete cylinder confined with FRP obtained from FEA is compared with design oriented and analysis oriented models which corroborate with present analysis. The peak compressive strength, flexural and fracture strength of the confined concrete from present analysis compared with experimental results which shows a good correlation.

The behaviour of the strengthened and conventional RC beam under two point loading is modeled using finite element analysis. The evolution of crack pattern in concrete at different load steps is studied to understand the failure mechanism of FRP strengthened reinforced concrete beam analytically. Load deflection relation, crack pattern at failure, yield and ultimate loads of FRP strengthened RC beams obtained from FEA are compared with the experimental results which shows a good

agreement. Also, the ultimate loads from finite element analysis are calculated using design models; a good correlation was obtained with the failure loads.

The load defection relationship obtained from finite element analysis of strengthened RC portal shows that the post cracking stiffness of the unreinforced portal increases with increase in number of CFRP layers. For present model, four layers of CFRP found to be sufficient to retrofit the portal to sustain during seismic events. The present analysis of reinforced concrete portal using ANSYS 14.0 software corroborated with standard research.

# Table of Contents

**Page no.**

# List of Figures

**Caption** **Page no.**

# List of Tables

# List of Notations

$a_v$ length of shear zone (mm)

$A_f$ area of FRP reinforcement

$A_i$ parameter in stress Sargin [49] model

$A_j$ parameter in stress Toutanji [34] model

$A_s$ area of steel reinforcement

$A_v$ area of transverse reinforcement

$b$ width of the beam (mm)

$c_1$ constant in the strength enhancement expression

$c_2$ constant in the strain enhancement expression

$C_j$ parameter in stress Toutanji [34] model

$D$ diameter of concrete cylinder (mm)

$d$ effective depth of the beam (mm)

$d_f$ effective depth of FRP (mm)

$D_i$ parameter in stress Sargin [49] model

$D_j$ parameter in stress Toutanji [34] model

$E'_{c2}$ tangent slope of the second branch of axial stress–strain curve at $f'_{c1}$ (MPa)

$E_c$ Young's modulus of unconfined concrete (MPa)

$E_{c1}$ initial slope of axial stress–strain curve of FRP-confined concrete (MPa)

$E_{c2}$ slope of the second branch of axial stress–strain curve of FRP-confined concrete (MPa)

$E_{co}$ secant elastic modulus of unconfined concrete at $f'_{co}$ (MPa)

$E_f$ Young's modulus of fibers (MPa)

$E_{frp}$ Young's modulus of FRP material (MPa)

$E_l$ lateral confinement stiffness; $E_l = 2E_f\ t_f / D$ or $2\ E_{frp}t_{frp}/D$ (MPa)

$f'_{c1}$ axial compressive stress of FRP-confined concrete at first peak (MPa)

$f'_{cc,u}$ ultimate axial compressive stress of FRP-confined concrete (MPa)

$f'_{cc}$* ultimate axial compressive stress of actively confined concrete (MPa)

$f_{ck}$ ultimate axial compressive stress of unconfined concrete (MPa)

$f'_{co}$ ultimate axial compressive stress of unconfined concrete (MPa)

$f'_{cu}$ axial compressive stress of FRP-confined concrete at $\varepsilon_{cu}$ (MPa)

$f_c$ axial compressive stress of concrete (MPa)

$f_{fu}$ ultimate tensile strength of fibers; $f_{fu} = E_f \varepsilon_f$ (MPa)

$f_{frp}$ ultimate tensile strength of FRP material; $f_{frp} = E_{frp} \varepsilon_{frp}$ (MPa)

$f_{c,A}$ axial compressive stress of concrete at $\varepsilon_{c,A}$ (MPa)

$f_l$ lateral confining pressure (MPa)

$f_l$* lateral confining pressure of actively confined concrete (MPa)

$f_{lu}$ ultimate lateral confining pressure; $f_{lu} = E_l \varepsilon_f$ or $f_{lu} = E_l \varepsilon_{frp}$ (MPa)

$f_{lu,a}$ effective lateral confining pressure at ultimate; $f_{lu,a} = E_l \varepsilon_{h,rup}$ (MPa)

$f_o$ intercept stress at the stress axis of axial stress–strain curve (MPa)

$f_r$ rupture strength of concrete (MPa)

$f_y$ yield strength of steel (MPa)

$h$ depth of beam (mm)

$H$ FRP confined concrete specimen height (mm)

$k_1$ axial strength enhancement coefficient

$k_2$ axial strain enhancement coefficient

$k_5$ parameter in Girgin [37] model

$k_\varepsilon$ hoop strain reduction factor

$k_{\varepsilon,f}$ hoop strain reduction factor of fibers

$k_{\varepsilon,frp}$ hoop strain reduction factor of FRP material

$l$ length of the beam (mm)

$m$ parameter in Youssef et al. [36] model

$m_1$ parameter in Fahmy and Wu [38] model

$m_2$ parameter in Fahmy and Wu [38] model

$n$ constant in Richard and Abbott [46] model

$n_f$ number of FRP layers

$r$ concrete brittleness constant in Popovics [53] model proposed

$s$ spacing of the transverse reinforcement (mm)

$s_f$ spacing of the FRP strips (mm)

$t_f$ total nominal thickness of fibers (mm)

$t_{frp}$ total thickness of FRP material (mm)

$V_f$ shear capacity of FRP (kN)

$V_T$ total shear capacity of beam (kN)

$x$ depth of concrete in compression (mm)

$w_f$ width of FRP strips (mm)

$\varepsilon_{cc}$* axial strain of actively confined concrete at $f'_{cc}$*

$\varepsilon_c$ axial strain of concrete

$\varepsilon_{c,A}$ axial strain of concrete at $\varepsilon_{l,A}$

$\varepsilon_{c,cr}$ axial strain of concrete at concrete cracking

$\varepsilon_{c1}$ axial strain of FRP-confined concrete at $f'_{c1}$

$\varepsilon_{c,\lambda}$ axial strain of FRP-confined concrete at the first peak in Miyauchi et al. [33] model

$\varepsilon_{co}$ axial strain of unconfined concrete at $f'_{co}$

$\varepsilon_{co,i}$ axial strain of unconfined concrete in model

$\varepsilon_{co,u}$ ultimate axial strain of unconfined concrete in model

$\varepsilon_{cc,u}$ ultimate axial strain of FRP-confined concrete

$\varepsilon_f$ ultimate tensile strain of fibers

$\varepsilon_{frp}$ ultimate tensile strain of FRP material

$\varepsilon_{h,rup}$ hoop rupture strain of FRP shell

$\varepsilon_l$ lateral strain of concrete

$\varepsilon_{lo}$ lateral strain of concrete at axial strain $\varepsilon_{co}$

$\varepsilon_{l,A}$ lateral strain of concrete at axial strain $\varepsilon_{c,A}$

$\varepsilon_{l1}$ lateral strain of concrete at $f'_{c1}$

$\varepsilon_o$ intercept strain of the axial strain axis of axial strain-lateral strain curve

$\beta$ inclination angle of FRP strips in shear strengthening

$\gamma_c$ density of concrete

$\gamma$ strain ratio used in Berthet et al.[40]

$\lambda$ parameter in Miyauchi et al. [33] model

$\mu$ lateral-to-axial strain ratio or dilation ratio of concrete

$\mu_s$ secant dilation ratio of confined-concrete

$\mu_{su}$ secant dilation ratio of confined-concrete at $\varepsilon_{cu}$

$\mu_t$ tangent dilation rate of confined-concrete

$\mu_{u,asym}$ asymptotic tangent dilation rate of FRP-confined concrete

$\mu_{max}$ maximum tangent dilation rate of FRP-confined concrete

$\mu_{tu}$ average tangent dilation rate of confined-concrete at $\varepsilon_{cu}$

$v_c$ initial Poisson's ratio of concrete

# CHAPTER 1

# INTRODUCTION

## 1.1 GENERAL

The deterioration of concrete structures reinforced with steel rebar due to environmental effects counting corrosion of internal steel reinforcements and gradual loss of strength with aging. Also, the damaged civil engineering structures due to natural phenomenon like earthquake are one of the major concerns. Further, the infrastructure constructed over many years, may be in need of strengthening due to changes in the use of the structure (increased dead load, live load or both), seismic codes and modern design practices which was not followed earlier at the time when the structure was built. Thus, a successful rehabilitation technique is required to address these problems. Within the span of rehabilitation of concrete structures, it is essential to distinguish between the terms *repair*, *strengthening* and *retrofitting*[1]. In *repairing* a structure, the material is used to upgrade a structural or functional deficiency such as a crack or a critically degraded structural component to provide same level of strength and ductility which the building had prior to the damage. In contrast, the *strengthening* of a structure is peculiar to those cases where the addition or application of the material would enrich the existing designed performance level i.e. higher strength and higher ductility than the original building and upgrade it to the current code of practice. The term *retrofit* is the concept including strengthening, repairing and remodeling of the structure, which is used to show the seismic upgrade of structure, such as in the case of the use of composite jackets for the confinement of columns. The first method of external strengthening employed by bonding steel plates to the tension faces of structures. The effectiveness in strengthening was acceptable; however several problems including durability, heavy weight, handling and shoring, had to be resolved; thus need for alternative materials aroused. Strengthening/ rehabilitating/retrofitting of existing structures, manufactured from the more conventional materials, by employing advanced fibre reinforced polymer (FRP) composites is a powerful and workable alternative to the use of steel. Since the 1980s, the realization amongst civil/structural engineers of the importance of the specific weight and stiffness, the resistance to corrosion, durability

and ease of installation is encouraging the use of FRP composites in the rehabilitation of structures throughout the world.

The repairing and retrofitting techniques adopted for a particular on the basis of study should not increase the dimensions of the members as it increases the dead load of the structure. The repairing should increase the strength and ductility appreciable and should make the structure brittle. Fiber reinforced polymer jacketing is the method which is much efficient due to the following advantages:

- FRP jacketing can be used to strengthen RC structures suffering corrosion induced deterioration, and to reduce the rate of corrosion. FRP jacketing slows down iron depletion due to continued post-repair exposure.
- Fibre reinforced polymer exhibits linear-elastic behaviour up to failure, thus these properties are interrelated by Hooke's law. And the strength and elastic modulus of the FRP is much higher.
- The FRP composites give high strength with minimal weight density and increase the strength of the member. It does not change the dimension of the structure, thus can be mold in any geometry.
- It is light weight can be easily transportable at the construction sites. Ease to cut and take less time for construction.
- The FRP composites require minimal maintenance thus it reduces the cost of maintenance. It also increases the durability or life of the structure.
- FRP technique can be used for any member such as beam, column, slab and walls.

## 1.2 FRP-DEFINATION AND TYPES

Fiber-reinforced polymer (FRP) is a high-strength composites material made up of high strength fibers and a polymer matrix to forge it properly over the structural member. The use of FRP composites by the civil engineering spans about four decades. Common fiber types include basalt, carbon, glass, and high-strength steel; common matrices are epoxies and esters. The use of composite by adulterating two different types of fibers is gaining its importance day by day. FRP Composites are known for their high specific strength, high stiffness, and corrosion resistance.

The commonly used varieties of the fiber reinforced polymers which are used in the present study are as follows:

A. Basalt fibers
B. Carbon fibers
C. Glass fibers

**Basalt fibers**: These fibers made from extremely fine fibers of basalts, which are composed of the minerals plagioclase, pyroxene and olivine. It have better physical and mechanical property than fiber glass and economical than the carbon fiber. It used for fire proof in aerospace and automatic industries. It has higher strength and elastic modulus than glass fiber and can used as alternative to carbon fibers

**Carbon fibers**: The fiber offers high stiffness, high tensile strength, low weight, high temperature tolerance and a very high strength-to-weight ratio. The manufacturing process for the carbon fibers includes a sequence of procedures, stabilization, carbonization, graphitization and surface treatment. These procedures depend upon the pyrolysis and crystallization of certain organic precursors. These fibers are expensive than the other fibers. These fibers are available in high strength and high modulus and divided in categories depending upon these properties.

**Glass fibers**: These fibre are one of the strongest and most commonly used structural fiber materials. The manufacturing process for the production of glass fiber includes direct melt in which the fine filaments of diameter 3-24 micrometer are produced by continuous and rapid drawing from the melt. There are different grades of glass fibers are available for the rehabilitation of the structural members such as E-glass, S-glass, A-glass, etc. High stiffness carbon fibers are used for reinforced and pre-stressed concrete beams and columns. The fiber is more economical than the other fibers make it more suitable for the practical use.

## 1.3 PRESENT STUDY: ITS IMPORTANCE

FRP repair is a simple way to increase both the strength and design life of a structure. But of its high strength to weight ratio and resistance to corrosion, this repair method is ideal for deteriorated concrete structures due to exposure to de-icing salts and other environmental factors. By encasing concrete members, FRP protects existing steel and

concrete from deleterious effects. It was noted that in many bridges majority of corrosive damages occur on exterior girders. This indicates that deleterious effects may be a direct result of surface exposure, to spray of water, de-icing agents and environmental effects. Encasement of these girders not only increase design life but also protects the members from surface attacks. FRP is a versatile material. It can be applied to various ranges of members. It is a highly cost effective method of maintaining or upgrading existing structures. Quick application results in lower disruption and shorter contract periods. Reasons for strengthening structures may include upgrading to accommodate higher loads (such as traffic), existing reinforcement pre stress loss or degrading of structure (e.g. corrosion of reinforcement). The technique may allow continue usage of structures or facility during strengthening works. Higher material costs of CFRP are outweighed by the numerous advantages over steel. GFRP or BFRP offer lower cost alternative, in some instances, to CFRP.

The present study focus on the analysis of the plain concrete members; reinforced concrete beam and portals externally bonded with FRP sheets using the finite element tool. The study checks the reliability and accuracy of the analytical results over the experimental results. The present study can provide a cheap, reliable and time saving approximation of the capacity of the reinforced concrete members bonded with external fiber reinforced polymer sheets. It will also predict the compression and flexural behaviour of the plain concrete member confined with different types of FRP sheets.

## 1.4 OBJECTIVE

The main objectives of the present report are as follows:

(i) To model and simulate the confining effect of different types of FRP wrapped on circular concrete cylinder under direct compression.

(ii) To study and compare the different confinement model with present study on confinement effectives of circular column with FRP.

(iii) To simulate flexural behaviour of plain concrete prisms affix with different FRP at the soffit.

(iv) To simulate fracture behavior of concrete prisms affix with different FRP types at the soffit.

(v) To simulate the effect of different types of FRP strengthening techniques on flexural deficient beams.

(vi) To simulate the effect of different types of FRP strengthening techniques on shear deficient beams.

(vii) To study the evolution of crack pattern of strengthened RC beam using finite element analysis.

(viii) To study the accuracy and reliability of the FE analysis over the experimental results.

(ix) To analytically study the behaviour of the reinforced concrete portal designs with gravity loads under lateral load analysis.

(x) To study the behaviour of RC portal reinforced with different layers of CFRP.

## 1.5 SCOPE OF STUDY

3-D Finite Element Model of concrete cylinders, prisms and prism with groove created using finite element tool ANSYS 14.0. Concrete cylinders wrapped with different FRP simulated in the ANSYS 14.0 for direct compression. The FRP sheets modeled by affixing at the bottom face of the prism in the ANSYS 14.0 for the flexure and fracture analysis. In the modeling of the prism the loads and supports produced by creating a contact between the loading arrangement and the prism. The model validated by the published experimental and analytical results. The confinement effectiveness of different FRP on the cylinder and prism model in the ANSYS 14.0 studied and increased in the strength compared with the controlled cylinder and prism. Also, the different confinement model given by researchers is used for the comparison of the results. Further, 3D finite element model of reinforced concrete beam modeled with two different compressive strength of the concrete. All the plain concrete members and RC beam then confined with different types of FRP (BFRP, CFRP and GFRP). The dimensions and material data used for the analysis were taken from the experimental study carried out last year in the department by Kumar, 2015; Kumar, 2015a[2,3]. To appropriately check the behavior of the experimental results; the models are generated with the existing physical boundary conditions. The results obtained from the analysis are validated by comparing with the published experimental results. Finally, a reinforced concrete (RC) portal is design considering the gravity loads and 3D finite

element model generated using ANSYS 14.0 for lateral load analysis of the RC portal. The RC portal then wrapped with different layers of FRP at the weaker section to check the confining effect of CFRP during the lateral loads. Material data of the FRP is taken from the literature. The results are compared with the results from the previous studies[4].

## 1.6 ORGANISTION OF THE REPORT

The present report consists of seven chapters including the introductory chapter:

Chapter 1: Introduction of the FRP material as retrofitting is discussed. It consists of importance of present study, objective and scope of the study.

Chapter 2: This chapter gives a state of art reviews of the work done in the field of FRP strengthening for concrete members and RC beams in flexure and shear. Mechanism of confinement and confinement models are discussed. A brief review of finite element analysis used by different researcher is conferred.

Chapter 3: This chapter is about of finite element model in ANSYS 14.0. It discusses the different element type used for finite element analysis. Behaviour of the different material in ANSYS 14.0 and material property used for study is also incorporated.

Chapter 4: In this chapter, modeling of plain concrete member confinement with FRP is discussed. The result obtained from finite element analysis is validated using past model is included.

Chapter 5: The chapter deals with modeling of FRP strength RC beam. Modeling of RC beam and its behaviour using finite element analysis is discussed.

Chapter 6: The behaviour of conventional and strengthened RC portal under lateral load analysis is discussed in this chapter.

Chapter 7: The chapter concludes the dissertation with a note on future scope.

# CHAPTER 2

# STATE OF THE ART

## 2.1 GENERAL

Many research works has been done to study the effect of FRP in enhancing the strength of the structural elements. The behavior of the FRP reinforced confined concrete cylinder under direct axial compressive load develops a bilinear stress-strain curve. Various stress-strain models predicted that the FRP start confining the concrete once the ultimate crushing strength of the concrete is reached. Study related to different failure pattern with FRP was also carried out. Many experimental and analytical works were carried out to examine the influence of FRP on the strength and ductile behaviour of the RC elements. The use of finite element method to study the behavior of the concrete confined externally with FRP has been adopted for economic reasons. This chapter focuses on the work done related to the FRP confinement of concrete elements

## 2.2 FRP CONFINED CONCRETE

Starting from Richart et al.,1928[5], Newman and Newman,1969[6], Ahmed and Shah, 1982[7] and Mander et al, 1988[8] developed stress-strain models for actively confined concrete reinforced with steel under uniaxial compressive loads; various stress-strain models for FRP confined concrete [9–11] were adopted directly from above mentioned researchers. The main disadvantage in the model predicted by Fardis and Khalili, 1982[9], Ahmad et al.,1991[10] and Saadatmanesh et al., 1994[11] was difference in the stress-strain characteristics of FRP confined and steel confined concrete which was identified by various research groups [12–16]. An enormous number of analytical stress-strain models have been predicted by various researchers. From which many of the models were predicted from narrow numbers of experimental data. As previously reviewed and assessment done by Lam and Teng, 2003[17], De Lorenzis and Tepfers, 2003[18], Bisby et al., 2005[19] and Ozbakkaloglu et al., 2013[20] found that the performances of these models reduces appreciably when assessed for significant number of data with range of parameters.

Over two decades, the predictions of the stress-strain models were mainly based on the experimental work done on CFRP and GFRP confined concrete. Some researchers like Lam and Teng, 2003[17], Bisby et al., 2005[19], and Wu et al., 2009[21] consider the Aramid FRP in their stress-strain model. From the past the stress-strain models are grouped on basis of their similarity and differences. The stress-strain models are mainly categorized into two parts i.e. Design oriented models and Analysis-oriented models[17]. Before going to the details of the FRP confined concrete model; it is important to understand the mechanism of FRP confinement.

### 2.2.1 Confining mechanism of FRP

The behaviour of an FRP-confined concrete cylinder differs from that of a conventional cylinder in that the behaviour of concrete now depends on the amount of FRP confinement. The behaviour and modeling of FRP-confined concrete is thus fundamental to the prediction of the behaviour and the design of FRP confined concrete cylinder. When an FRP confined concrete cylinder is subject to axial compressive pressure, the concrete is the first load bearing member. The concrete expands laterally when its ultimate crushing strength is reached and this expansion is now confined by the FRP which provides a lateral confining pressure ( $f_l$ ) assumed distributed uniformly over the circumference as indicated in Figure 2.1. The pressure apply due to confining action of the FRP is of passive type because it arises due to the lateral expansion of the concrete and the FRP is subjected to tensile forces on its hoop direction. The confining pressure ( $f_l$ ) of FRP increases correspondingly with the increase in the lateral expansion of the concrete. The failure of system appears once the FRP ruptures. For the FRP confined circular column sections, based on force equilibrium between the concrete and FRP; the lateral confinement pressure ( $f_l$ ) can be calculated theoretical using the Eqn. (2.1). The ultimate lateral confining pressure ( $f_{lu}$ ) is a function of ultimate strain in the fibre ( $\varepsilon_f$ ). Later, it has been reported in previous studies by a number of researchers [17,18,22–28] that the measured ultimate strain on FRP at the time of FRP hoop rupture is lower than the ultimate strain of the fibres ( $\varepsilon_f$ ).Thus, a strain reduction factor ( $k_e$ ) was introduced by Pessiki et al., 2001[25] keeping in view the importance of this factor to form a relationship between ultimate tensile strain of

fibre ( $\varepsilon_f$ ) and hoop rupture strain of FRP ( $\varepsilon_{h,rup}$ ) during failure defined by Eqn. (2.2). Then, Lam et al., 2003[17] defined actual confining pressure at ultimate ( $f_{lu,a}$ ) using the hoop rupture strain of FRP ( $\varepsilon_{h,rup}$ ) (Eqn. (2.3)).

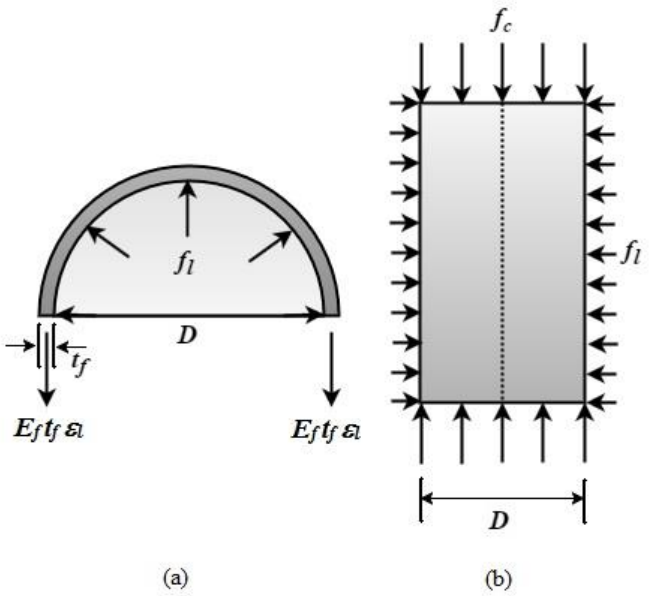


Figure 2.1 Ultimate confining mechanism of (a) FRP on (b) Circular concrete core

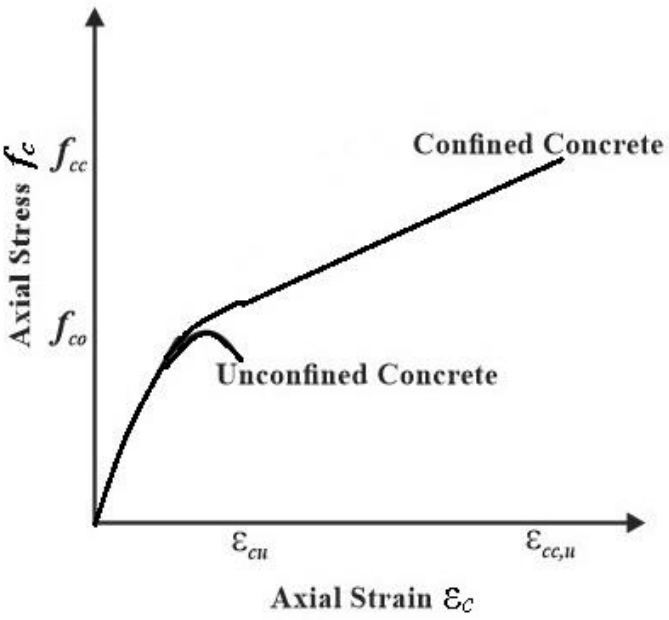


Figure 2.2 Stress-strain plot for FRP confined concrete

$$f_{lu} = \frac{2E_f t_f \varepsilon_f}{D} \tag{2.1}$$

$$\varepsilon_{h,rup} = k_e \varepsilon_f \tag{2.2}$$

$$f_{lu,a} = \frac{2E_f t_f \varepsilon_{h,rup}}{D} \tag{2.3}$$

As observed in majority of tests that the stress–strain curve of FRP confined concrete features a monotonically ascending bilinear shape with sharp softening in a transition zone around the stress level of the unconfined concrete strength (Figure 2.2).

### 2.2.2 Design oriented confinement models

The models which are directly derived from the experimental test results with closed form expressions called as design oriented models. The expressions proposed by Richert et al., 1928[5] become the basis for most of the stress-strain models. Most of the models were derived considering CFRP. GFRP and AFRP were taken in account by some authors. A detail insight of the design oriented model is discussed in the present section.

Most of the FRP confined stress-strain models were derived from the confinement model proposed by Richart et al., 1928[5] from test conducted on concrete specimens confined with hydrostatic pressure. The proposed stress-strain relationship follows a linear trend and is indicated by the Eqn. (2.4) and Eqn. (2.5).

$$f'_{cc,u} = f'_{co}\left[1 + k_1\left(\frac{f_{lu}}{f'_{co}}\right)\right] \tag{2.4}$$

$$\varepsilon_{cc,u} = \varepsilon_{co}\left[1 + k_2\left(\frac{f'_{cc,u}}{f'_{co}} - 1\right)\right] \tag{2.5}$$

The Eqn. (2.4) shows linear relationship with the normalized confining pressure of the FRP ( $f_{lu} / f'_{co}$ ). The value of $k_1$ and $k_2$ based on test result by Richart et al., 1928[5] was 4.1 and 5 respectively.

Mander et al., 1988[8] proposed a model for appraising the effect of confinement on the axial strength of concrete column with steel confinement. The expression (Eqn. (2.35)) for the peak stress ( $f'_{cc}$ ) was mostly used in the actively confined model. This

expression was calibrated with test results of Elwi and Murry, 1979[29] and was based on the expression proposed by Willam and Warnke, 1975[30].

$$f_{cc}^{'} = f_{co}^{'}\left(2.254\sqrt{1+\frac{7.94\,f_l}{f_{co}^{'}}}-2\frac{f_l}{f_{co}^{'}}-1.254\right) \tag{2.6}$$

Table 2.1 presents the summary of ultimate stress and strain expression predicted by different researchers. Fardis and Khalili,1982[9], Saadatmanesh et al., 1994[11]; Mirmiran, 1996[31]; Karbhari and Gao, 1997[32]; Samaan et al., 1998[22]; Miyauchi et al., 1999[33]; Saafi et al., 1999[15]; Spolestra and Monti, 1999[16]; Toutanji,1999[34]; Lin and Chen, 2001[35], Youssef et al., 2007[36]; Girgin, 2009[37]; Fahmy and Wu[38], 2010 does not consider the FRP hoop strain reduction in their model. So, the confining pressure in their case calculated using Eqn. (2.1).The actual confining pressure ( $f_{lu,a}$ ) were consider by Lam and Teng, 2003[17]; Ilki et al., 2004[39]; Berthet et al., 2006[40]; Mathys et al., 2005[41]; Jiang and Teng, 2006[42]; Teng et al., 2009[43]; Realfonzo and Napoli, 2011[44] in their model with experimentally determined or recommended strain efficiency factor ( $k_e$ ).

The Miyauchi et al., 1999[33] and Mathys et al., 2005[41] suggested the stress-strain curve adopted from Hognestad's parabola[45] (Eqn.(2.7)) for first advancing portion of the curve of confined concrete with FRP. The second ascending straight line obtained by connecting with the ultimate condition.

$$f_c = f_{c1}^{'}\left[2\left(\frac{\varepsilon_c}{\varepsilon_{c1}}\right)-\left(\frac{\varepsilon_c}{\varepsilon_{c1}}\right)^2\right] \text{for } \varepsilon_c \le \varepsilon_{c1} \tag{2.7}$$

$$f_c = f_{c1}^{'} + E_{c2}\left(\varepsilon_c - \varepsilon_{c1}\right) \text{for } \varepsilon_c \ge \varepsilon_{c1} \tag{2.8}$$

Where,

$$E_{c2} = \frac{f_{cc,u}^{'} - f_{c1}^{'}}{\varepsilon_{cc,u} - \varepsilon_{c1}} \tag{2.9}$$

The Miyauchi et al., 1999 purposed a different expression for second straight line defined by the following

$$f_c = f_{cc,u}^{'} - \lambda\left(\varepsilon_{cu} - \varepsilon_{c,\lambda}\right) \text{for } \varepsilon_c \ge \varepsilon_{c,\lambda} \tag{2.10}$$

Where,

$$\varepsilon_{c,\lambda} = \varepsilon_{co} - \frac{\lambda \varepsilon_{co}^{\ 2}}{2 f_{co}^{'}} \tag{2.11}$$

$$\lambda = \frac{-2 f_{co}^{'}\left(\varepsilon_{cu} - \varepsilon_{co}\right) + \sqrt{4 f_{co}^{'}\left(f_{co}^{'}\varepsilon_{cc,u}^{\ 2} - 2 f_{co}^{'}\varepsilon_{co}\varepsilon_{cu} + f_{cc,u}^{'}\varepsilon_{co}^{\ 2}\right)}}{\varepsilon_{co}^{\ 2}} \tag{2.12}$$

The value of transition strain ($\varepsilon_{c1}$) was taken as $\varepsilon_{co}$ wherever separate expression is not provide for transition strain.

Table 2.1 Proposed design oriented models

| **Model** | **Ultimate strength ( $f_{cc,u}^{'}$ )** | **Ultimate strain ( $\varepsilon_{cc,u}$ )** |
|---|---|---|
| Fardis and Khalili, 1982[9] | Richart et al., 1928[5] $f_{cc,u}^{'} = f_{co}^{'}\left[1 + 4.1\left(\frac{f_{lu}}{f_{co}^{'}}\right)\right]$ Newman and Newman, 1969[6] $f_{cc,u}^{'} = f_{co}^{'}\left[1 + 3.7\left(\frac{f_{lu}}{f_{co}^{'}}\right)^{0.86}\right]$ | $\varepsilon_{cc,u} = 0.002 + 0.001\left(\frac{E_f t_f}{D f_{co}^{'}}\right)$ |
| Saadamantesh et al., 1994[11] | Adopted Mander et al., 1988[8] model (Eqn. (2.35)) | Adopted Richert et al., 1928[5] model $\varepsilon_{cc,u} = \varepsilon_{co}\left[1 + 5\left(\frac{f_{cc}^{'}}{f_{co}^{'}} - 1\right)\right]$ |
| Mirmiran, 1996[31] | $f_{cc,u}^{'} = f_{co}^{'} + 4.269\, f_{lu}^{\ 0.587}$ | N/A |
| Karbhari and Gao, 1997[32] | $f_{cc,u}^{'} = f_{co}^{'}\left[1 + 2.1\left(\frac{f_{lu}}{f_{co}^{'}}\right)^{0.87}\right]$ | $\varepsilon_{cc,u} = \varepsilon_{co} + 0.01\left(\frac{f_{lu}}{f_{co}^{'}}\right)$ |
| Samaan et al., 1998[14] | $f_{cc,u}^{'} = f_{co}^{'} + 6.0\left(f_{lu}\right)^{0.7}$ | $\varepsilon_{cc,u} = \frac{f_{cc,u}^{'} - f_{co}^{'}}{E_{c2}}$ $E_{c2} = m_2\left(245.61 f_{co}^{' m_1} + 0.6728 E_l\right)$ $m_1 = 0.2; m_2 = 1.0$ |

Table 2.1(Continue)

| **Model** | **Ultimate strength ( $f'_{cc,u}$ )** | **Ultimate strain ( $\varepsilon_{cc,u}$ )** |
|---|---|---|
| Miyauchi et al., 1999[33] | $f'_{cc,u} = f'_{co} + 2.98(f_{lu})$ | $\varepsilon_{cc,u} = \varepsilon_{co} + \varepsilon_{co}\left(15.87 - 0.093 f'_{co}\right) X \left(\frac{f_{lu}}{f'_{co}}\right)^{\left(0.246+0.0064 f'_{co}\right)}$ |
| Saafi et al., 1999[15] | $f'_{cc,u} = f'_{co} + 2.2\left(\frac{f_{lu}}{f'_{co}}\right)^{-0.16}(f_{lu})$ | $\varepsilon_{cc,u} = \varepsilon_{co}\left[1 + k_2\left(\frac{f'_{cc,u}}{f'_{co}} - 1\right)\right]$ $k_2 = 537\varepsilon_{lu} + 2.6$ |
| Spolestra and Monti, 1999[16] | $f'_{cc,u} = f'_{co}\left[0.2 + 3\left(\frac{f_{lu}}{f'_{co}}\right)^{0.5}\right]$ | $\varepsilon_{cc,u} = \varepsilon_{co}\left[2 + 1.25\frac{E_c}{f'_{co}}\varepsilon_{lu}\left(\frac{f_{lu}}{f'_{co}}\right)^{0.5}\right]$ |
| Toutanji, 1999[34] | $f'_{cc,u} = f'_{co} + 3.5\left(\frac{f_{lu}}{f'_{co}}\right)^{-0.15}(f_{lu})$ | $\varepsilon_{cc,u} = \varepsilon_{co}\left[1 + k_2\left(\frac{f'_{cc,u}}{f'_{co}} - 1\right)\right]$ $k_2 = 310.57\varepsilon_{lu} + 1.9$ |
| Lin and Chen, 2001[35] | $f'_{cc,u} = f'_{co} + 2.0(f_{lu})$ | N/A |
| Lam and Teng, 2003[17] | $f'_{cc,u} = f'_{co}\left[1 + 3.3\left(\frac{f_{lu,a}}{f'_{co}}\right)\right]$ | $\varepsilon_{cc,u} = \varepsilon_{co}\left[1.75 + 12\left(\frac{f_{lu,a}}{f'_{co}}\right)\left(\frac{\varepsilon_{h,rup}}{\varepsilon_{co}}\right)^{0.735}\right]$ |
| Ilki et al., 2004[39] | $f'_{cc,u} = f'_{co}\left[1 + 2.4\left(\frac{f_{lu,a}}{f'_{co}}\right)\right]$ | $\varepsilon_{cc,u} = \varepsilon_{co}\left[1 + 20\left(\frac{f_{lu,a}}{f'_{co}}\right)^{0.5}\right]$ |
| Berthet et al., 2006[40] | $f'_{cc,u} = f'_{co} + k_1(f_{lu})$ $k_1 = 3.45$ if $20 \le f'_{co} \le 50$ MPa $k_1 = \frac{9.5}{\left(f'_{co}\right)^{1/4}}$ if $50 \le f'_{co} \le 200$ MPa | $\varepsilon_{cc,u} = \varepsilon_{co} + \frac{\varepsilon_{h,rup} - \upsilon_c\varepsilon_{co}}{\gamma_B}$ $\gamma_B = \frac{1}{\sqrt{2}}\left(\frac{E_l}{f'^{\,2}_{co}}\right)^{-2/3}$ |
| Jiang and Teng, 2006[42] | $f'_{cc,u} = f'_{co}\left[1 + 3.3\left(\frac{f_{lu,a}}{f'_{co}}\right)\right]$ | $\varepsilon_{cc,u} = \varepsilon_{co}\left[1.65 + 6.5\left(\frac{E_l}{f'_{co}/\varepsilon_{co}}\right)^{0.8}\left(\frac{\varepsilon_{h,rup}}{\varepsilon_{co}}\right)^{1.45}\right]$ |

Table 2.1(Continue)

| **Model** | **Ultimate strength ( $f'_{cc,u}$ )** | **Ultimate strain ( $\varepsilon_{cc,u}$ )** |
|---|---|---|
| Mathys et al., 2005[41] | $f'_{cc,u} = f'_{co}\left[1+3.5\left(\frac{f_{lu,a}}{f'_{co}}\right)^{0.85}\right]$ | $\varepsilon_{cc,u} = \varepsilon_{co}\left[1+k_2\left(\frac{f'_{cc,u}}{f'_{co}}-1\right)\right]$<br>$k_2 = 310.57\varepsilon_{lu}+1.9$ |
| Youssef et al., 2007[36] | $f'_{cc,u} = f'_{co}\left[1+2.25\left(\frac{f_{lu,a}}{f'_{co}}\right)^{5/4}\right]$ | $\varepsilon_{cc,u} = 0.003368+0.2590\left(\frac{f_{lu}}{f'_{co}}\right)\left(\frac{f_{frp}}{E_{frp}}\right)^{1/2}$ |
| Girgin, 2009[37] | $f'_{cc,u} = f_{lu}+\sqrt{f'^{2}_{co}+k_5 f'_{co} f_{lu}}$<br>$k_5 = 2.9$ if $f'_{co}$ =7 to 18 MPa<br>$k_5 = 6.34-0.076 f'_{co}$ if $f'_{co}$ =20 to 82 MPa<br>$k_5 = 0.1$ if $f'_{co}$ =82 to 108 MPa | N/A |
| Teng et al., 2009[43] | $f'_{cc,u} = f'_{co}\left[1+3.5(k_1-0.01)k_2\right]$<br>$k_1 = \frac{E_l}{f'_{co}/\varepsilon_{co}}$ | $\varepsilon_{cc,u} = \varepsilon_{co}\left[1.75+6.5(k_1)^{0.8}(k_2)^{1.45}\right]$<br>$k_2 = \frac{\varepsilon_{h,rup}}{\varepsilon_{co}}$ |
| Fahmy and Wu, 2010[38] | $f'_{cc,u} = f'_{co}+k_1(f_{lu})$<br>$k_1 = 4.5 f_{lu}^{-0.3}$ if $f'_{co} \le 40$ MPa<br>$k_1 = 3.75 f_{lu}^{-0.3}$ if $f'_{co} \ge 40$ MPa | $\varepsilon_{cc,u} = \frac{f'_{cc,u}-f'_{co}}{E_{c2}}$<br>$E_{c2} = m_2\left(245.61 f'^{m_1}_{co}+0.6728E_l\right)$<br>$m_1 = 0.5; m_2 = 0.83$ if $f'_{co} \le 40$ MPa<br>$m_1 = 0.2; m_2 = 1.73$ if $f'_{co} \ge 40$ MPa |
| Realfonzo and Napoli, 2011[44] | $f'_{cc,u} = f'_{co}\left[1+3.49\left(\frac{f_{lu,a}}{f'_{co}}\right)^{0.86}\right]$<br>$f'_{cc,u} = f'_{co}\left[1+3.57\left(\frac{f_{lu,a}}{f'_{co}}\right)\right]$ | N/A |

Youssef et al., 2007[36] modified the Hognestad's parabola[45] (Eqn. (2.7)) to establish the stress-strain curve of the FRP confined concrete defined by below expression.

$$f_c = E_c\varepsilon_c\left[1-\frac{1}{m}\left(\frac{\varepsilon_c}{\varepsilon_{c1}}\right)^{m-1}\right] \text{ for } \varepsilon_c \le \varepsilon_{c1} \tag{2.13}$$

Where,

$$m = \frac{E_c\varepsilon_{c1}}{E_c\varepsilon_{c1} - f_{c1}^{'}} \tag{2.14}$$

For second ascending straight line Youssef et al., 2007[36] uses the same Eqn. (2.8) with modified $f_{c1}^{'}$ and $\varepsilon_{c1}$ values as suggested below.

$$\frac{f_{c1}^{'}}{f_{co}^{'}} = 1+3\left(\frac{4t_{frp}E_{frp}\varepsilon_{l1}}{Df_{co}^{'}}\right)^{5/4} \tag{2.15}$$

$$\varepsilon_{c1} = 0.002748 + 0.1169\left(\frac{4t_{frp}E_{frp}\varepsilon_{l1}}{f_{co}^{'}}\right)^{6/7}\left(\frac{f_{frp}}{E_{frp}}\right)^{0.5} \tag{2.16}$$

$$\varepsilon_{l1} = 0.002$$

The Richard and Abbott, 1975[46] (Eqn. (2.17)) curve has been broadly used for modeling the stress—strain relationship of FRP confined concrete. Samaan et al., 1998[14]; Lam and Teng, 2003[17], Jiang and Teng, 2006[42], Ilki et al., 2004[39], Fahmy and Wu, 2010[38] modified the original form of the stress-strain expression to form a new model expressions.

$$f_c = \frac{\left(E_{c1}-E_{c2}\right)\varepsilon_c}{\left\{1+\left[\frac{\left(E_{c1}-E_{c2}\right)\varepsilon_c}{f_o}\right]^n\right\}^{1/n}} + E_{c2}\varepsilon_c \tag{2.17}$$

$$f_o = f_{cc,u}^{'} - E_{c2}\varepsilon_{cc,u} \tag{2.18}$$

$$n = 1+\frac{1}{\frac{E_{c1}}{E_{c2}}-1} \tag{2.19}$$

Most of the researchers use the expression of elastic modulus of concrete $E_c = 4730\sqrt{f_{co}^{'}}$ given by ACI 318-95[47] to determine the slope of the initial ascending curve ($E_{c1}$). Samaan et al., 1998[14] due to higher modulus of elasticity of concrete use

a different expression $E_{c1} = 3950\sqrt{f_{co}^{'}}$ . The expression used to determine $E_{c2}$ is given in Table 2.1. Lam and Teng, 2003[17] (Eqn. (2.20, 2.21)) uses a modified form of Richard and Abbott, 1975[46] stress-strain expression which was further adopted by ACI 440.2R-08[48]. The Jiang and Teng, 2006[42] and Fahmy and Wu, 2010[38] use the same expression adopted by Lam and Teng, 2003[17] given below

$$f_c = E_{c1}\varepsilon_c - \frac{\left(E_{c1} - E_{c2}\right)^2 \varepsilon_c^{\,2}}{4 f_o} \text{ for } \varepsilon_c \le \varepsilon_{c1};\ f_o = f_{co}^{'} \tag{2.20}$$

$$f_c = f_{co}^{'} + E_{c2}\varepsilon_c \text{ for } \varepsilon_c \ge \varepsilon_{c1} \tag{2.21}$$

Where,

$$\varepsilon_{c1} = \frac{2 f_{co}^{'}}{\left(E_{c1} - E_{c2}\right)};\ E_{c2} = \frac{f_{cc,u}^{'} - f_{co}^{'}}{\varepsilon_{cu}} \tag{2.22}$$

From the general expression given by Sargin, 1971[49] (Eqn. (2.23)) for stress-strain relationship, Ahmad and shah, 1982[7] proposed a model for spiral confinement of concrete. Then, the expression was modified by Toutanji, 1999[34] (Eqn. (2.24)).

$$f_c = f_{co}^{'}\left[\frac{A_i\left(\frac{\varepsilon_c}{\varepsilon_{co}}\right) + \left(D_i - 1\right)\left(\frac{\varepsilon_c}{\varepsilon_{co}}\right)^2}{1 + \left(A_i - 2\right)\left(\frac{\varepsilon_c}{\varepsilon_{co}}\right) + D_i\left(\frac{\varepsilon_c}{\varepsilon_{co}}\right)^2}\right] \tag{2.23}$$

$$f_c = \frac{A_j \varepsilon_c}{1 + C_j \varepsilon_c + D_j \varepsilon_c^{\,2}} \tag{2.24}$$

Where,

$$A_j = E_{c1} \tag{2.25}$$

$$C_j = \frac{E_{c1}}{f_{c1}^{'}} - \frac{2}{\varepsilon_{c1}} + \frac{E_{c1}E_{c2}\varepsilon_{c1}}{f_{c1}^{1}} \tag{2.26}$$

$$D_j = \frac{1}{\varepsilon_{c1}^{\,2}} - \frac{E_{c1}E_{c2}}{f_{c1}^{1}} \tag{2.27}$$

The different parameter stress at first peak ( $f_{c1}^{'}$) corresponding strain($\varepsilon_{c1}$), initial slope of stress strain curve($E_{c1}$) and slope of second branch($E_{c2}$) to find the stress-strain curve (Eqn.(2.24)), tabulated in Table 2.2.

Table 2.2 Parameter to define Eqn. (2.24)

| **Models** | **Stress-strain curve parameters** |
|---|---|
| Saafi et al., 1999[15] | $f_{c1}^{'} = f_{co}^{'}\left[1+0.0213\left(\frac{t_{frp}E_{frp}}{Df_{co}^{'}}\right)^{0.84}\right]$ |
| | $\varepsilon_{c1} = \varepsilon_{co}\left[1+0.0783\left(\frac{t_{frp}E_{frp}}{Df_{co}^{'}}\right)^{0.84}\right]$ |
| | $E_{c1} = 10200\left(f_{co}^{'}\right)^{1/3}$ |
| | $E_{c2} = 0.272\left(\frac{f_{co}^{'}}{\varepsilon_{co}}\right)$ |
| Toutanji, 1999[34] | $f_{c1}^{'} = f_{co}^{'}\left[1+0.0178\left(\frac{E_l}{f_{co}^{'}}\right)^{0.85}\right]$ |
| | $\varepsilon_{c1} = \varepsilon_{co}\left[1+0.0448\left(\frac{E_l}{f_{co}^{'}}\right)^{0.85}\right]$ |
| | $E_{c1} = 10200\left(f_{co}^{'}\right)^{1/3}$ |
| | $E_{c2} = 0.3075\left(\frac{f_{co}^{'}}{\varepsilon_{co}}\right)$ |
| Berthet et al., 2006[40] | $f_{c1}^{'} = f_{cc,u}^{'} - E_{c2}\left(\varepsilon_{h,rup} - 0.002\right)$ |
| | $\varepsilon_{c1} = \varepsilon_{co} + \frac{0.002 - \upsilon_c\varepsilon_{co}}{\gamma}$ |
| | $E_{c1} = E_c\frac{E_c + \left(1-\upsilon_c\right)E_l}{E_c + \left(1-\upsilon_c - 2\upsilon_c^{\,2}\right)E_l}$ |
| | $E_{c2} = 2.73E_l - 163$ |

ACI 440.2R-08[48] adopts the Lam and Teng, 2003[17] stress-strain relationship using unified strain efficiency factor ($k_e$) for all type of FRP i.e. 0.55. Lam and Teng, 2003[17] experimentally calculated the value of $k_e$ for different types of FRP. Jiang and Teng, 2006[42] use different $k_e$ for different FRP for CFRP he suggested 0.5 and for GFRP 0.7. Fahmy and Wu, 2010[38] recommended $k_e = 0.55$. ACI 440.2R-08[48]

also considers a reduction factor of $\psi_f = 0.95$ for all types of FRP in calculation of peak confined strength calculation.

### 2.2.3 Analysis oriented confinement model

Analysis-oriented model uses an incremental iterative procedure for determining the stress-strain curves for FRP confined concrete. It provides unique treatment to both well confined and weak confined concrete. Analysis oriented models are more versatile and powerful than design oriented model [50]. It requires an incremental iterative procedure to derive the stress-strain curves crossing a family of stress-strain curve of same concrete under different lateral confining pressure and thus can be used directly in design. Analysis-oriented model are generally used for advanced studies using nonlinear finite element method. It is closely valid for uniformly FRP confined concrete with circular sections. The primary assumption in most of the these model is that axial stress and axial strain of confined concrete at a particular lateral strain ($\varepsilon_l$) are same as those of the same concrete actively confined with a constant confining pressure equal to that of FRP for stress-strain models using active confinement model which means the stress path of confined concrete does not affect its stress-strain behavior[50]. Based on the investigations on FRP high strength concrete (HSC) by Xiao et al., 2010[51] stated that assumption of the stress path independence was incorrect for the high strength concrete confined with FRP and they suggested that confinement efficacy of FRP confined HSC could be lower than that of actively confined HSC. Further reported that the assumption of stress path independence diverge the actual behavior significantly for the confining FRP was softer or for higher unconfined strength of the concrete. These observations were supported by the experimental test results conducted by Ozbakkaloglu et al., 2012[52].

In the Figure 2.3 the stress strain curves of actively confined concrete are served as the base curve. Then stress-strain model for FRP-confined concrete is determined using a step by step incremental procedure crossing a series of stress-strain curve for the same concrete with different confining pressure. This requires a relationship between the lateral strain to axial strain ($\mu$) i.e. dilation relationship. The steps for determination of stress strain curve of FRP confined concrete can be outline as follows.

- For a particular axial strain $\varepsilon_{c,A}$, if the lateral to axial strain relationship is known, then find the corresponding lateral strain using the strength of the unconfined concrete.
- The lateral confining pressure for FRP can be calculates using the Eqn. (2.1) for the known lateral strain.
- Then actively confined stress strain curve for this confining pressure can be selected from the Figure 2.3 Generation of stress-strain curve for FRP confined concrete. Then the corresponding axial stress calculated leading to identification of one point on stress strain curve for FRP confined concrete.
- Repeat the above three steps with increase axial strain to generate the whole stress strain model.

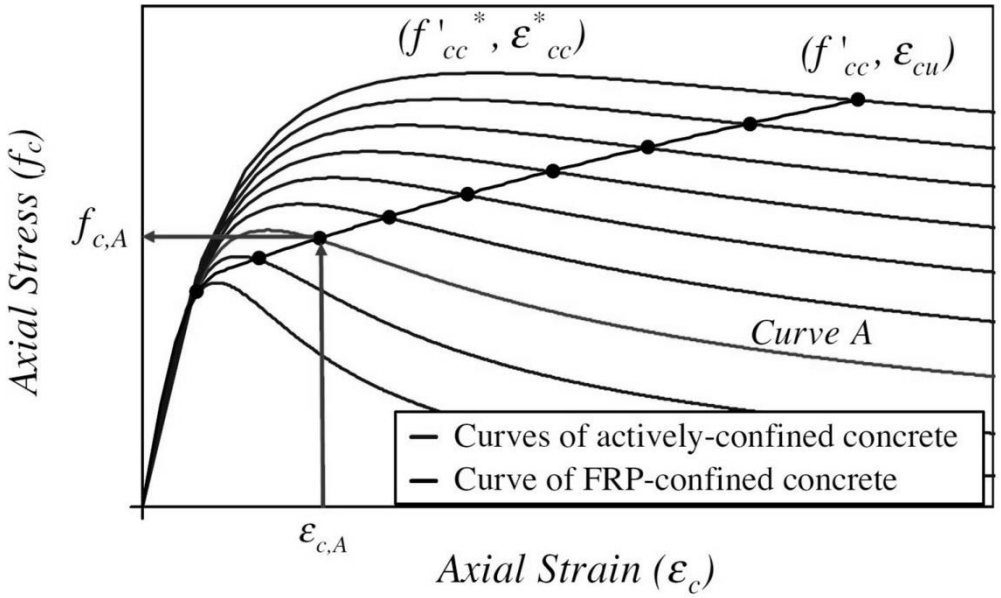


Figure 2.3 Generation of stress-strain curve for FRP confined concrete[1,20]

For the prediction of the stress strain curves of actively confined concrete requires a stress strain with peak stress and peak strain equation. The stress strain expression proposed by Popovics, 1973[53] (Eqn. (2.28)), mostly adopted for the determination of stress strain model of actively confined concrete base curves [16,50,51,54–57].

$$f_c = \frac{f'^{*}_{cc}.x.r}{r-1+x^r} \tag{2.28}$$

Where, constant $r = 0.058 f'_{co} + 1$ accounts for brittleness of concrete modified later by Carreira and Chu, 1985[58] (Eqn. (2.29)).

$$r = \frac{E_c}{E_c - f_{cc}^{'*} / \varepsilon_{cc}^{*}} \tag{2.29}$$

$$x = \varepsilon_c / \varepsilon_{cc}^{*} \tag{2.30}$$

The elastic modulus of concrete ($E_c$) expression given by ACI 318-95[47] $E_c = 4730\sqrt{f_{co}^{'}}$ was used by most of the researchers. Spoelstra and Monti, 1999[16] used expression $E_c = 5700\sqrt{f_{co}^{'}}$ and Xiao et al., 2010[51] used $E_c = 4700\sqrt{f_{co}^{'}}$.

The most widely used expression for the peak stress ($f_{cc}^{'*}$) was given by Manders et al., 1982[8] (Eqn. (2.31)). Researchers like Teng et al., 2007[50] (Eqn. (2.32)) and Xiao et al. 2010[51] (Eqn. (2.33)) used a different expression for peak stress of actively confined concrete based on their investigation.

$$f_{cc}^{'*} = f_{co}^{'}\left(2.254\sqrt{1+\frac{7.94 f_l^{*}}{f_{co}^{'}}} - 2\frac{f_l^{*}}{f_{co}^{'}} - 1.254\right) \tag{2.31}$$

$$\frac{f_{cc}^{'*}}{f_{co}^{'}} = 1 + 3.5\frac{f_l^{*}}{f_{co}^{'}} \tag{2.32}$$

$$\frac{f_{cc}^{'*}}{f_{co}^{'}} = 1 + 3.24\left(\frac{f_l^{*}}{f_{co}^{'}}\right)^{0.80} \tag{2.33}$$

The widely used expression for the prediction of the axial strain ($\varepsilon_{cc}^{*}$) at peak stress was proposed by Richart et al., 1928[5] (Eqn. (2.34)).

$$\varepsilon_{cc}^{*} = \varepsilon_{co}\left[1 + 5\left(\frac{f_{cc}^{'*}}{f_{co}^{'}} - 1\right)\right] \tag{2.34}$$

The Xiao et al., 2010[51] proposed a confinement model which is applicable to both high strength concrete and normal strength concrete proposed a different expression for axial strain ($\varepsilon_{cc}^{*}$) at peak stress (Eqn. (2.35)).

$$\frac{\varepsilon_{cc}^{*}}{\varepsilon_{co}} = 1 + 17.4\left(\frac{f_l^{*}}{f_{co}^{'}}\right)^{1.06} \tag{2.35}$$

Different researchers have given different dilation properties based on the conducted test results and investigation. Some which are derived explicitly from FRP confined

concrete test results [50,54,55] and some are adopted from an actively confined concrete model [16]. The different given for dilation behaviour of FRP confined concrete are compiled in Table 2.3.

Table 2.3 Dilation expression for actively confined concrete

| **Models** | **Dilation expression** |
|---|---|
| Mirmiran Shahawy, 1997[54,55] | $\mu = \dfrac{\upsilon_c - 2\upsilon_c\left(\dfrac{\varepsilon_c}{\varepsilon_{co}}\right) + \mu_{u,asym}\left(\dfrac{\mu_{\max} - \upsilon_c}{\mu_{\max} - \mu_{u,asym}}\right)\left(\dfrac{\varepsilon_c}{\varepsilon_{co}}\right)^2}{1 - 2\left(\dfrac{\varepsilon_c}{\varepsilon_{co}}\right) + \left(\dfrac{\mu_{\max} - \upsilon_c}{\mu_{\max} - \mu_{u,asym}}\right)\left(\dfrac{\varepsilon_c}{\varepsilon_{co}}\right)^2}$ Where, $\mu_{\max} = -0.7611\ln\left(\dfrac{E_l}{f_{co}^{'}}\right) + 4.0167$ $\mu_{u,asym} = -0.1375\ln\left(\dfrac{E_l}{f_{co}^{'}}\right) + 0.8646$ |
| Spoelstra and Monti., 1999[16] | $\varepsilon_l\left(\varepsilon_c, f_l\right) = \dfrac{E_c\varepsilon_c - f_c^{'}\left(\varepsilon_c, f_l\right)}{2\beta f_c^{'}\left(\varepsilon_c, f_l\right)}$ Where, $\beta = \dfrac{E_c}{\left\|f_{co}^{'}\right\|} - \dfrac{1}{\left\|\varepsilon_{co}\right\|}$ |
| Teng et al., 2007[50] | $\dfrac{\varepsilon_c}{\varepsilon_{co}} = 0.85\left(1 + 8\dfrac{f_l}{f_{co}^{'}}\right) \times \left\{\left[1 + 0.75\left(\dfrac{\varepsilon_l}{\varepsilon_{co}}\right)\right]^{0.7} - \exp\left[-7\left(\dfrac{\varepsilon_l}{\varepsilon_{co}}\right)\right]\right\}$ |
| Xiao et al., 2010[51] | Same as Teng et al., 2007[50] |

### 2.2.4 Finite element analysis

Mirmiran et al., 2000[59] carried out the nonlinear finite element analysis (FEA) modeling of CFRP confined concrete column for both circular and square section in ANSYS 14.0 using SOLID65 element to model the concrete and SHELL41 element to model the FRP. The focus of the study was to reduce the parameters by utilizing the Drucker-Prager type plasticity, assuming an elastic perfectly plastic response through a sensitivity analysis. The cohesion ($c$) and the angle of internal friction ($\phi$) for the concrete was calculated using the expression given by Rochette and Labossiere,

1996[60]. The purposed model fairly predicts the axial stress-strain response of the FRP confined concrete. Shahawy et al., 2000[61] tested and analytically modeled the CFRP reinforced concrete column by adopting the procedure of the Mirmiran et al., 2000[59] for FE modeling which produce reasonable results when compared with test results. Wu et al., 2009[21] with the same approach conducted 3D nonlinear FEA on circular HSC cylinder confined with Aramid FRP (AFRP) which gives a good agreement when compared with experimental and theoretical results for both uniformly and strip confined concrete. Feng et al., 2002[62] also uses the same element in ANSYS 14.0 to the model FRP and concrete but utilize William and Warnke failure criterion for concrete for the investigation of square concrete column confined with FRP sheets under uniaxial compression. Li et al., 2003[63] uses SHELL99 element to model the FRP in ANSYS 14.0 to investigate the FRP repaired RC columns. Sadeghian et al., 2008[64] study the numerical modeling of CFRP confined concrete cylinders by creating a contact between the interface of fibre and concrete. The FRP was modeled with SHELL99 element and concrete with SOLID65 element using DP plasticity model. The numerical analysis results were in good agreement with the test results. Strength of the concrete confined by the CFRP was studied by the Seffo and Hamcho., 2012[65]. Comparison between the experimental results and analytical results from finite element were studied. A cylinder of 150 mm X 300 mm was test with FRP orientation to know the effectiveness of the FRP in different orientation and number of layers. The FE model uses SOLID46 element to model FRP composites and concrete was modeled with SOLID65 element The conclusions made from the study were fiber orientation and FRP wall thicknesses have considerable effect on the stress-strain behaviour. It was also reported that the failure of the all confined cylinders was marked by the rupture of carbon fibers.

## 2.3 REVIEW ON FRP STRENGTHENED RC BEAM

*Ritchie et al., 1991*[66] conducted experimental investigation by strengthening 14 RC beams in flexure using aramid, carbon and glass fibers. To prevent the brittle mode of failure beams were design as under reinforced section. On the basis of initial failure mode separation between concrete and steel reinforcement, four different types of FRP attachment techniques were adopted. Using FRP sheets to beam sides change the failure mode was concluded.

*Saadamantesh et al., 1992*[67] experimentally investigated the GFRP strengthened RC beam in flexure. GFRP significantly improves the flexural strength of conventional beam as well as the epoxy improves the crack behaviour was the major outcomes.

*Norris et al., 1997*[68] experimentally and analytically study the shear and flexural strengthening of RC beams reinforced with CFRP sheets. Depending on the orientation of CFRP different failure patterns and ultimate strength were observed.

*Kachlakev et al., 2001*[69]studied four models of beams strengthened in flexure and shear using FE tool ANSYS 14.0 which shown a good agreement with experimental data conducted by Kachalakev and McCurry, 2000[70]. The outcome of the analytical study was ANSYS 14.0 can be utilizing to model strengthened beam efficiently. The crack behaviour was predicted for flexural shear strengthening which was consistent with the hand calculations. The shear strengthening efficiently increases the ductility of the RC beam.

*Wolanski, 2004*[71] analytically modeled the RC beam using ANSYS 14.0 to study its flexural behaviour. SOLID65, LINK8 and SOLID45 element was to model the concrete, rebar and steel plate respectively. A good agreement was concluded when compared with experimental load deflection plot.

*Camata et al., 2004*[72] conducted experimental and nonlinear finite element studies of RC beams strengthened with FRP plates. The main aim was to study the brittle failure of RC members strengthened by the FRP plates. The conclusion made from the study were for short FRP plates, failure starts at the plate end, while for longer FRP plates failure starts at mid span. A comparison between CFRP and GFRP strengthening with same axial stiffness but different contact showed that increasing the plate width increases greatly the peak load and the deformation level of the strengthened beam.

*Coccia et al., 2005*[4] carried out the work on effect of FRP strengthening on global response of RC portal to account for nonlinear phenomenon. The numerical analysis was carried using ATENA program and validated with a nonlinear procedure. The result confirms the effectiveness of the techniques adopted for the retrofitting.

*Barros et al., 2006*[73] experimentally studied the behaviour of reinforced concrete beams strengthened in flexure and shear with near surface mounted (NSM) and externally bonded reinforcement (EBR) strengthening techniques with CFRP. The study

was conducted to check the efficiency of strengthening techniques. The experimental results obtained were compared with analytical formulation of ACI, fib and Italian guidelines. A numerical model was also implemented to check the effective FRP strain applicability. The result shows NSM technique was most effective for strengthening.

*Esfahani et al., 2006*[74] investigates the flexural behaviour of the RC beams strengthened with CFRP sheets. Beams sections with three different reinforcing ratios were manufactured. Nine beams were strengthened with CFRP sheets with different layers. The conclusion made from the study was as the reinforcing ratio increases, the ratio of the test load to the load calculated by ACI 440.2 and ISIS Canada, also increase. With large reinforcing bar ratio failure of the strengthened beams occurs with adequate ductility.

*Godat et al., 2007*[75] studied the numerical modeling of FRP shear-strengthened reinforced concrete beams with aiming to develop an efficient FEM model. The conclusion drawn from the analysis by comparison with the experimental trends were the number of FRP plies influences the slip values; it is very important parameter as the interfacial slip values are directly affected by the strains that develop in the bonded FRP laminates. Also the existence of the crack affects the interfacial slip profiles along the beam depth.

*Ibrahim et al., 2009*[76] presented an analytical model for the RC beams externally reinforced with fiber reinforced polymer laminates using ANSYS 14.0. The results from the analysis were compared with the experimental data for the six beams and it was concluded that the numerical solution adopted to evaluate the ultimate shear strength of the RC beams reinforced with FRP laminates in simple, cheap and rapid way compared with experimental full scale test. The result also compared that the carbon fiber polymer is more efficient than glass polymer fiber in strengthening of the RC beams for shear.

*Godat et al., 2010*[77] investigated the shear performance of different sized rectangular RC beams strengthened by using CFRP strips. It was found that the contribution of the strip is higher in smaller specimen compare with the larger one.

*Julio et al., 2012*[78] studied the effect of adhesive thickness and concrete strength on FRP- concrete bonds. It was found that adhesive when mixed with low strength concrete member, failure occurred in the weakest part that was concrete. On the other

hand when the adhesive was fixed with the stronger concrete, failures occurs at the concrete-adhesive interface which was the weakest part.

*Ouyang et al., 2012*[79] conducted experimental study on flexural strength of BFRP strengthened RC beam. Increasing in layers of BFRP sheets improves the stiffness and yielding of steel was concluded along with other conclusions

*Dong et al., 2013*[80] conducted experimental research on RC beams strengthened with FRP in flexure and flexural-shear to check how different reinforcing scheme affect the behaviour of strengthened RC beams. Also, the experimental results compared with design models. Flexural shear strengthening of RC beam increases the stiffness more efficiently was concluded.

*Hawileh et al., 2013*[81] carried FE simulation of RC beam for short length CFRP plates using ANSYS 14.0. The aim of the study was to develop FE model to accurately simulate the behaviour of strengthened RC beams. A good agreement with experimental results was obtained using the FE model with bond slip properties.

*Sasmal et. al., 2013*[82] carried out study on the nonlinear finite element analysis of FRP strengthened RC beams by using ANSYS 14.0 software. The study shows that FRP with SHELL41 element is recommended when single layer of FRP laminate is used. When multilayered FRP is used SOLID46 can be a reasonably good choice.

*Ronagh and Baji, 2014*[83] compared the elements use for FRP and material model for concrete in ANSYS 14.0 for beam column assemblies. SHELL181 and SHELL41 element was used to model the FRP with smeared element REINF265. They concluded that their model takes less time for simulation and ANSYS 14.0 predict monotonic load very well

*Tomilnson and Fam, 2014*[84] check the performance of RC beam reinforced with BFRP for flexure and shear strengthening. They found that the ultimate capacity does not depend on the failure modes. ACI code method was found to be adequate in predicting the ultimate strength.

*Abu-Obeidah et al., 2015*[85] utilizes ANSYS 14.0 to develop a 3D nonlinear FE model for shear deficient RC beams strengthened with aluminum plates. SHELL63 and

INTER205 element was used to model the aluminum plates and interface. The developed model predicts the behaviour of the experimental work accurately.

*Kumar, 2015*[2] experimentally study the behaviour of strengthened RC beam with different types of FRP. Different scheme of FRP wrapping was used for 18 RC beams with M20 and M30 grade of concrete. The dimension of all RC beams was identical. From the shear and flexural-shear strengthening of RC beams, concluded that FRP significantly help in energy dissipation and increases the stiffness of the unreinforced RC beam.

## 2.4 REMARKS

The confinement models show an approximate prediction of the stress-strain curve of the FRP confined concrete. For more accurate predication it must be compared with more number of test results. The finite element modeling of FRP confined concrete can be effectively carried out when a proper numerical model is used. The results obtained from finite element analysis can be validated with the previously available results. The finite element analysis gives a better theoretical understanding to proceed towards an accurate confinement model or strength predication.

# CHAPTER 3

# FINITE ELEMENT MODEL

## 3.1 GENERAL

This chapter deals with basic of the finite element method (FEM), and material properties used for the modeling in finite element tool ANSYS 14.0. Details of element formulation and material properties for concrete, rebar, FRP are described. For analytical study, it is important to understand the material behaviour and its failure criteria which are describe in this segment.

## 3.2 FINITE ELEMENT ANALYSIS

Finite element method (FEM) is a capable tool to effectively simulate the behaviour of the concrete member confined with FRP. The FE software ANSYS 14.0 has been used for the numerical studies. In ANSYS 14.0, different element type defined the behaviour of different geometries. Each element has different degrees of freedom condition at each node, connectivity types, output option and capability of carrying particular load types etc. ANSYS 14.0 provides special element which capture the behaviour of brittle materials like concrete. The ANSYS 14.0 also provide the layered elements for the material like FRP which is used as adhesive layers between the concrete member and the FRP. For contact analysis different element is defined in ANSYS 14.0 which able the contact between the two surfaces.

## 3.3 ELEMENT FORMULATION

### 3.3.1 FRP Composites

In confined cylinder, a 3-D layered structural element SOLID185 was used to model FRP composites. The element has three degree of freedom at each node i.e. translation in x, y, z directions. The element is defined by the eight nodes, layer thickness, layer material, direction, angles and material properties. The geometry and coordinate system is shown in Figure 3.1. For beams and portal, SHELL181 was used to model the FRP composites. The element stiffness option considered for the SHELL181 was membrane

only. Thus, the element has three degree of freedom. The element accommodates option for defining the material number, orientation, thickness and number of integration points through the thickness of each layer[86]. The geometry of the SHELL181 element is shown in Figure 3.2.

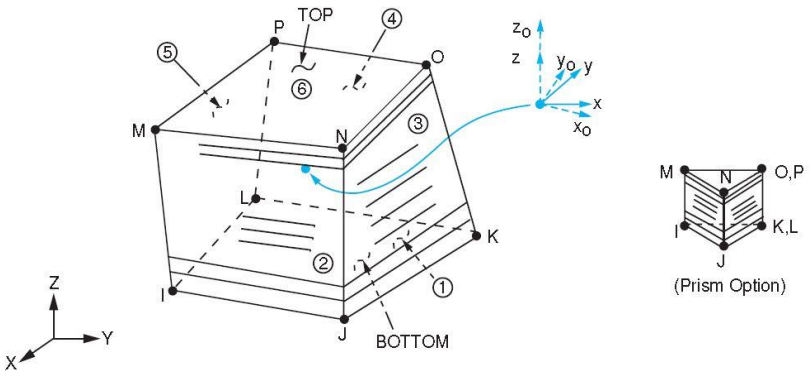


Figure 3.1 Geometry and coordinate system of SOLID185 Layered element[86]

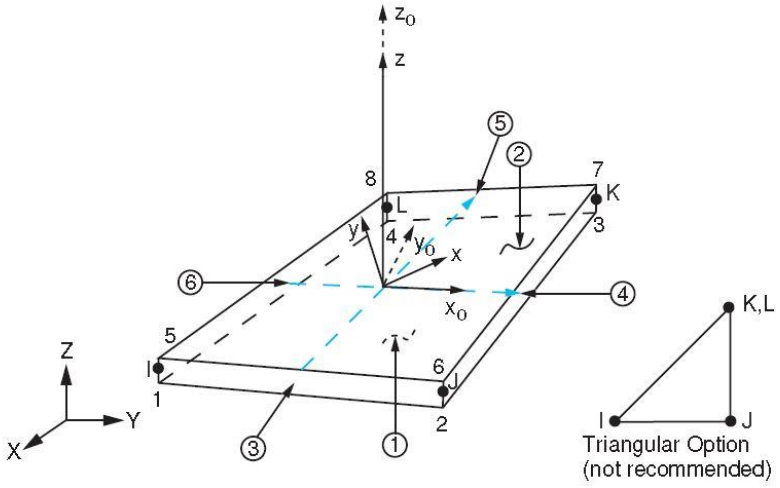


Figure 3.2 Geometry and coordinate system of SHELL181 element[86]

### 3.3.2 Reinforced Concrete

For the modeling of concrete, a 3-D reinforced concrete solid element SOLID65 was used. The element is capable of cracking in tension and crushing in compression. The element is defined by the eight nodes having three degrees of freedom at each node i.e. translations in x, y, z directions. The element support isotropic property, nonlinear properties and plastic deformation[86]. The geometry and coordinate system is shown in Figure 3.3.

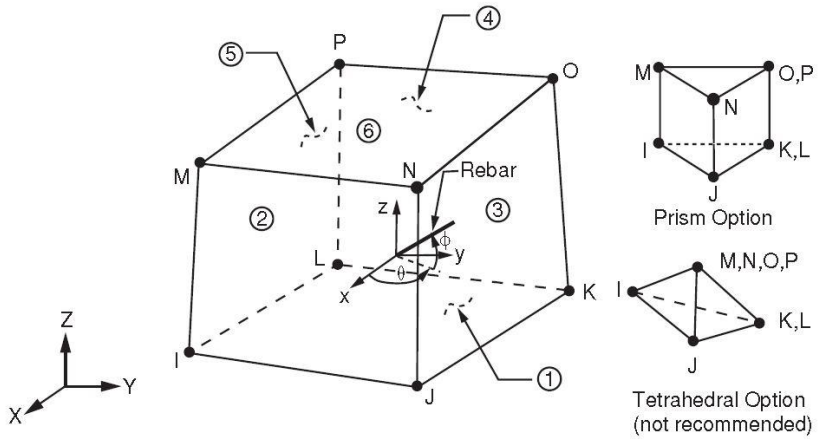


Figure 3.3 Geometry and coordinate system of SOLID65 element [86]

### 3.3.3 Steel reinforcement

A LINK180 element was used to model the steel reinforcement. The element is a 3D spar element and it has two nodes with three degrees of freedom at each node i.e. translations in nodal x, y, and z directions. The element is capable of plastic deformation[86]. This element is shown in Figure 3.4.

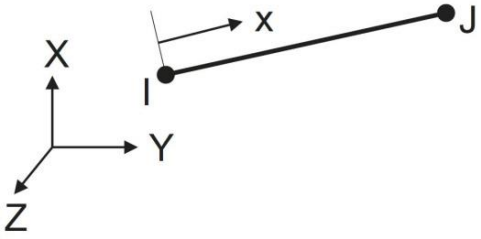


Figure 3.4LINK180 element [86]

### 3.3.4 Support and loading arrangements

The support and loading cylinder was modeled with eight node 3D SOLID185 element having three degree of freedom at each node: translations in x, y, z directions[86]. The nodal location with coordinate system is shown in Figure 3.5.

### 3.3.5 Contact element

ANSYS 14.0 provide different contact elements for the 2-D and 3-D geometries. In this study, CONTA174 and TARGET170 are used for creating the contact between the structural member and the loading arrangements. The structural member is considering

as source and the loading arrangement is consider as the target. As the deflected element act normal to the target element. In this study, a surface-to-surface contact was made taking the loading arrangement as rigid body. Figure 3.6 shows the geometry of the contact elements.

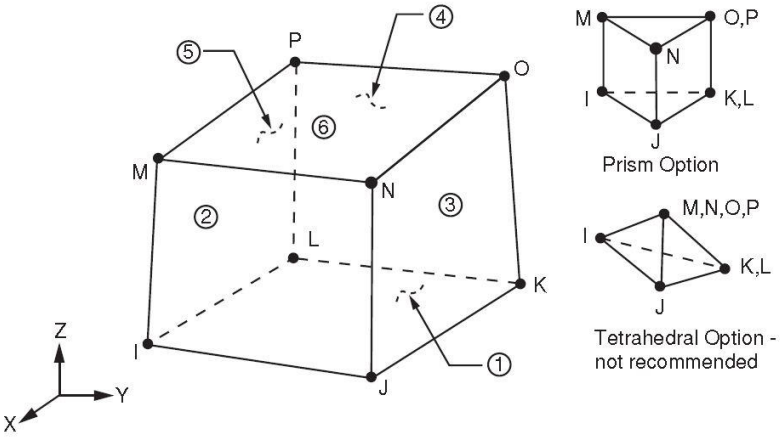


Figure 3.5 Geometry and coordinate for SOLID185 element[86]

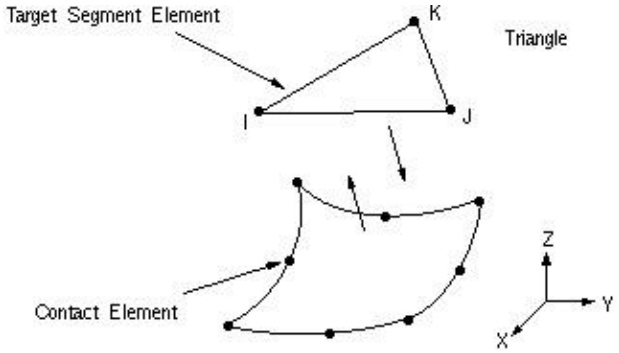


Figure 3.6 Geometry of CONTA174 and TARGET170 elements[86]

## 3.4 MATERIAL PROPERTIES

### 3.4.1 FRP sheets

As defined by the element the input used are the numbers of layers, thickness of the layers, and orientation of the fiber direction for each layer. The composites are orthotropic materials therefore; nine different properties have to be input, the elastic modulus in three different directions ($E_x, E_y, E_z$), the shear modulus in the three directions ($G_{xy}, G_{yz}, G_{zx}$) and the Poisson's ratio in the three directions ($\upsilon_{xy}, \upsilon_{yz}, \upsilon_{zx}$).

Figure 3.7 gives the principal directions of the orthotropic material. The material properties determined depending upon the principal directions of the FRP composite.

$$E_x = E_1, E_y = E_2, E_z = E_3$$

$$\upsilon_{xy} = \upsilon_{12}, \upsilon_{yz} = \upsilon_{23}, \upsilon_{zx} = \upsilon_{31}$$

$$G_{xy} = G_{12}, G_{yz} = G_{23}, G_{zx} = G_{31}$$

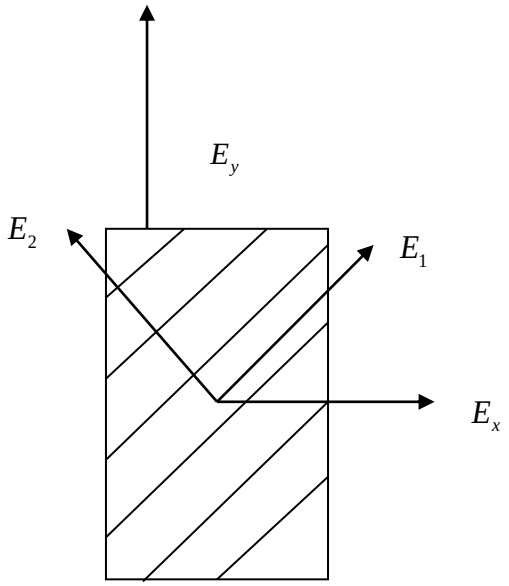


Figure 3.7 Principal directions of an orthotropic material

The properties of FRP (BFRP, CFRP and GFRP) for the modeling of concrete members and RC beams used from the experimental study conducted by Kumar, 2015[2] and acquire here are stated in Table 3.1. Due to non-availability of epoxy matrix property; only properties of FRP sheets is used for FE modeling which assure the conditions needed for a non-isotropic material in ANSYS 14.0 manual and also identified by Kachlakev et al., 2001[69]. The CFRP sheet is unidirectional whereas the BFRP and GFRP sheets are bidirectional. The elastic modulus of BFRP, CFRP and GFRP sheets are 89 GPa, 242 GPa and 69 GPa respectively, used by Kumar, 2015[2,3]. The property of CFRP for modeling the simple RC portal was adopted from Niroomandi et al., 2010[87] and is tabulated in Table 3.2. The CFRP characteristic tabulated in Table 3.3 is used for validation of the confined cylinder model.

The FRP is assumed to be linearly elastic until rupture. The ultimate fibre strength for all the three fibers is plotted against its ultimate strain as shown in Figure 3.8. The flexural and shear cracks of concrete can initiate debonding of the FRP sheets. To exclude such debonding of FRP sheets in finite element analysis, the effective FRP strain should be less than limiting strain recommended by ACI 440.2R-08[48]. ACI

440.2R-08[48] modified the debonding FRP strain equation which was originally proposed by Teng et al., 2003[88]. The effective FRP strain to consider debonding failure in modified form is given by

$$\varepsilon_{fd} = 0.41\sqrt{\frac{f_c^{'}}{n_f E_f t_f}} \leq 0.9\varepsilon_{fu} \tag{3.1}$$

Table 3.1 Material properties of FRP used for FE modeling of concrete member and RC beams

| **FRP** | **Elastic Modulus (MPa)** | **Poisson's Ratio** | **Shear Modulus (MPa)** | **Thickness of each layer (mm)** |
|---|---|---|---|---|
| Basalt fiber (BFRP) | $E_x$ =89000 | $\upsilon_{xy}$ = 0.3 | $G_{xy}$ = 8200 | |
| | $E_y$ = 89000 | $\upsilon_{yz}$ = 0.35 | $G_{yz}$ = 6630 | 0.111 |
| | $E_z$ = 17500 | $\upsilon_{zx}$ = 0.35 | $G_{zx}$ = 6630 | |
| Carbon fiber (CFRP) | $E_x$ =242000 | $\upsilon_{xy}$ = 0.2 | $G_{xy}$ = 12570 | |
| | $E_y$ = 17500 | $\upsilon_{yz}$ = 0.3 | $G_{yz}$ = 6640 | 0.222 |
| | $E_z$ = 17500 | $\upsilon_{zx}$ = 0.2 | $G_{zx}$ = 12570 | |
| Glass fiber (GFRP) | $E_x$ =69000 | $\upsilon_{xy}$ = 0..22 | $G_{xy}$ = 7500 | |
| | $E_y$ = 69000 | $\upsilon_{yz}$ = 0..25 | $G_{yz}$ = 6150 | 0.273 |
| | $E_z$ = 15000 | $\upsilon_{zx}$ = 0..25 | $G_{zx}$ = 6150 | |

Table 3.2 Material properties of CFRP used for RC portal FE modeling.

| **Data collected from** | **FRP Composite** | **Elastic Modulus (MPa)** | **Poisson's Ratio** | **Shear Modulus (MPa)** | **Thickness of each layer(mm)** |
|---|---|---|---|---|---|
| Niroomandi et al., 2010[87] | Carbon fiber | $E_x$ =240000 | $\upsilon_{xy}$ = 0.2 | $G_{xy}$ = 12576 | |
| | | $E_y$ = 18581 | $\upsilon_{yz}$ = 0.3 | $G_{yz}$ = 7147 | 0.165 |
| | | $E_z$ = 18581 | $\upsilon_{zx}$ = 0.2 | $G_{zx}$ = 12576 | |

Table 3.3 Material properties of CFRP used for model verification

| Data collected from | FRP Composite | Elastic Modulus (MPa) | Poisson's Ratio | Shear Modulus (MPa) | Thickness of each layer(mm) |
|---|---|---|---|---|---|
| Seffo and Hamcho, 2012[65] | Carbon fiber | $E_x$ =200000<br>$E_y$ = 48000<br>$E_z$ = 48000 | $\upsilon_{xy}$ = 0.22<br>$\upsilon_{yz}$ = 0.3<br>$\upsilon_{zx}$ = 0.22 | $G_{xy}$ = 3270<br>$G_{yz}$ = 1860<br>$G_{zx}$ = 3270 | 0.165 |

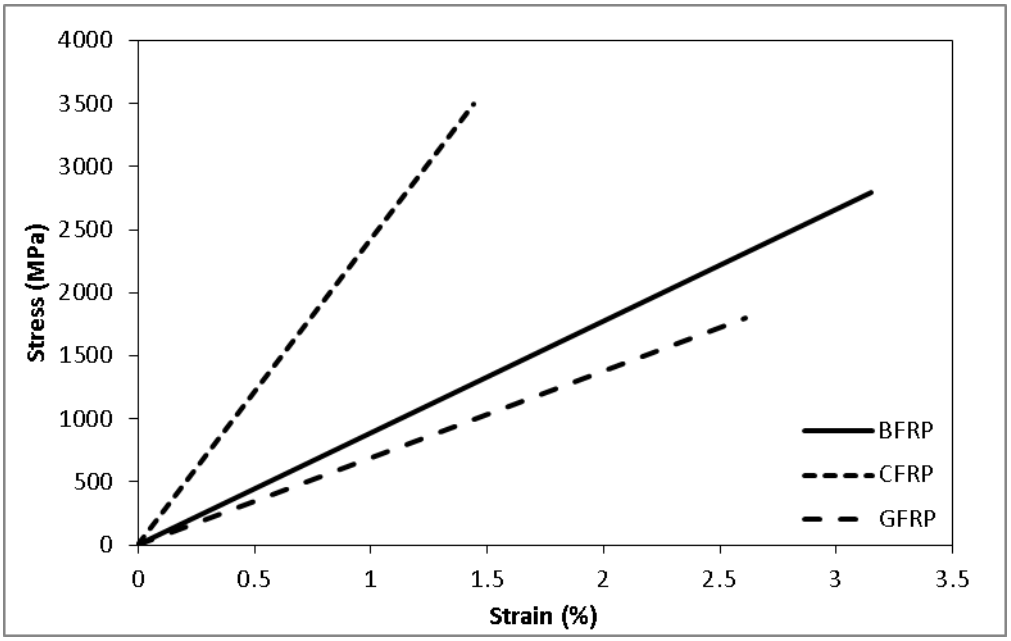


Figure 3.8 Stress-strain curves for FRP sheets

### 3.4.2 Concrete

The properties of the concrete were taken from the IS 456:2000[89]. The SOLID65 element requires linear isotropic and multi-linear isotropic material properties to model the concrete. The multi-linear isotropic uses the Von Mises failure criterion and the failure of the concrete was define using Willam and Warnke, 1975[30] model. The modulus of elasticity of the concrete ($E_c$) and modulus of rupture ($f_r$) were found out as:

$$E_c = 5000\sqrt{f_{co}^{'}} \tag{3.2}$$

$$f_r = 0.7\sqrt{f_{co}^{'}} \tag{3.3}$$

The material properties for concrete used in the present study are tabulated in the Table 3.4. The ultimate compressive strength of the concrete is taken from standard cylinder test results conducted by Kumar, 2015[2].

Table 3.4. Material properties of concrete used in the study[2]

| **Type** | **Compressive strength, $f_{ck}$. (MPa)** | **Elastic modulus, $E_c$ (MPa)** | **Tensile strength, $f_r$ (MPa)** | **Poisson's ratio, ν** |
|---|---|---|---|---|
| C1 | 25.52 | 25258.66 | 3.54 | 0.18 |
| C2 | 39.11 | 31276.60 | 4.38 | 0.18 |

The following parabola equation given by Hogesnatad[45] is used to compute the nonlinear compressive stress-strain curve for the concrete.

$$f_c = f_{ck}\left[2\left(\frac{\varepsilon_c}{\varepsilon_{co}}\right)-\left(\frac{\varepsilon_c}{\varepsilon_{co}}\right)^2\right] \text{ if } \varepsilon_c \le \varepsilon_{co} \tag{3.4}$$

$$f_c = f_{ck} \text{ if } \varepsilon_c \ge \varepsilon_{co} \tag{3.5}$$

$$\varepsilon_{co} = \frac{2 f_{ck}}{E_c} \tag{3.6}$$

Where,

$f_c$ = stress at any strain $\varepsilon_c$, MPa.

$\varepsilon_c$ = strain at stress $f_c$.

$\varepsilon_{co}$ = strain at the ultimate compressive strength $f_{ck}$

The first point on the multi-linear stress-strain curve is defined by the user and must satisfy the Hooke's law. The concrete compressive stress-strain curve is used to help with nonlinear solution convergence.

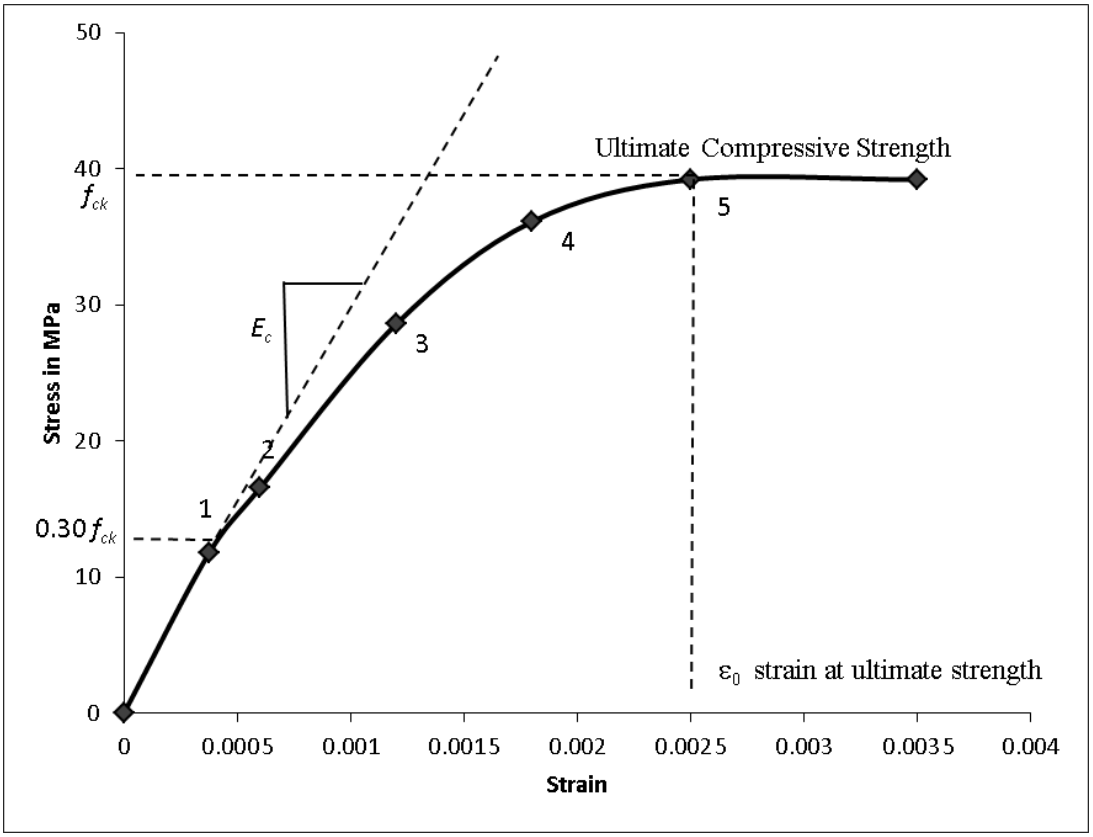


Figure 3.9 Uniaxial stress-strain curve of concrete

Figure 3.9 shows the non-linear stress-strain relationship used for the study and is based on IS 456:2000[89]. The point 1 on the curve defined the linear elastic limit of the concrete which is 30 percent of the ultimate compressive strength, $f_{ck}$ of the concrete and the point 5 represents the ultimate compressive strength of the concrete. Other points are calculated using the Eqn. (3.4). After the point 5, the behavior of the concrete was assumed to perfectly plastic. Strain at the ultimate was 0.0035 as per the IS 456:2000.

An example is enumerated here, to indicate the values of the five points using the ultimate compressive strength of concrete, $f_{ck}$ to be 39.11 MPa. At point 1, the strain at stress of 11.760 MPa (0.30 $f_{ck}$) is carried out for the linear behaviour of stress-strain curve i.e. 0.000376 mm/mm. The strain at ultimate compressive strength of concrete is carried out using the Eqn. (3.6) which is equal to 0.002504 mm/mm. All other values on stress-strain curve are carried out using the Eqn. (3.4) as presented in the Table 3.5.

Table 3.5 Stress-strain curve values for the concrete of compressive strength 39.11 MPa

| Point on curve as shown in Figure 3.9 | Strain | Stress (MPa) |
|---|---|---|
| 1 | 0.000376 | 11.760 |
| 2 | 0.000600 | 16.533 |
| 3 | 0.001200 | 28.566 |
| 4 | 0.001800 | 36.099 |
| 5 | 0.002504 | 39.110 |

The concrete model in ANSYS 14.0 required different constants to be defined. The condition of the crack face of concrete is characterized by shear transfer coefficient, for which the value ranges from 0.0 to 1.0. Here, value 0.0 illustrates a smooth crack which means total loss of shear transfer and 1.0 illustrates a rough crack which means zero loss of shear transfer[90]. The shear coefficient used for the present study is 0.3 as suggested by the previous researchers[69,71,91]. The uniaxial cracking stress based upon the modulus of rupture i.e. the tensile strength of the concrete.

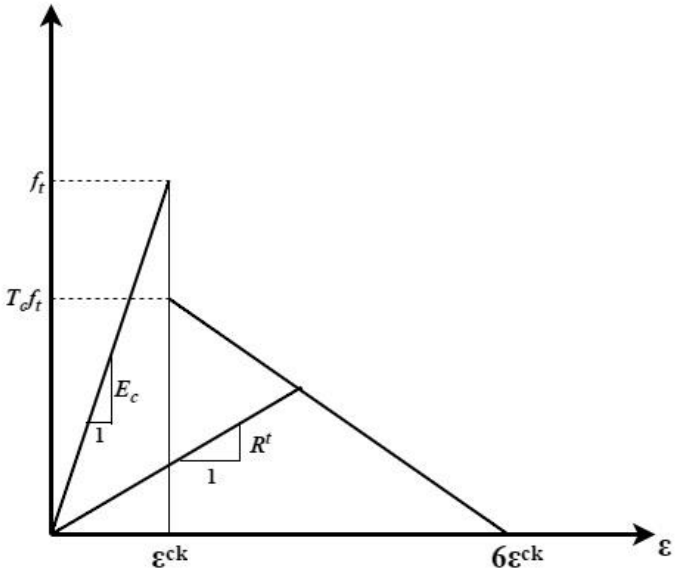


Figure 3.10 Stress of cracked condition of concrete[90]

Stress relaxation must be contemplated after cracking in order to consider tension stiffening. Figure 3.10 shows the model engaged in ANSYS 14.0 to deal with tension stiffening. A multiplier $T_c$ set to default constant value of 0.6 is used to control the amount of tensile stress relaxation. $f_t$ is the tensile cracking stress of the concrete. $R^t$

is the secant modulus as shown in the Figure 3.10 which value depend upon the key option 7 of the SOLID65 element. The $R^t$ help in solution convergence when tensile stress relaxation after cracking is considered using KEYOPT (7), the value of $R^t$ is set as one which gradually reduces to zero as solution converges[90].

Figure 3.11 shows the failure surface for concrete in three dimensions. The $\sigma_{xp}$, $\sigma_{yp}$ and $\sigma_{zp}$ represents the principal stresses in x, y and z directions respectively. In Figure 3.11, $\sigma_{xp}$ and $\sigma_{yp}$ are the most important nonzero principal stresses. The three failure surfaces $\sigma_{zp}$ marginally greater than zero, $\sigma_{zp}$ equal to zero and $\sigma_{zp}$ marginally less than zero are depicted as projections on the $\sigma_{xp}$ - $\sigma_{yp}$ plane which are nearly equivalent and the failure surface is continuous. The material failure status is the function of $\sigma_{zp}$ sign. For instance, if both $\sigma_{xp}$ and $\sigma_{yp}$ are negative (compressive) and $\sigma_{zp}$ is marginally positive then cracking would be concluded in a direction perpendicular to the $\sigma_{zp}$ direction. Despite, if the value of $\sigma_{zp}$ is zero or marginally negative, the failure of material is assumed to be crush [90].

If the failure surface lies outside the principal tensile stress in any direction then the concrete element cracks. After the cracking occurs, the modulus of elasticity of concrete element is fixed to zero in direction parallel to principle stress direction. The crushing in the concrete element appears when all the principal stresses are compressive and lie outside the failure surface. Consequently, the modulus of elasticity is fixed to zero in every direction and the concrete element completely disappears[90].

During the analysis using the concrete non-metal plasticity, it was found out that if the uniaxial crushing stress of concrete is set to be ultimate compressive strength of the concrete then the finite element model of the concrete member fails too early. As the crushing evolve in the concrete elements which are located directly under the loads. Consequently, the adjoining elements crushes within next load steps which significantly reducing the local stiffness. Lastly, the solution diverged by showing a large displacement and element distortion.

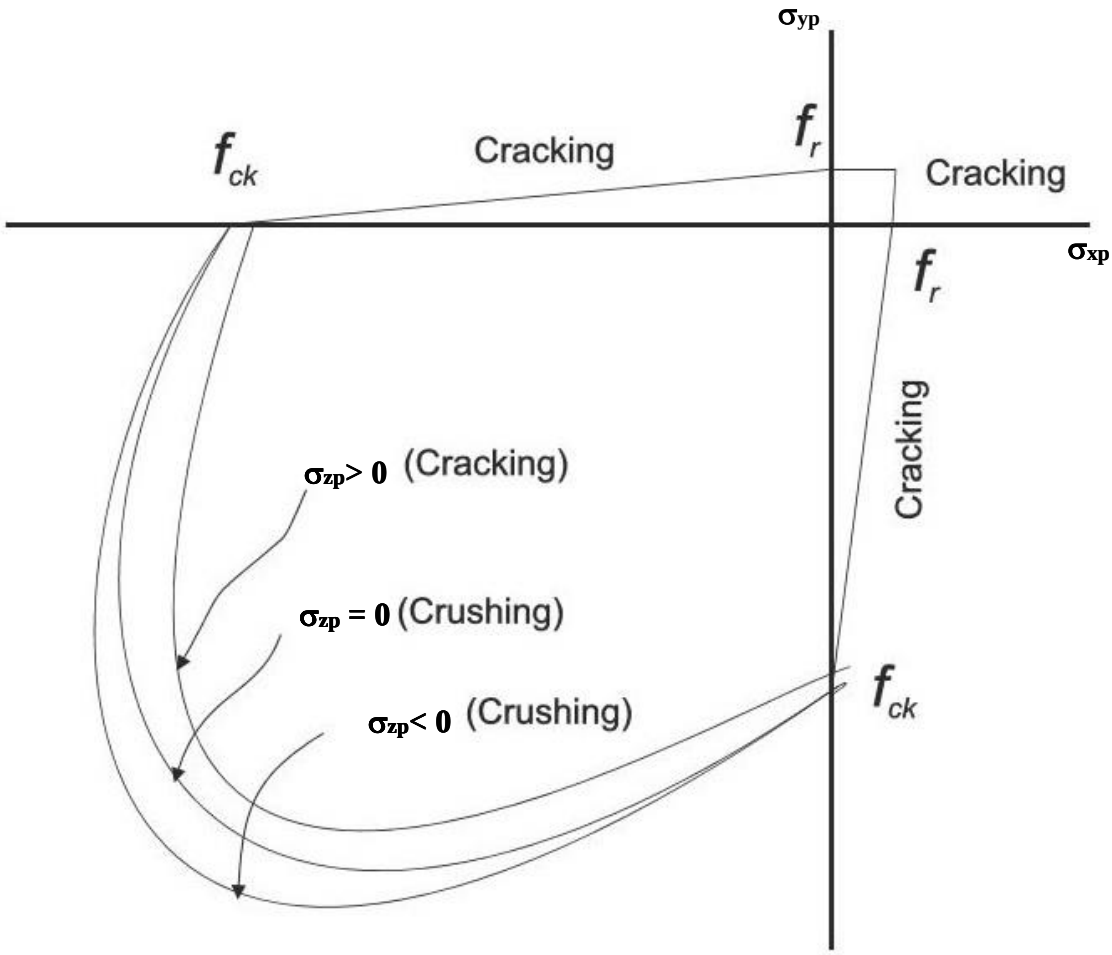


Figure 3.11. 3D failure surface for concrete[90]

The concrete rarely fails in pure compression. Considering the compression test of concrete in which concrete is subjected to uniaxial compressive load. And the tensile strains convinced by the Poisson's effect appear perpendicular to the load. Due to concrete is relatively weak in tension which causes cracking in concrete and ultimately the failure of concrete[92,93]. Thus, in the present study, the crushing capability of the concrete element was turned off by entering the uniaxial crushing stress as -1.

### 3.4.3 Steel reinforcement

The experimental beams were constructed with Fe500 grade steel reinforcing bar for main bars and Fe250 grade steel reinforcing bar for stirrups. The material properties such as modulus of elasticity and yield stress used in FEM analysis pursue the design material properties used for the experimental beams[2]. Bilinear isotropic model based on Von Mises failure criteria is used to model the steel reinforcement. The bilinear Von Mises plasticity need two values i.e. yield strength ( $f_y$ ) and tangential modulus of the

steel reinforcement. The tangential modulus ($E_T$) of steel for bilinear curve is taken as 20 MPa. The Fe250 grade of steel stirrup is model by assuming to be perfectly plastic material. Also, the behaviour assumed identical in both tension and compression. Figure 3.12 and Figure 3.13 shows the stress-strain curve for steel used in the study for both Fe500 and Fe250 grade of steel respectively. The steel reinforcement is model with Poisson's ratio of 0.3 and Young's modulus of 200 GPa. For RC portal only Fe500 grade of steel is used to model both steel reinforcement and the tie bars.

### 3.4.4 Loading arrangement and Contact

The support and loading arrangement is modeled rigidly with high modulus of elasticity and the Poisson's ratio of 0.3. The contact between the beam surface and the support cylinder is generated using the coefficient of friction equal to 0.05, normal penalty stiffness of 1.0 and penetration tolerance of 0.0001. Close gap is opted for the initial adjustment of the contact. The cylinder model is of 2 cm diameter.

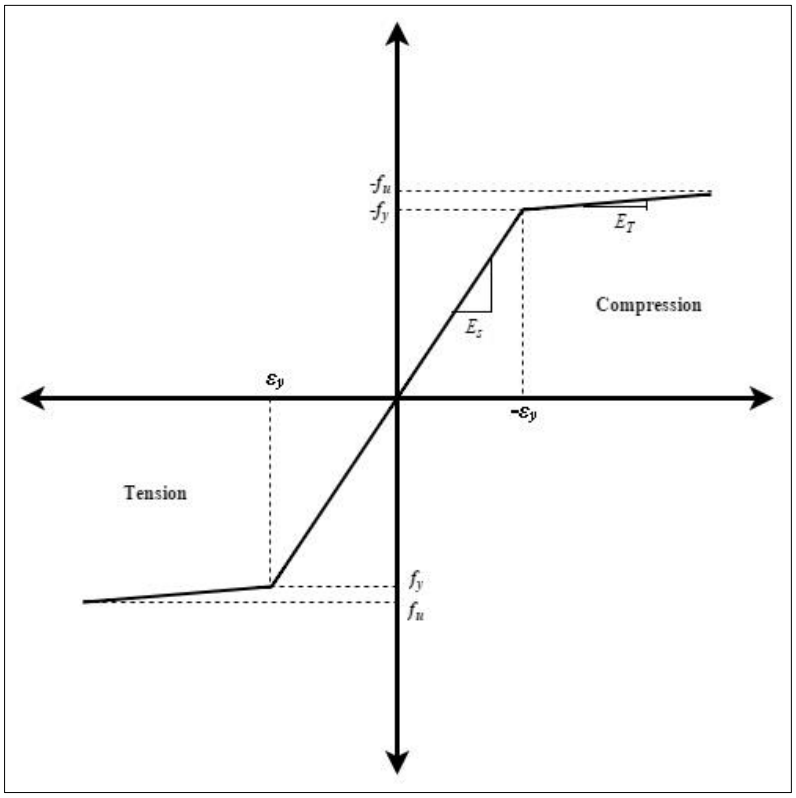


Figure 3.12. Stress-strain plot for Fe500 grade steel reinforcement

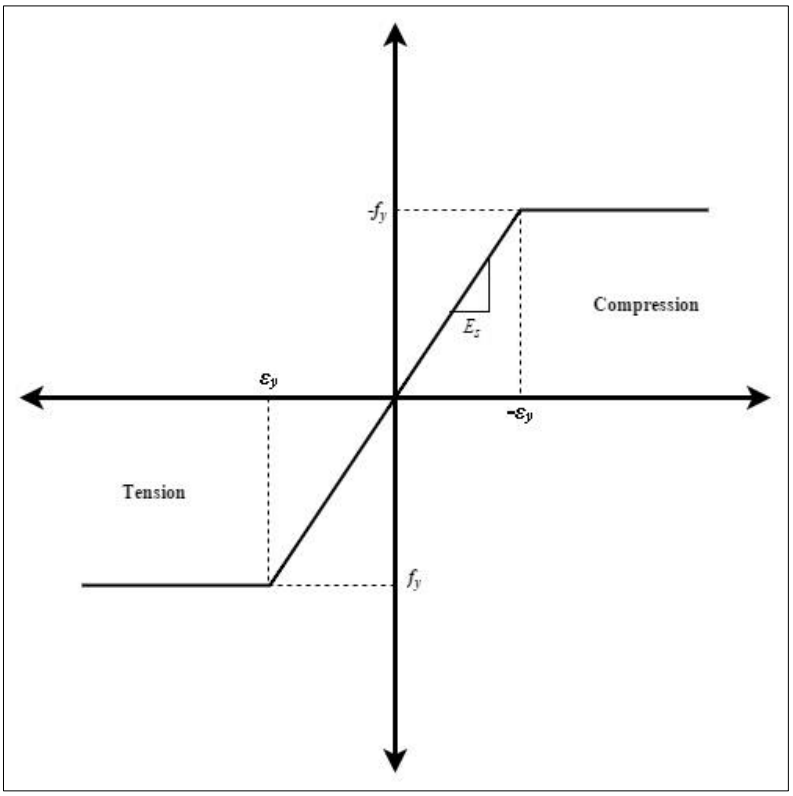


Figure 3.13. Stress-strain plot for Fe250 grade of steel reinforcement

.

## 3.5 REMARKS

The preceding chapter discusses about the element formulation and material data used for the finite element modeling in ANSYS 14.0. Using the above mentioned element and material data, the finite element analysis is simulated discuss in the next section.

# CHAPTER 4

# 3D FEM OF CONFINED CONCRETE MEMBERS

## 4.1 GENERAL

In order to understand the improvement in the performance of the confined concrete with FRP from the control concrete member; it is require designing the confined concrete analytically. Various confining model have been proposed for strength enhancement of the concrete cylinder confined with FRP. In the present section, FE modeling is used to understand the mechanical behavior of the confined concrete members. Concrete cylinder confined with FRP for direct compression, flexural and fracture strength of concrete prism with FRP sheet attached to the soffit of the prism are analyses. The model is validated with the earlier experimental work done in the department by Kumar, 2015[2]. Also, the confining model proposed by different researchers is used for comparison of FRP confined concrete strength.

## 4.2 SIMULATION OF DIRECT COMPRESSION

Previously, the nonlinear FE modeling of FRP confined concrete column is carried out in ANSYS 14.0 using SOLID65 element to model the concrete and SHELL41 element to model the FRP jacketing by Mirmiran et al., 2000[59]; Shahawy et al., 2000[61] and Wu et al., 2009[21]. They used a non-associative Drucker-Prager type plasticity model to account for failure criteria of concrete. Feng et al., 2002[62] also uses the same element to the model FRP and concrete. But utilize William and Warnke failure criterion[30] of concrete. Li et al., 2003[63] and Sadeghian et al., 2008[64] uses SHELL99 element to model the FRP in ANSYS 14.0 to investigate the FRP repaired RC columns. The researcher Seffo and Hamcho 2012[65] uses SOLID46 element to the FRP composites and concrete was modeled with SOLID65 element.

In present analysis, the concrete is modeled with SOLID65 element along with William and Warnke[30] concrete failure criteria and SOLID185 layered element is used to model the FRP. The material properties of the concrete and FRP described in the chapter 3. Some assumption has been made for the unavailable data.

Table 4.1 Confined concrete cylinder Designation

| Designation | Details |
|---|---|
| CYN-C1 | Control cylinder with C1=25.52 MPa |
| CYN-C2 | Control cylinder with C2=39.11 MPa |
| C1-CYN-BFRP-L1 | Confined with 1 layer BFRP and concrete strength C1 |
| C1-CYN-CFRP-L1 | Confined with 1 layer CFRP and concrete strength C1 |
| C1-CYN-GFRP-L1 | Confined with 1 layer GFRP and concrete strength C1 |
| C1-CYN-BFRP-L2 | Confined with 2 layer BFRP and concrete strength C1 |
| C1-CYN-CFRP-L2 | Confined with 2 layer CFRP and concrete strength C1 |
| C1-CYN-GFRP-L2 | Confined with 2 layer GFRP and concrete strength C1 |
| C2-CYN-BFRP-L1 | Confined with 1 layer BFRP and concrete strength C2 |
| C2-CYN-CFRP-L1 | Confined with 1 layer CFRP and concrete strength C2 |
| C2-CYN-GFRP-L1 | Confined with 1 layer GFRP and concrete strength C2 |
| C2-CYN-BFRP-L2 | Confined with 2 layer BFRP and concrete strength C2 |
| C2-CYN-CFRP-L2 | Confined with 2 layer CFRP and concrete strength C2 |
| C2-CYN-GFRP-L2 | Confined with 2 layer GFRP and concrete strength C2 |

### 4.2.1 Modeling of Concrete cylinder with FRP

A solid cylinder is produce by a creating a cylindrical coordinate system at the active working plane. Then a hollow cylinder is produced with given thickness, diameter and height. The solid cylinder resembles concrete and hollow cylinder resembles FRP sheet. Then both volumes are merged together to form a perfect bond between the composite and concrete. The dimension of the cylinder is the standard diameter of 150 mm and height of 300 mm. The model is meshed with mapped meshing which helps in governing the number of elements. Coarser mesh reduces the time of analysis and finer increases the accuracy of the analysis. The hollow cylinder is meshed with SOLID185 element and the solid cylinder is meshed with SOLID65 element. The coordinate axes of all the elements of the hollow cylinder are aligned to the cylindrical coordinate system. Figure 4.1 shows the finite element model of the FRP confined concrete cylinder.

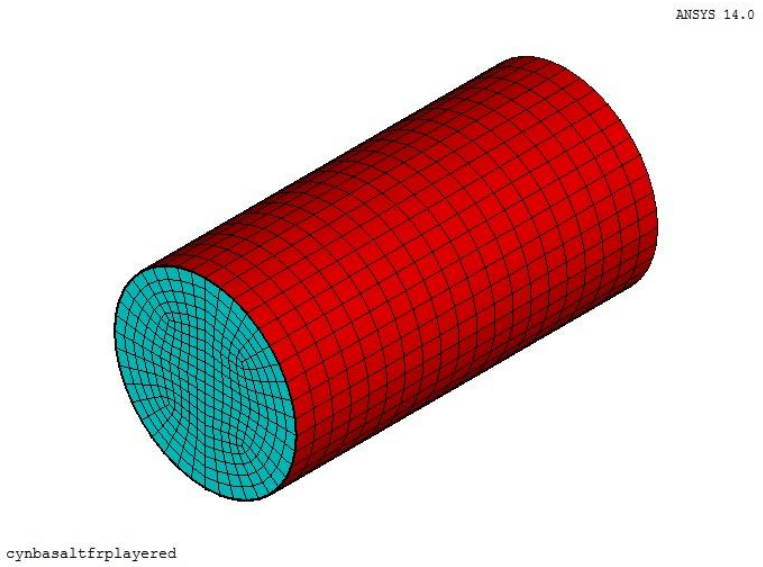


Figure 4.1 Finite element model of FRP concrete cylinder

### 4.2.2 Boundary condition and loading

The one end of the surface is fixed i.e. constrained all the degrees of freedom on that surface. An axial compressive pressure load applied on the other surface which increases gradually until the failure. This type of loading condition and boundary constraints are similar to cylinders under uniaxial compression test. Figure 4.2shows the loading and boundary conditions for the FRP confined concrete column.

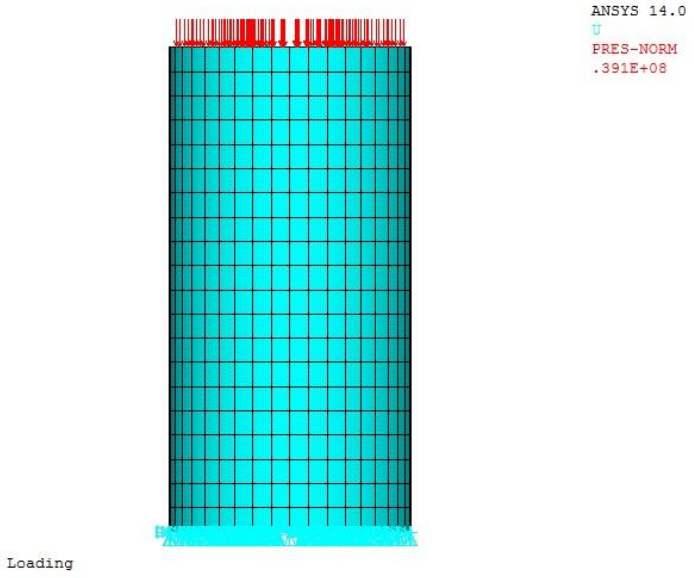


Figure 4.2 Loading and boundary condition on an FRP confined cylinder.

### 4.2.3 Simulation and Output

A nonlinear structural analysis is performed, to include the nonlinear material behaviour of concrete. To solve nonlinear problems, the Newton- Raphson approach is engaged in ANSYS 14.0. The applied pressure is divided into several load steps. The increment in every load steps is applied over several sub steps which follows an iterative procedure until the problem converges. To increase the possibility of convergence the auto time stepping is activated. The force tolerance is set to 0.005 for the convergence. Also, the equilibrium iteration is increased to 200 for an individual sub steps.

When an axial compressive load is applied to concrete cylinder confined with FRP, the concrete is the basic load resisting member. With gradual increase in the load the concrete starts cracking with visible micro-cracks and finally concrete crush when the ultimate crushing strength of concrete is reached. Now the concrete is confined by the FRP which collaboratively bear the loads along with concrete. The FRP fails when its rupture strain is reached. The failure of the confined concrete appears when FRP rupture. The premature failure in the confined concrete may occur if the bulging of the concrete appears.

Figure 4.3 shows the displacement modeling studied in the ANSYS 14.0 program for the direct compression in which maximum displacement occur at the top of the surface. The cracking and crushing of the concrete using SOLID65 element can be shown. The cracking behavior of the FRP confined concrete obtained from analytical study is shown in Figure 4.4. The crushing capability of the SOILD65 is turn off due to premature failure. The cracking pattern shows the primary crack start in concrete near the fixed end. No visible/few cracks develop at the middle of the confined column. More cracks maximum crack developed near the end surface of the FRP confined cylinder. This behaviour follows the Saint Venant's Principle "the difference between the effects of two different but statistically equivalent loads becomes very small at sufficiently large distances from the load" adopted from Wikipedia[94] originally the statement published in French by Saint-Venant in 1855.

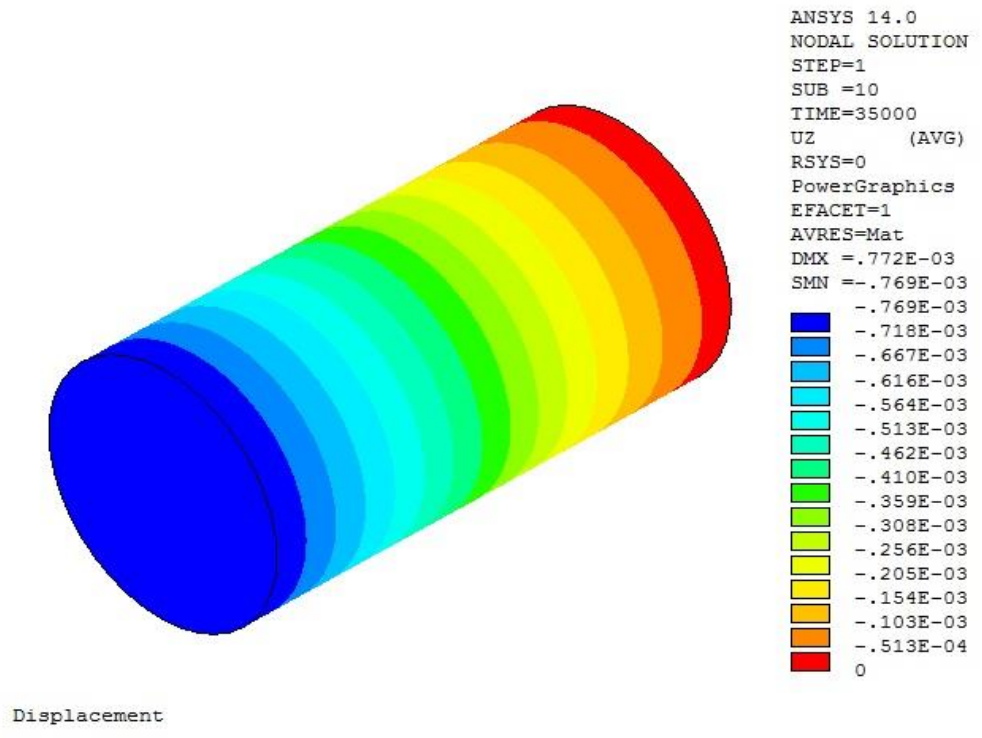


Figure 4.3 Displacement modeling in cylinder studied from ANSYS 14.0 program.

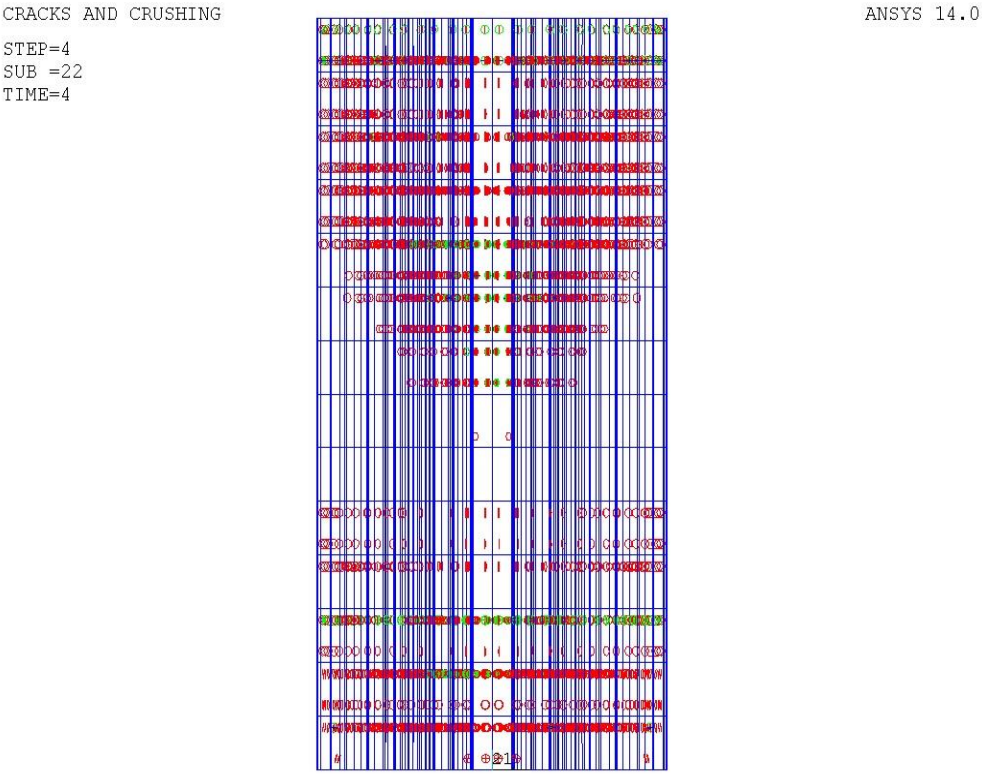


Figure 4.4 Failure pattern of FRP confined concrete

### 4.2.4 Results and Discussion

The model is validity with the experimental and analytical works done in the literature. The analytical work carried out by Seffo and Hamcho, 2012[65] on the performed experiment confined concrete test is taken for the validation. The Experiment carried out in the department by Kumar, 2015[2] is compared with present analytical work for the confined concrete under direct compression of concrete wrapped with FRP. The stress-strain plot obtained from FEA compared with experimental plots, some design oriented and experimental oriented models.

The FEM work done by the Seffo and Hamcho, 2012[65] report the confined compressive strength for single layered unidirectional Carbon FRP was to be 48.6 MPa and results from the present analysis with same condition is about 48.4 MPa which is comparatively closed. So the model can use for the modeling for compression cylinder confined with FRP.

The comparison between the experimental and finite element result for the different types of FRP with concrete strength C1=25.52 MPa and C2=39.11 MPa tabulated in table 4.2 and table 4.3 respectively. The experimental data taken from the M. Tech dissertation by the Kumar (May, 2015), Department of Earthquake Engineering, IIT Roorkee[2].

Table 4.2 Comparison of analytical strength with experimental data for C1=25.52 MPa

| **Type** | **Experimental results (MPa)** | **FEA Results (MPa)** | **Differences (%)** | $f'_{cc,u} / f'^{*}_{co}$ |
|---|---|---|---|---|
| CYN-C1 | 25.52 | 25.52 | | 1.00 |
| C1-CYN-BFRP-L1 | 33.24 | 31.28 | 5.90 | 1.23 |
| C1-CYN-CFRP-L1 | 54.72 | 46.86 | 14.37 | 1.84 |
| C1-CYN-GFRP-L1 | 28.95 | 34.64 | -19.66 | 1.36 |
| C1-CYN-BFRP-L2 | 34.11 | 36.44 | -6.82 | 1.43 |
| C1-CYN-CFRP-L2 | 60.78 | 61.89 | -1.82 | 2.43 |
| C1-CYN-GFRP-L2 | 37.84 | 44.07 | -16.47 | 1.73 |

$f'_{cc,u} / f'^{*}_{co}$ *Comparison of FEA results with C1 strength*

Table 4.3 Comparison of analytical strength with experimental data for C2=39.11 MPa

| Type | Experimental results (MPa) | FEA Results (MPa) | Differences (%) | $f'_{cc,u} / f'^{*}_{co}$ |
|---|---|---|---|---|
| CYN-C2 | 39.11 | 39.11 | | 1.00 |
| C2-CYN-BFRP-L1 | 48.00 | 44.88 | 6.50 | 1.15 |
| C2-CYN-CFRP-L1 | 57.24 | 61.81 | -7.99 | 1.58 |
| C2-CYN-GFRP-L1 | 55.45 | 50.33 | 9.23 | 1.29 |
| C2-CYN-BFRP-L2 | 48.04 | 52.08 | -8.40 | 1.33 |
| C2-CYN-CFRP-L2 | 83.62 | 79.58 | 4.83 | 2.03 |
| C2-CYN-GFRP-L2 | 46.90 | 58.57 | -24.88 | 1.50 |

$f'_{cc,u} / f'^{*}_{co}$ *Comparison of FEA results with C2 strength*

From the above table, the comparison between the FEA and the experimental results show that analytical predictions of FRP confined concrete are reliable. The two layered GFRP confined cylinder with concrete strength 39.11 MPa gives the maximum error of 24.88 % which may be due to deficiency during the experimental program. Also, it was stated that the failure of C2-CYN-GFRP-L2 specimen occur due to the rupture of the GFRP at the bottom part. The failure of C2-CYN-GFRP-L2 may be occur due to the less strength of concrete at the bottom part which further contributes to the bulging of concrete at the bottom part during the load increment. For rest, the error is in between 20% which indicates the accuracy and reliability of the analytical model for the simulation of FRP confined concrete.

The comparison of FE results with conventional concrete strength point out that CFRP is good in increasing the strength of concrete. More than 200% increase in the strength can be seen with two layer of CFRP for both concrete types. The effect of FRP confinement is more with concrete strength 25.52 MPa. The effect of confinement follows CFRP >GFRP>BFRP.

The comparison of final stress obtained from FEA with different proposed confinement model in literature [16,31,36,38,40,43,48] summarized in Table 4.4 Comparison of FEA results with confinement models for C1 and C2 concrete strength are shown in Table 4.4 and Table 4.5 respectively. The table shows the comparison of confined part with percentage of error from finite element analysis results.

From the Table 4.4 and Table 4.5, it can be concluded that the model proposed by ACI 440.2R-08[48] adopted from the confinement model given by Teng et al., 2003[17] with some modification like reduction factor ($\psi_f$ =0.95) in peak strength calculation and taking a uniform strain reduction factor of $k_e = 0.55$ for all types of FRP is found to be suitable for predicting the peak confined concrete strength for all types of FRP. It shows percentage of error of less than 10% for all type of FRP with both concrete type C1 and C2 when compared with the FEA results. The confinement models of Berthet et al., 2006[40] and Youssef et al., 2007[36] are also good in predicting the peak strength. The model by Mirmiran 1996[31] fair for the basalt and glass type FRP also for single layer carbon fibre but produce error of more than 15% when confined with two layered of CFRP. Fahmy and Wu, 2010[38] shows good agreement in peak strength for CFRP confined concrete.

Table 4.4 Comparison of FEA results with confinement models for C1

| **Type**<br>**Stress in MPa** | **C1-CYN-BFRP-L1** | **C1-CYN-CFRP-L1** | **C1-CYN-GFRP-L1** | **C1-CYN-BFRP-L2** | **C1-CYN-CFRP-L2** | **C1-CYN-GFRP-L2** |
|---|---|---|---|---|---|---|
| **FEA Results** | 31.28 | 46.86 | 34.64 | 36.44 | 61.89 | 44.07 |
| **ACI 440.2R-08**[48] | 32.67 | 43.38 | 36.82 | 39.83 | 61.24 | 48.13 |
| **(error)** | (-4.5%)* | (7.4%) | (-6.3%) | (-9.3%) | (1.0%) | (-9.2%) |
| **Mirmiran, 1996**[31] | 35.36 | 42.36 | 38.39 | 40.30 | 50.81 | 44.86 |
| **(error)** | (-13.0%) | (9.6%) | (-10.8%) | (-10.6%) | (17.9%) | (-1.8%) |
| **SM model 1999**[16] | 35.97 | 53.8 | 43.91 | 48.76 | 74.08 | 59.98 |
| **(error)** | (-15.0%) | (-15.0%) | (-26.7%) | (-33.8%) | (-19.7%) | (-36.1%) |
| **Berthet model, 2006**[40] | 33.39 | 45.17 | 37.96 | 41.27 | 64.83 | 50.40 |
| **(error)** | (-6.8%) | (3.6%) | (-9.6%) | (-13.3%) | (-4.8%) | (-14.4%) |
| **Youssef model, 2007**[36] | 31.45 | 44.12 | 36.02 | 39.62 | 69.76 | 50.49 |
| **(error)** | (-0.5%) | (5.8%) | (-4.0%) | (-8.7%) | (-12.7%) | (-14.6%) |
| **Teng model, 2009**[43] | 26.05 | 41.96 | 33.54 | 37.67 | 61.90 | 49.60 |
| **(error)** | (16.7%) | (10.4%) | (3.2%) | (-3.4%) | (0.0%) | (-12.6%) |
| **FW model 2010**[38] | 37.70 | 48.64 | 42.30 | 45.31 | 63.07 | 52.78 |
| **(error)** | (-20.5%) | (-3.8%) | (-22.1%) | (-24.4%) | (-1.9%) | (-19.8%) |

** Error in percentage for FEA result*

Table 4.5 Comparison of FEA results with confinement models for C2

| **Type** **Stress in MPa** | **C2-CYN-BFRP-L1** | **C2-CYN-CFRP-L1** | **C2-CYN-GFRP-L1** | **C2-CYN-BFRP-L2** | **C2-CYN-CFRP-L2** | **C2-CYN-GFRP-L2** |
|---|---|---|---|---|---|---|
| **FEA Results** | 44.88 | 61.81 | 50.33 | 52.08 | 79.58 | 58.57 |
| **ACI 440.2R-08**[48] | 46.26 | 56.97 | 50.41 | 53.42 | 74.83 | 61.72 |
| **(error)** | (-3.1%)* | (7.8%) | (-0.2%) | (-2.6%) | (6.0%) | (-5.4%) |
| **Mirmiran, 1996**[31] | 48.95 | 55.95 | 51.98 | 53.89 | 64.40 | 58.45 |
| **(error)** | (-9.1%) | (9.5%) | (-3.3%) | (-3.5%) | (19.1%) | (0.2%) |
| **SM model 1999**[16] | 46.04 | 68.20 | 55.86 | 61.87 | 93.21 | 75.75 |
| **(error)** | (-2.6%) | (-10.3%) | (-11.0%) | (-18.8%) | (-17.1%) | (-29.3%) |
| **Berthet model, 2006**[40] | 46.98 | 58.76 | 51.55 | 54.86 | 78.42 | 63.99 |
| **(error)** | (-4.7%) | (4.9%) | (-2.4%) | (-5.3%) | (1.5%) | (-9.2%) |
| **Youssef model, 2007**[36] | 44.44 | 55.83 | 48.55 | 51.78 | 78.87 | 61.56 |
| **(error)** | (1.0%) | (9.7%) | (3.5%) | (0.6%) | (0.9%) | (-5.1%) |
| **Teng model, 2009**[43] | 39.11 | 54.70 | 45.17 | 48.55 | 74.64 | 61.23 |
| **(error)** | (12.9%) | (11.5%) | (10.3%) | (6.8%) | (6.2%) | (-4.5%) |
| **FW model 2010**[38] | 51.29 | 62.23 | 55.89 | 58.90 | 76.66 | 66.37 |
| **(error)** | (-14.3%) | (-0.7%) | (-11.0%) | (-13.1%) | (3.7%) | (-13.3%) |

** Error in percentage for FEA result*

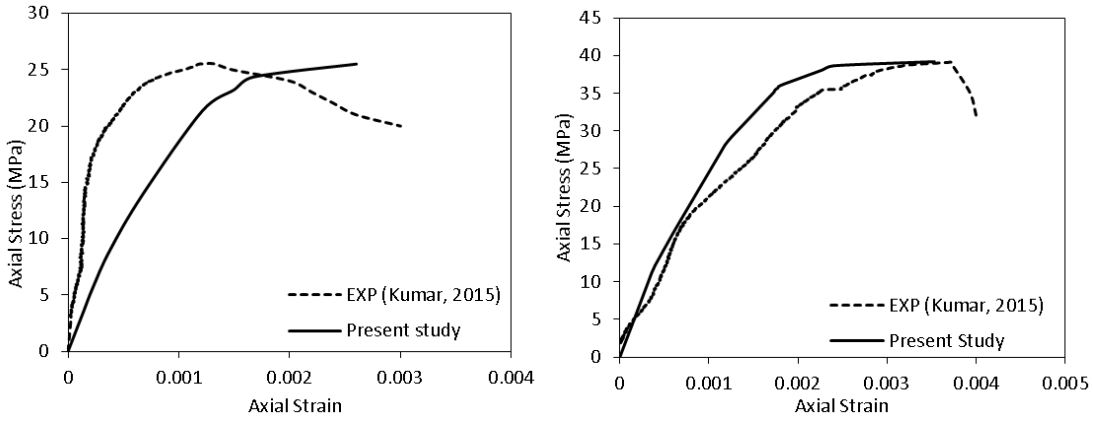


(a) CYN-C1 (b) CYN-C2

Figure 4.5 Comparison of stress strain plot for control concrete strength

The stress strain plot for control specimen CYN-C1 and CYN-C2 with concrete strength 25.52 MPa and 39.11 MPa obtained analytically from ANSYS 14.0 is compared with the experimental data [2]. In CYN-C2 specimen, the stress strain plot

from FE analysis stiffer than the experimental plots. But in case of CYN-C1 specimen the experimental plot is found to be stiffer than FEA plot.

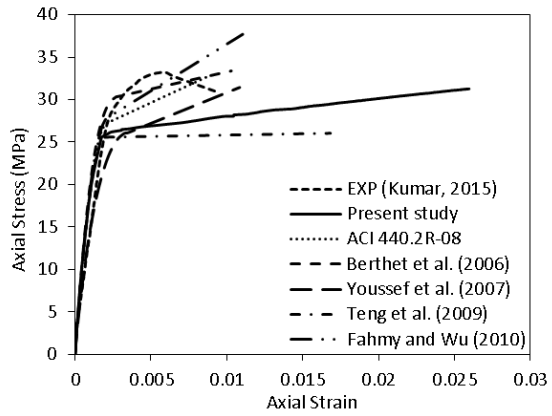


(a) C1-CYN-BFRP-L1

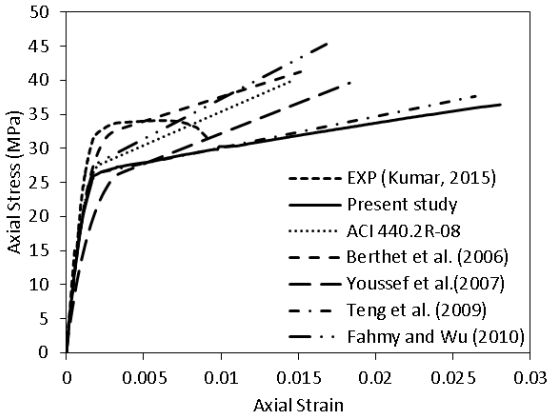


(b) C1-CYN-BFRP-L2

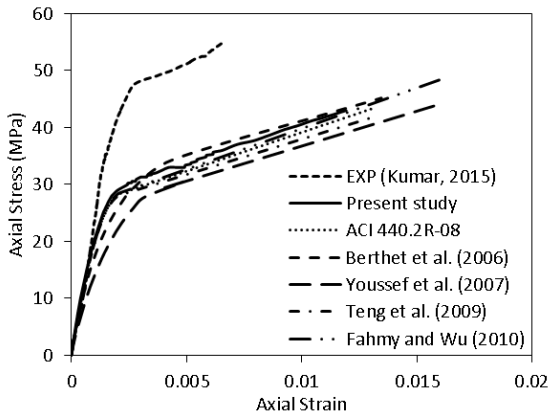


(c) C1-CYN-CFRP-L1

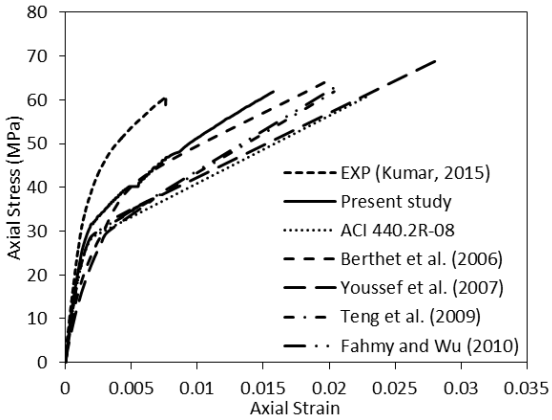


(d) C1-CYN-CFRP-L2

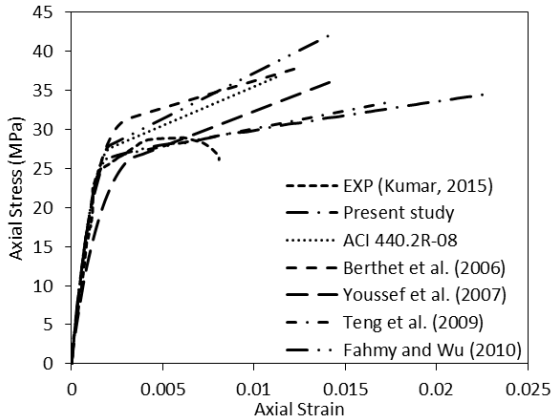


(e) C1-CYN-GFRP-L1

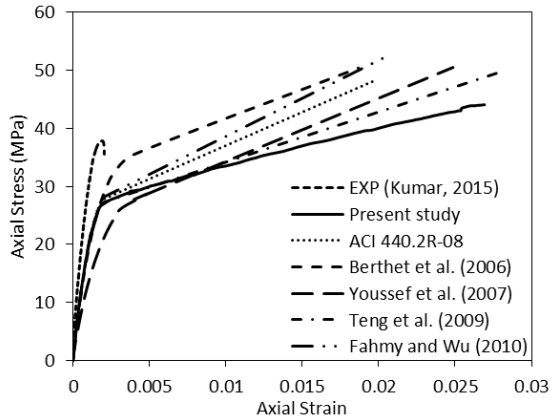


(f) C1-CYN-GFRP-L2

Figure 4.6 Comparison of stress-strain plot with design oriented model for C1

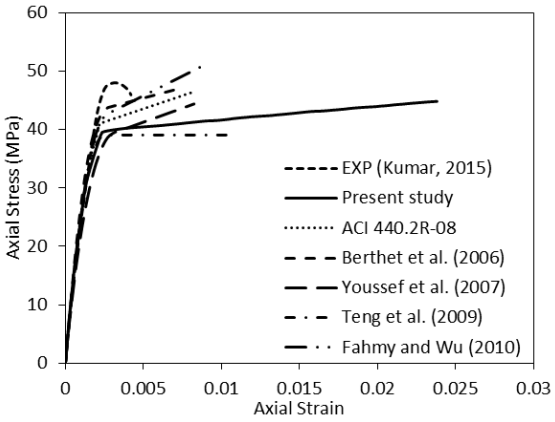


(a) C2-CYN-BFRP-L1

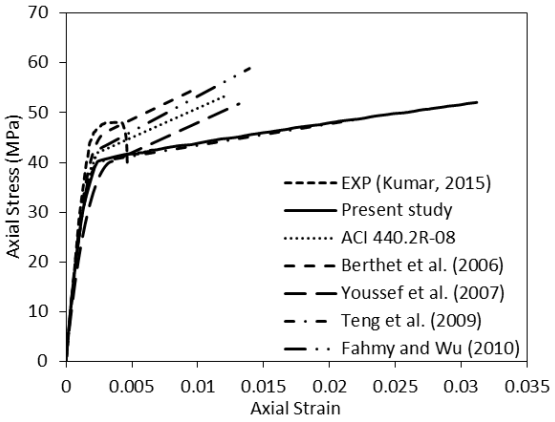


(b) C2-CYN-BFRP-L2

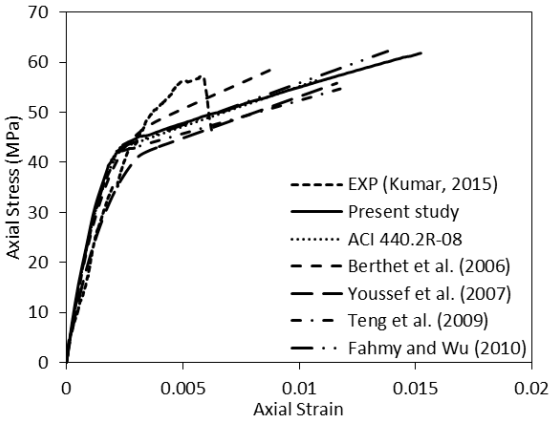


(c) C2-CYN-CFRP-L1

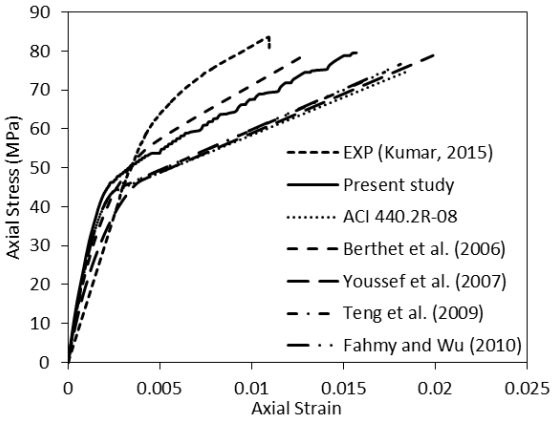


(d) C2-CYN-CFRP-L2

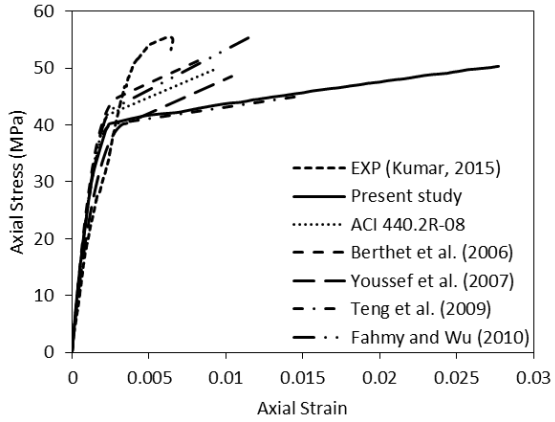


(e) C2-CYN-GFRP-L1

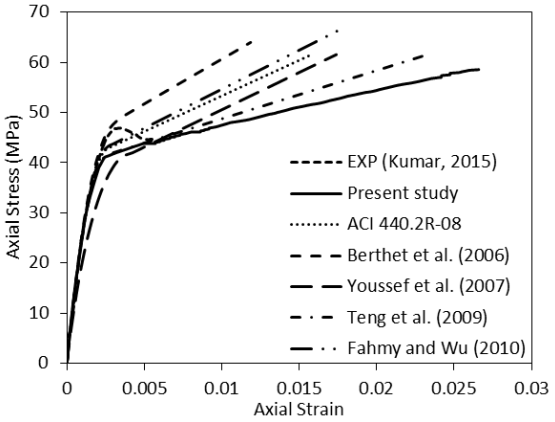


(f) C2-CYN-GFRP-L2

Figure 4.7 Comparison of stress-strain plot with design oriented model for C2

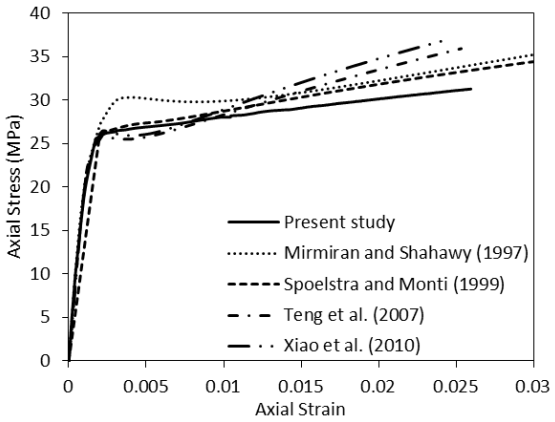


(a) C1-CYN-BFRP-L1

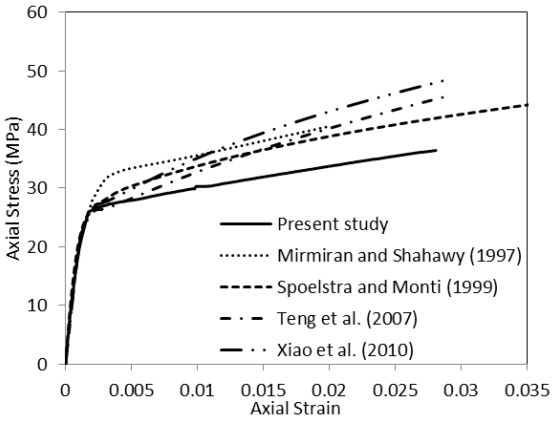


(b) C1-CYN-BFRP-L2

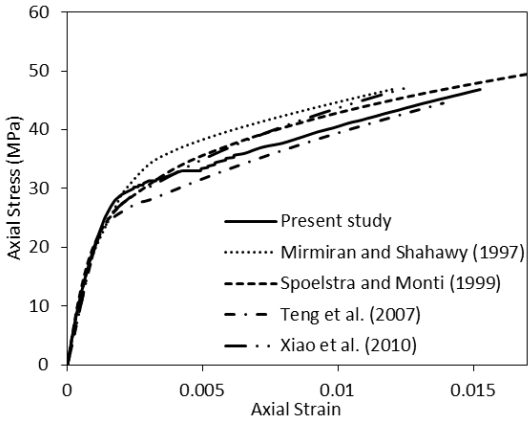


(c) C1-CYN-CFRP-L1

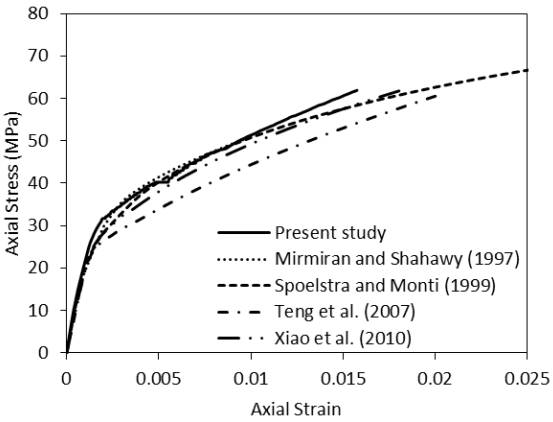


(d) C1-CYN-CFRP-L2

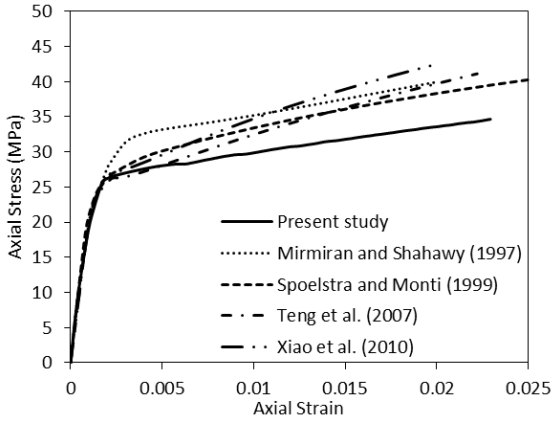


(e) C1-CYN-GFRP-L1

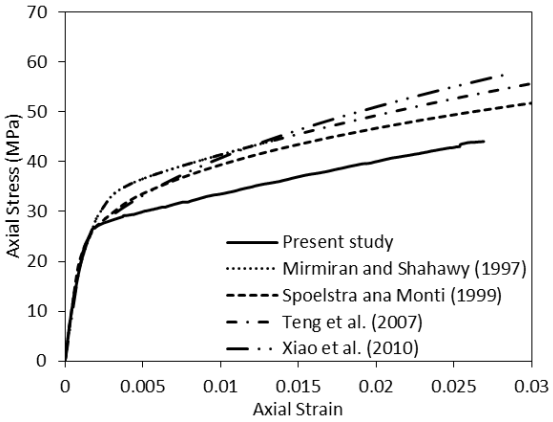


(f) C1-CYN-GFRP-L2

Figure 4.8 Comparison of stress-strain plot with analysis oriented model for C1

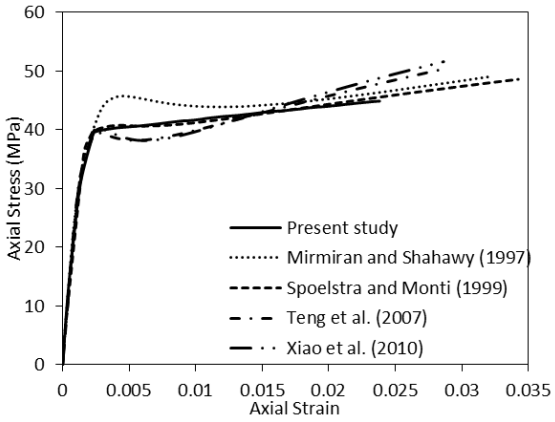


(a) C2-CYN-BFRP-L1

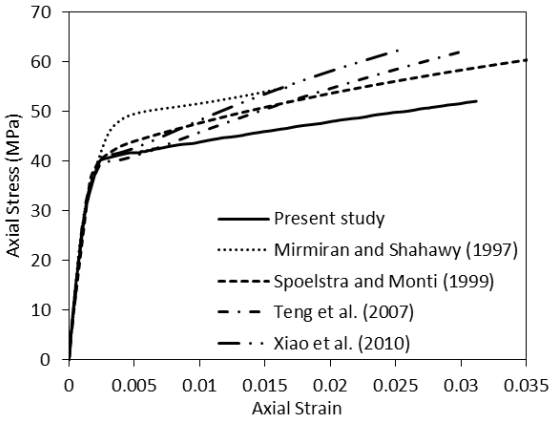


(b) C2-CYN-BFRP-L2

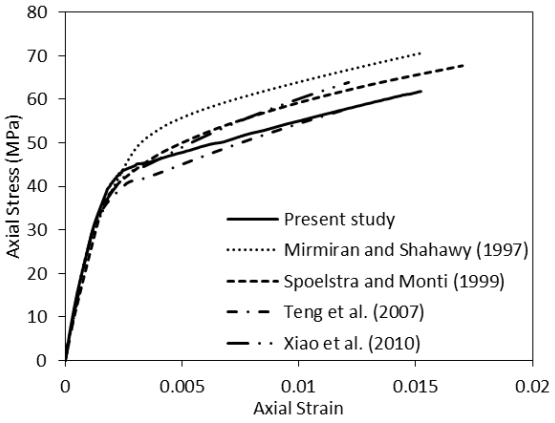


(c) C2-CYN-CFRP-L1

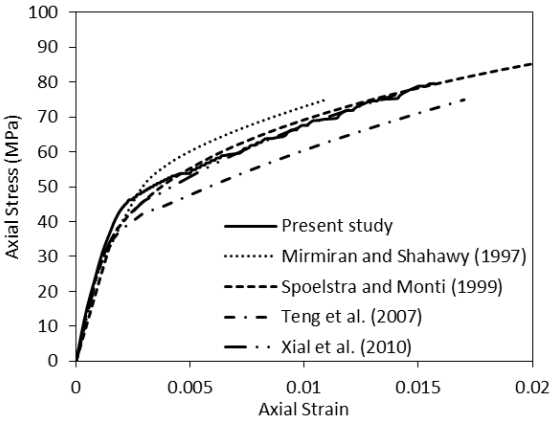


(d) C2-CYN-CFRP-L2

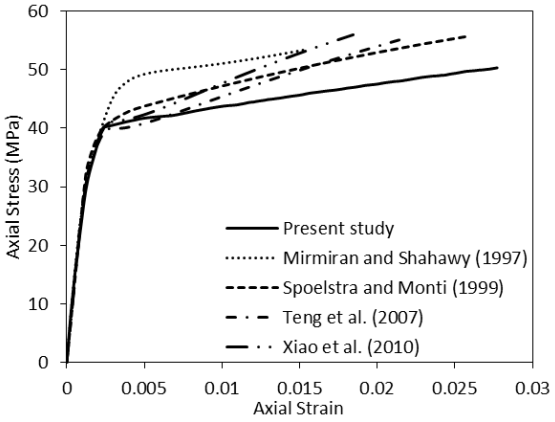


(e) C2-CYN-GFRP-L1

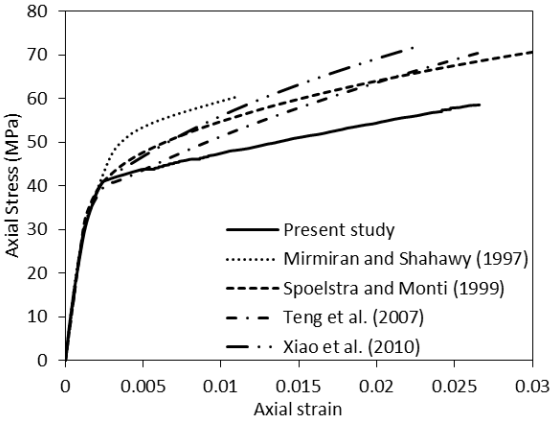


(f) C2-CYN-GFRP-L2

Figure 4.9 Comparison of stress-strain plot with analysis oriented model for C2

Figure 4.6 and Figure 4.7 shows the comparison of stress strain plot for all FRP confined concrete obtained from finite element analysis with experimental plot[2] and design oriented model[36,38,40,43,48] having concrete strength C1=25.52 MPa and C2=39.11 MPa respectively. A fair agreement is noted when compared with the experimental plots. There is deviation or more plasticity in present model after the yielding which corresponds to assumed elastic-perfectly plastic behaviour of concrete using Von Mises plasticity. Further, a good agreement is noted with the Teng et al., 2009[43] design oriented model for all types of FRP. The model predicted by Youssef et al., 2007[36], Fahmy and Wu, 2010[38], ACI 440.2R-08[48] show a good agreement for CFRP and GFRP confined concrete but show marginal differences with BFRP confined concrete. As most of the predicted model was derived using CFRP and GFRP confined concrete experimental results. The model given by Berthet et al., 2006[40] shows a good agreement with the experimental plots.

Figure 4.8 and Figure 4.9 shows the comparison of present finite element model with analysis oriented models [16,50,51,54,55] for all FRP types. A good agreement is noted for single and double layered CFRP confined concrete for both concrete strength C1 and C2. For the BFRP and CFRP confined concrete, a minor refinement is needed in consideration with the present finite element model for the stress strain curve prediction using analysis oriented models.

Comparison with both design oriented and analysis oriented models as well experimental results shows that the present finite element model can be used to predict the behaviour of the single and double layer FRP confined concrete with circular section. However, the present model cannot be used for predicting strength degradation after the peak stress.

## 4.3 SIMULATION OF INDIRECT SPLIT TENSION

A concrete cylinder of diameter 100 mm and height 150 mm is modeled using SOLID65 element for the indirect split tension test condition to be simulated in the ANSYS 14.0. Two plates with SOLID185 element modeled in the opposite faces of the cylinder along the length to be acts as loading and supporting condition for the cylinder. Contact is then made between the plate and cylinder surfaces using CONTA 174 for sources element i.e. plate and TARGET 170 element for target element i.e. the flexible

member cylinder. A rigid- flexible contact between the surfaces of the cylinder and plate generated. The material property used to model concrete with concrete strength C1=25.52 MPa and C2=39.11 MPa is described in chapter 3. The support and loading plate is model with rigid material property to simulate the real experimental condition. One of plate fixed at bottom and from the other plate loading is applied gradually on the cylinder length for indirect split tension. Figure 4.10 shows the finite element model for the indirect split tension.

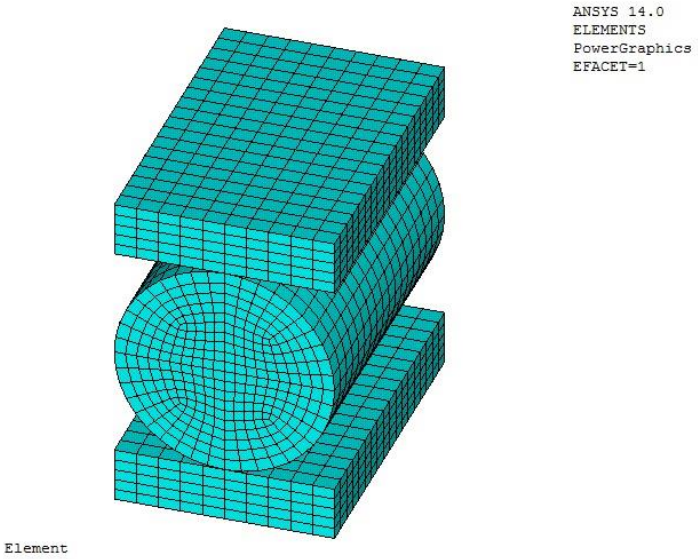


Figure 4.10 FE model for the indirect split tension

The load applied incrementally by dividing the loads in different load steps till the cylinder fail in tension. The failure stress at the time of failure is noted and compared with the experimental value from the literature. The average tensile strength from experiment was 3.46 MPa and 4.11 MPa for concrete strength C2=39.11 MPa and C1=25.52 MPa respectively. And tensile strength obtained from FE analysis is 4.05 MPa and 3.20 MPa for concrete strength C2=39.11 MPa and C1=25.52 MPa respectively which shows FEA analysis is reliable and can approximate the experimental condition. Further it should be noted that we cannot directly apply the loads on FRP material thus the split tensile strength of confined concrete with FRP is not carried out analytically.

## 4.4 SIMULATION OF PRISM FOR FLEXURAL BEHAVIOUR

The designation used for the entire specimens in the present study is tabulated in Table 4.6 for both concrete type C1 and C2. The material property used for FRP and concrete is defined in chapter.

Table 4.6 Prism affix with FRP for flexural behavior designation

| Designation | Details |
|---|---|
| FL-C1 | Control prism with C1=25.52 MPa |
| FL-C2 | Control prism with C2=39.11 MPa |
| C1-FL-BFRP-L1 | Soffit affix with 1 layer BFRP and concrete strength C1 |
| C1-FL-CFRP-L1 | Soffit affix with 1 layer CFRP and concrete strength C1 |
| C1-FL-GFRP-L1 | Soffit affix with 1 layer GFRP and concrete strength C1 |
| C1-FL-BFRP-L2 | Soffit affix with 2 layer BFRP and concrete strength C1 |
| C1-FL-CFRP-L2 | Soffit affix with 2 layer CFRP and concrete strength C1 |
| C1-FL-GFRP-L2 | Soffit affix with 2 layer GFRP and concrete strength C1 |
| C2-FL-BFRP-L1 | Soffit affix with 1 layer BFRP and concrete strength C2 |
| C2-FL-CFRP-L1 | Soffit affix with 1 layer CFRP and concrete strength C2 |
| C2-FL-GFRP-L1 | Soffit affix with 1 layer GFRP and concrete strength C2 |
| C2-FL-BFRP-L2 | Soffit affix with 2 layer BFRP and concrete strength C2 |
| C2-FL-CFRP-L2 | Soffit affix with 2 layer CFRP and concrete strength C2 |
| C2-FL-GFRP-L2 | Soffit affix with 2 layer GFRP and concrete strength C2 |

### 4.4.1 Modeling

The prism, load and support cylinder modeled as volumes. A quarter of beam is modeled by considering the symmetry of section, loading and constraints. The model is 250 mm long, with a cross section of 50 mm X 100 mm. Figure 4.11 shows the complete prism with cross section and loading arrangement for two point load flexural tests of the concrete beam. To reduce the stress concentration at the loading and support; cylinder is modeled to provide the support and to induce the loading to the prism. The prism is modeled with SOLID65 element with no reinforcement and the loading arrangement modeled with SOLID185 element. And the FRP modeled as the layered SHELL181 element and smeared at the bottom face of the prism to have a perfect adhesive bond between prism and FRP composite. The model is meshed using map meshing with an element size of 10 mm by assigning appropriate material property

to each volume or area. After meshing the surface contact is generated between the load cylinder and prism also between the support and prism using CONTA174 and TARGET170 element. The loading arrangements made rigid to form a rigid-flexible contact between the two surfaces. Figure 4.12 shows the finite element model of the prism with loading arrangements.

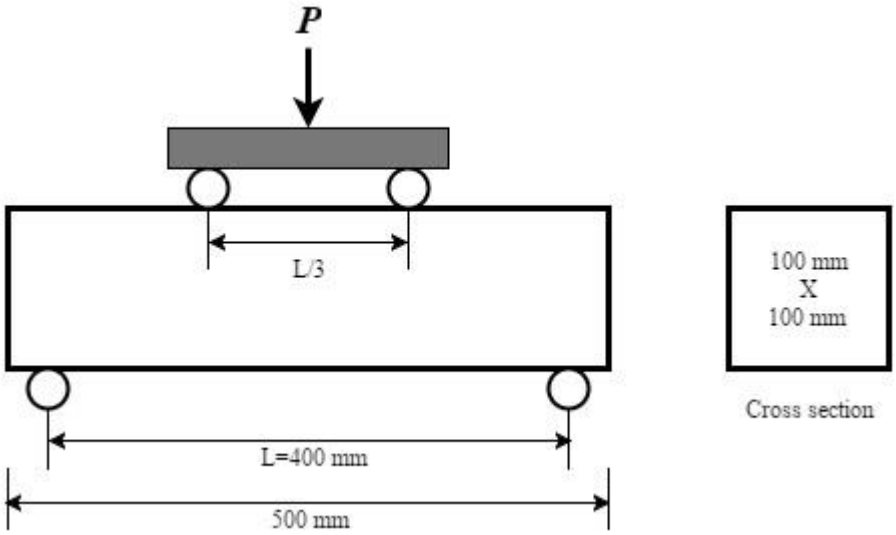


Figure 4.11 Test set up for flexural behaviour

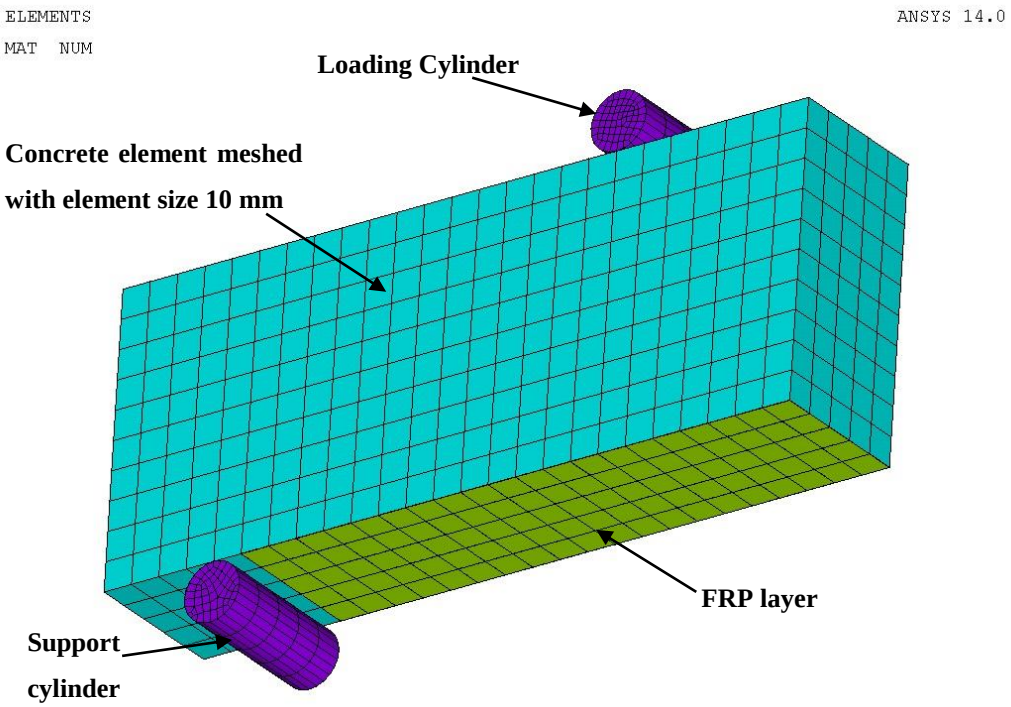


Figure 4.12 Finite element model of prism with loading arrangement

### 4.4.2 Boundary condition and loading

For the prism to be acted as same way as the experimental prism, boundary conditions need to be applied at points of symmetry, where the supports and loading exist. The symmetry boundary condition is set at the two planes. At the support cylinder vertical constraint is provided in $u_y$ direction with zero displacement such that a roller is created. The load applied at the centerline of the loading cylinder. The force applied at each node is one twelfth of the actual force applied. Figure 4.13 shows the loading arrangement with symmetry boundary conditions.

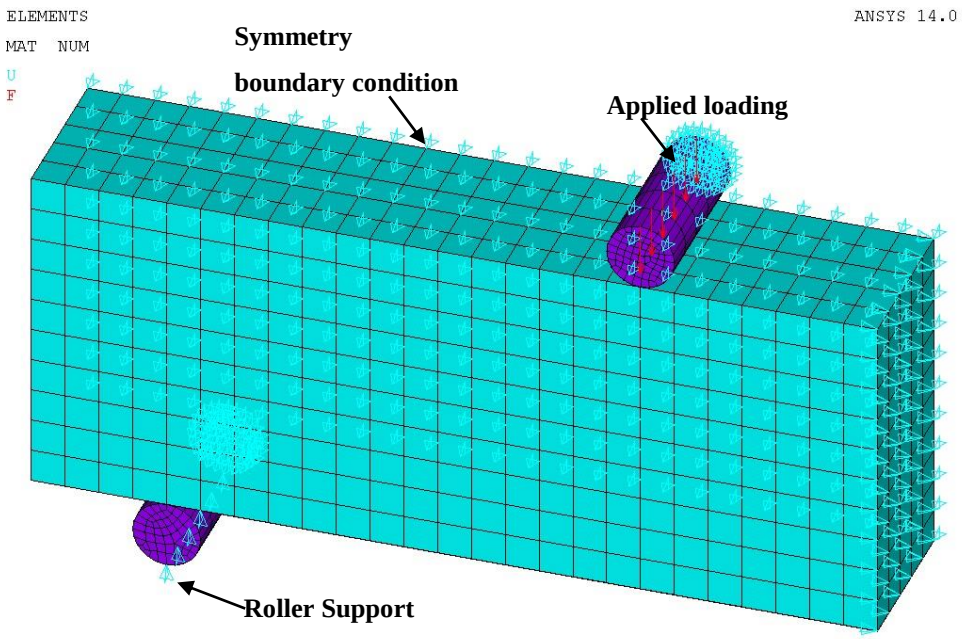


Figure 4.13 Loading arrangement with symmetry boundary condition

### 4.4.3 Simulation, Results and Discussion

For the purpose of this model, the static analysis type utilized. The sol-n-controls command edict the use of linear or nonlinear solution for the finite element model. The applied load divided into number of load steps to apply the load in incremental process. The load steps further divide into the sub steps to apply load gradually on the prism. The force convergence set to five times the default value. Automatic time stepping is activated so that ANSYS 14.0 can help in solving the problem more efficiently. The Newton-Raphson method is used to compute the nonlinear response. The loads applied

incrementally until failure of the prism. The failure of the control prism occurs when the peak load achieved showing a brittle mode of failure. Prism with FRP affixed at the soffit takes the loads once the concrete achieve its tensile strength. The failure in FRP confined prism occurs due to severe tensile crack in the concrete element and FRP reaches the tensile strength.

The displacement modeling and the stress in x-direction showing the maximum tensile strength in control beam for concrete strength of C1=25.52 MPa is shown in Figure 4.14 and Figure 4.15 respectively.

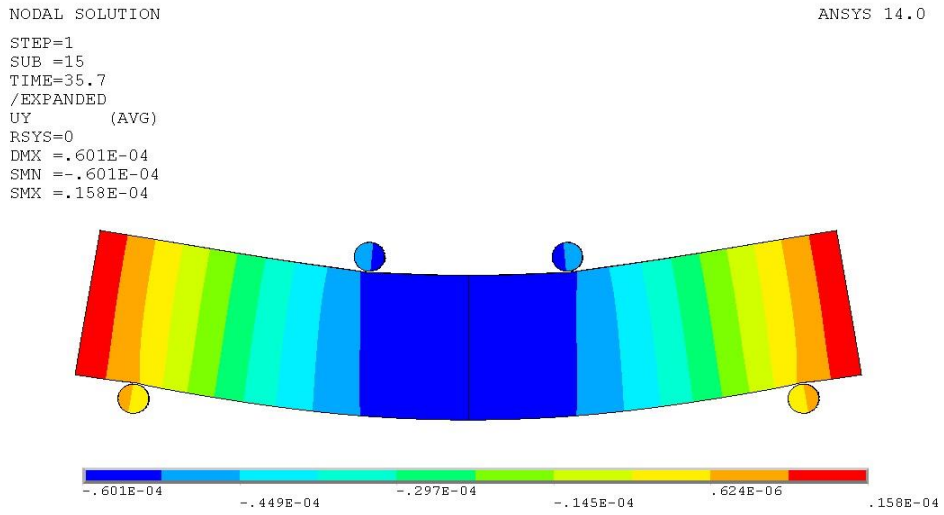


Figure 4.14 Displacement contour for control prism FL-C1 in ANSYS 14.0

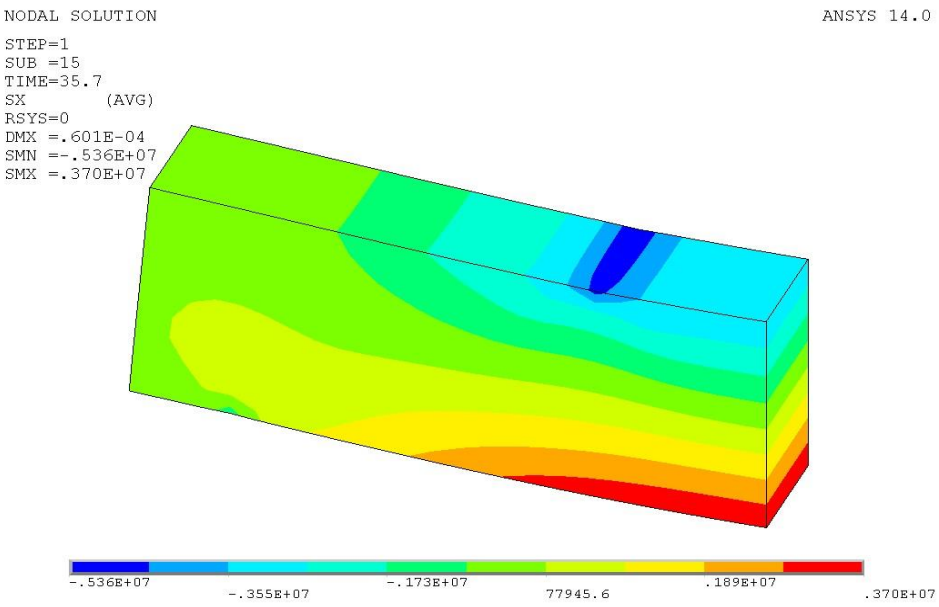


Figure 4.15 Horizontal stress counter in the control prism FL-C1

Table 4.7 Comparison of flexural strength with experimental data for concrete strength C1

| Type | Experimental Results (MPa) | FEA results (MPa) | Differences (%) | Compared with FL-C1 |
|---|---|---|---|---|
| FL-C1 | 4.93 | 3.70 | 24.95 | 1.00 |
| C1-FL-BFRP-L1 | 6.40 | 4.95 | 22.70 | 1.34 |
| C1-FL-CFRP-L1 | 12.46 | 11.12 | 10.75 | 3.01 |
| C1-FL-GFRP-L1 | 7.24 | 6.45 | 10.91 | 1.74 |
| C1-FL-BFRP-L2 | 8.01 | 7.16 | 10.61 | 1.94 |
| C1-FL-CFRP-L2 | 16.47 | 15.18 | 7.85 | 4.10 |
| C1-FL-GFRP-L2 | 7.49 | 8.65 | -15.49 | 2.34 |

Table 4.8 Comparison of flexural strength with experimental data for concrete strength C2

| Type | Experimental Results (MPa) | FEA results (MPa) | Differences (%) | Compared with FL-C2 |
|---|---|---|---|---|
| FL-C2 | 4.50 | 4.58 | -1.78 | 1.00 |
| C2-FL-BFRP-L1 | 5.63 | 5.57 | 0.99 | 1.22 |
| C2-FL-CFRP-L1 | 11.46 | 12.09 | -5.49 | 2.64 |
| C2-FL-GFRP-L1 | 6.94 | 7.14 | -2.92 | 1.56 |
| C2-FL-BFRP-L2 | 7.69 | 8.41 | -9.33 | 1.84 |
| C2-FL-CFRP-L2 | 12.03 | 16.66 | -38.49 | 3.64 |
| C2-FL-GFRP-L2 | 8.19 | 9.58 | -16.93 | 2.09 |

The flexural strength calculated using the formula $f_{cr} = M/Z$ i.e.

$$f_{cr} = \frac{Pl}{bd^2} \tag{4.1}$$

Where,

$P$ = peak load in Newton.

$l$= length of the prism.

$b$ and $d$ = cross section of the prism.

Table 4.7 and Table 4.8 show the comparison of the finite element results with experimental results[2]; also the increase in the flexural strength due to the FRP affix at

the soffit of the concrete beam with concrete strength C1=25.52 MPa and C2=39.11 MPa respectively.

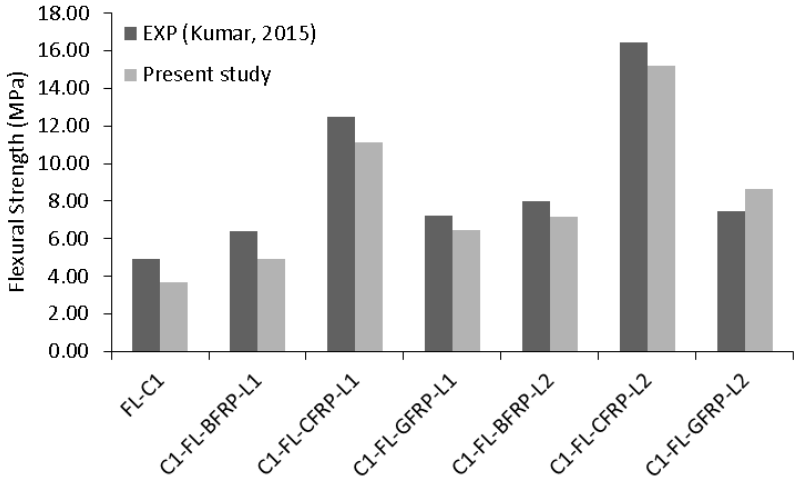


Figure 4.16 Comparison of flexural strength for concrete strength C1 with experimental data

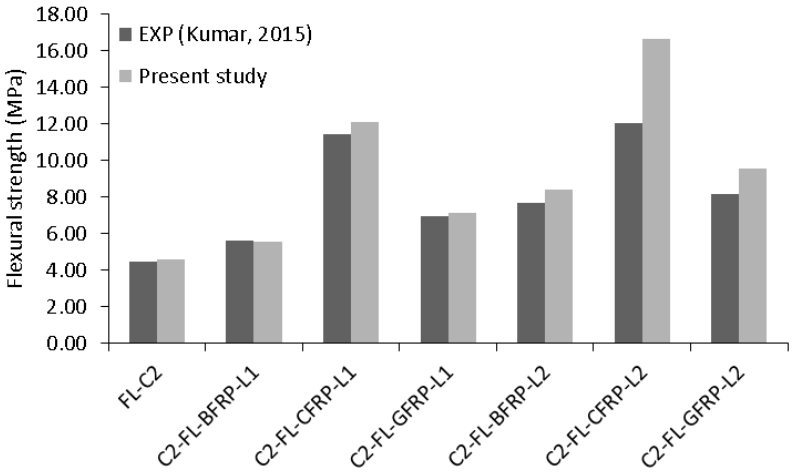


Figure 4.17 Comparison of flexural strength for concrete strength C2 with experimental data

From the above Figure 4.16 and Figure 4.17, it can be observed that the FEA model gives reasonable results when compared with experimental data. There is large difference in the flexural strength for the concrete strength C1 as the present finite element model use a unique strength and material data for concrete as obtained from the cylinder strength of concrete experimentally[2] for modeling the flexural beam affix with FRP for concrete strength C1. In experiment, the flexural strength for C1 group with lower concrete strength found to be higher which cannot be true in finite element modeling. As the finite element model behavior depend upon the entered material data and the availability of the concrete strength for a particular beam can change or refine

the present result obtained from finite element analysis. The percentage of error in some cases found to be less than 10%. Considering the above points, the present finite element model found to be reliable and accurate for simulating the flexural strength of the concrete. Significant increase in the flexural strength for the carbon fibre affix prism can be observed for both concrete types which in parallel to the experimental finding.

## 4.5 SIMULATION OF CONCRTE FRACTURE BEHAVIOR

The designation used for the entire specimens in the present study for fracture behavior of the concrete beam with a vertical groove of 20 mm length at the centre is tabulated in Table 4.9 for both concrete type C1 and C2.

Table 4.9 Prism affix with FRP for fracture behavior designation

| Designation | Details |
|---|---|
| FR-C1 | Control specimen with C1=25.52 MPa |
| FR-C2 | Control specimen with C2=39.11 MPa |
| C1-FR-BFRP-L1 | Soffit affix with 1 layer BFRP and concrete strength C1 |
| C1-FR-CFRP-L1 | Soffit affix with 1 layer CFRP and concrete strength C1 |
| C1-FR-GFRP-L1 | Soffit affix with 1 layer GFRP and concrete strength C1 |
| C1-FR-BFRP-L2 | Soffit affix with 2 layer BFRP and concrete strength C1 |
| C1-FR-CFRP-L2 | Soffit affix with 2 layer CFRP and concrete strength C1 |
| C1-FR-GFRP-L2 | Soffit affix with 2 layer GFRP and concrete strength C1 |
| C2-FR-BFRP-L1 | Soffit affix with 1 layer BFRP and concrete strength C2 |
| C2-FR-CFRP-L1 | Soffit affix with 1 layer CFRP and concrete strength C2 |
| C2-FR-GFRP-L1 | Soffit affix with 1 layer GFRP and concrete strength C2 |
| C2-FR-BFRP-L2 | Soffit affix with 2 layer BFRP and concrete strength C2 |
| C2-FR-CFRP-L2 | Soffit affix with 2 layer CFRP and concrete strength C2 |
| C2-FR-GFRP-L2 | Soffit affix with 2 layer GFRP and concrete strength C2 |

### 4.5.1 Modeling

A block of length 500 mm and cross section 100 mm X 100 mm modeled with a vertical groove of 20 mm at the center of the rectangle to be act as the fracture concrete beam. The effective span of the beam is 400 mm. The loading cylinder modeled at the centre of the beam and two support cylinder modeled for three point bending analysis of the fracture beam. The line diagram of the beam along with cross section is shown in

Figure 4.18. Then, the complete model meshed with an effective element size of 10 mm. The beam meshed using 3-D reinforced concrete SOLID65 element with no reinforcement and the cylinder for boundary condition and loading meshed using SOLID185 element. FRP meshed using the layered SHELL181 element with only membrane option and smeared at the bottom face of the prism to have a perfect adhesive bond between beam and FRP composite. Then the surface to surface contact generated between the load cylinder and concrete beam also between the support cylinder and bottom face of the concrete beam using CONTA174 and TARGET170 element. Figure 4.19 shows the finite element model of the concrete beam with loading arrangements for three point bending.

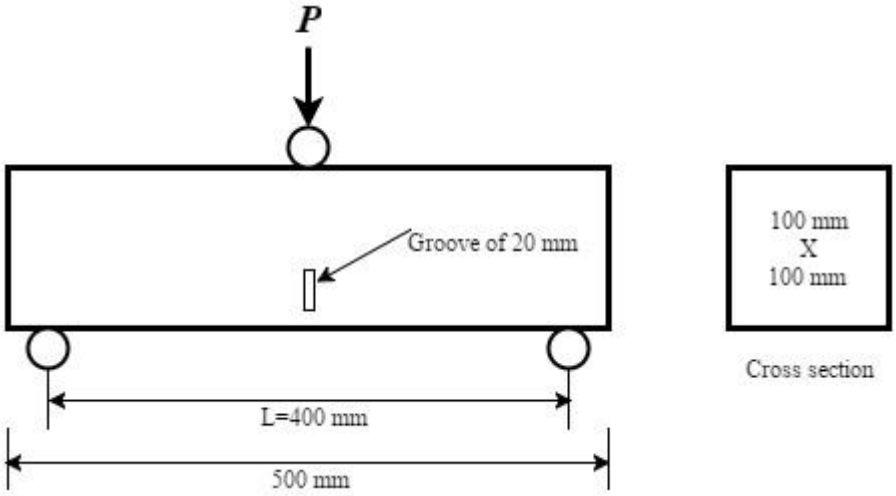


Figure 4.18 Test set up for the fracture behaviour

### 4.5.2 Boundary condition and loading

The concrete beam to be acted as same way as the experimental beam, the boundary condition need to be consistent with existing physical conditions. The complete 3-D beam modeled with simply supported boundary condition. At left support cylinder, constraint is provided in all three directions with zero displacement. At right support cylinder, vertical constraint is provided in $u_y$ direction with no displacement. The gradual load applied at the centerline of the loading cylinder at the middle of the beam. The total load applied is divided into eleven parts for each node. Figure 4.20 shows the loading arrangement with symmetry boundary conditions.

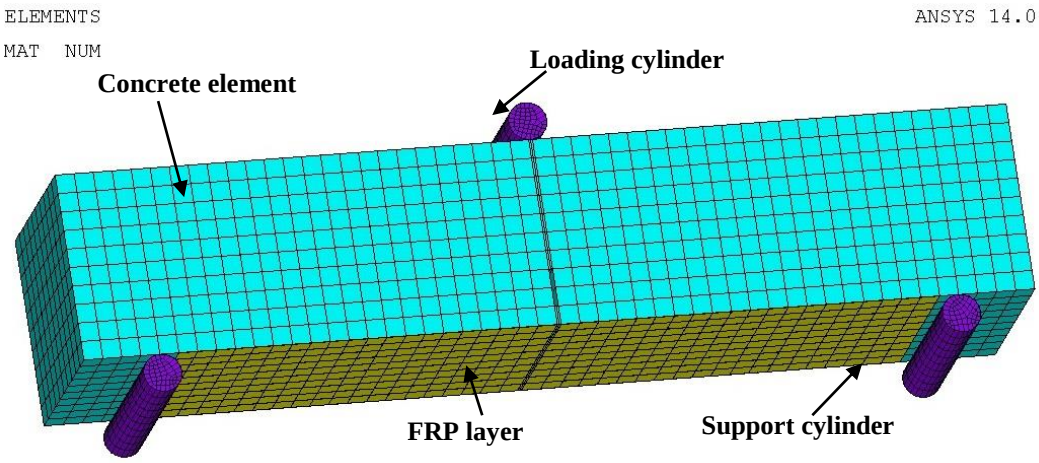


Figure 4.19 Finite element model for fracture behavior in ANSYS 14.0

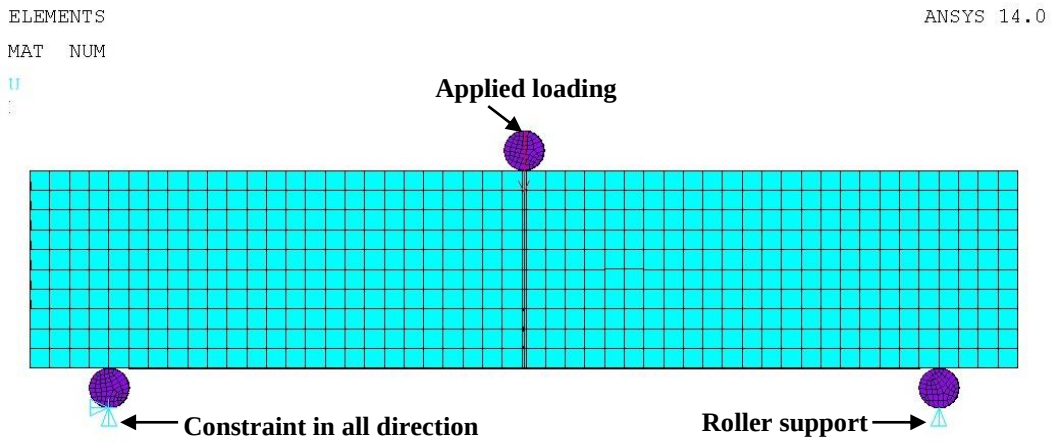


Figure 4.20 Boundary condition and loading for fracture behaviour

### 4.5.3 Results and Discussion

Simulation process is same as explained for flexural behavior of the concrete. The failure of the control specimen occurs due to failure of the concrete at the center of the beam with stress concentrated near the groove section. The failure in FRP confined prism occur due to more tensile crack in the concrete element near the groove part with stress concentration, large deflection or opening of the groove and FRP reaches it capacity. The failure in the concrete and FRP is check with failure criteria as mention in the ANSYS 14.0.

The displacement modeling and the stress in x-direction in control beam for concrete strength of C1=25.52 MPa is shown in Figure 4.21 and Figure 4.22 respectively. From

the figure, it is visible that the vertical groove is opened up with stress concentrated inside the opening.

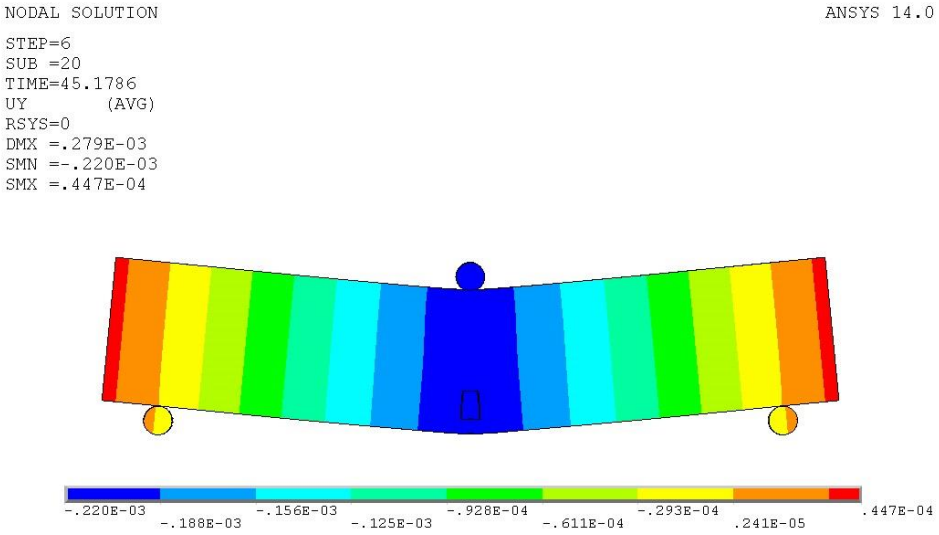


Figure 4.21 Deflection modeling for control specimen FR-C1

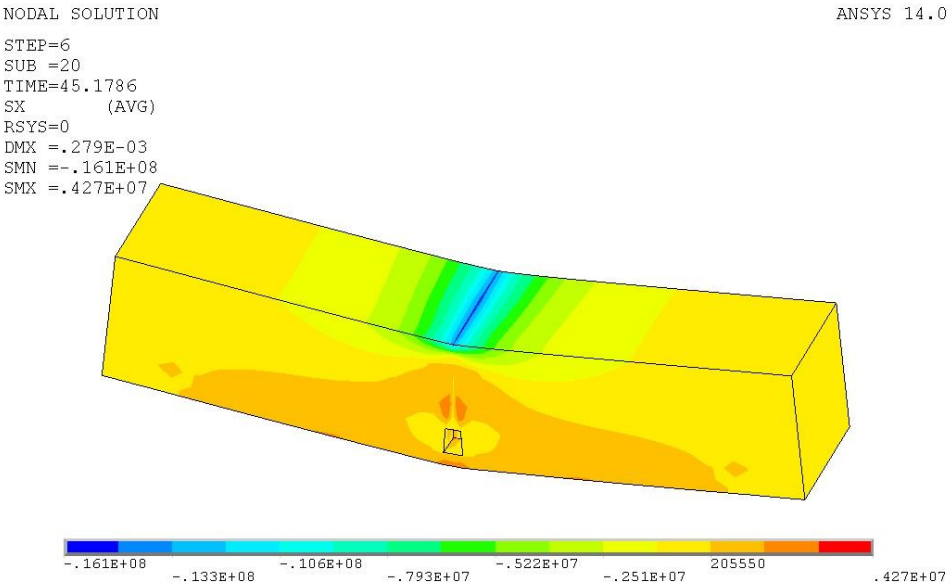


Figure 4.22 Horizontal stress counter for control FR-C1

Table 4.10 and Table 4.11 depict the comparison of the fracture strength obtained from present finite element study with experimental results[2]. The increase in load due to beam affix with different types of FRP with single and double layer at the soffit is also shown.

Table 4.10 Comparison of fracture strength with experimental data for concrete strength C1

| Type | Experimental Results (MPa) | FEA results (MPa) | Differences (%) | Compared with FR-C1 |
|---|---|---|---|---|
| FR-C1 | 2.31 | 1.99 | 13.95 | 1.00 |
| C1-FR-BFRP-L1 | 2.95 | 2.66 | 9.68 | 1.34 |
| C1-FR-CFRP-L1 | 9.93 | 8.21 | 17.32 | 4.13 |
| C1-FR-GFRP-L1 | 3.11 | 3.08 | 0.97 | 1.55 |
| C1-FR-BFRP-L2 | 3.40 | 3.30 | 2.89 | 1.66 |
| C1-FR-CFRP-L2 | 11.47 | 9.69 | 15.49 | 4.88 |
| C1-FR-GFRP-L2 | 4.25 | 3.96 | 6.79 | 1.99 |

Table 4.11 Comparison of fracture strength with experimental data for concrete strength C2

| Type | Experimental Results (MPa) | FEA results (MPa) | Differences (%) | Compared with FR-C2 |
|---|---|---|---|---|
| FR-C2 | 2.08 | 2.58 | -24.01 | 1.00 |
| C2-FR-BFRP-L1 | 2.74 | 2.98 | -8.93 | 1.16 |
| C2-FR-CFRP-L1 | 9.39 | 9.16 | 2.44 | 3.55 |
| C2-FR-GFRP-L1 | 2.60 | 3.60 | -38.49 | 1.40 |
| C2-FR-BFRP-L2 | 3.95 | 3.78 | 4.20 | 1.47 |
| C2-FR-CFRP-L2 | 9.31 | 11.22 | -20.52 | 4.35 |
| C2-FR-GFRP-L2 | 4.37 | 4.71 | -7.77 | 1.83 |

The Figure 4.23 and Figure 4.24shows the comparison of the experimental results with analytical results for the fracture behavior of concrete with concrete strength C1 and C2 respectively. The analytical result produces reasonable agreement with the experimental results. The deviation of result in some case is due to same concrete material data is used to model all type of concrete beam with 20 mm vertical groove for particular set of concrete strength. The result obtained from experiment is not certain as in case of finite element modeling a perfect bond assumption is made between the concrete and FRP which is not true during the experiment. Further, the material data of concrete for particular beam can change the behavior in the finite element modeling which can produce more reliable results.

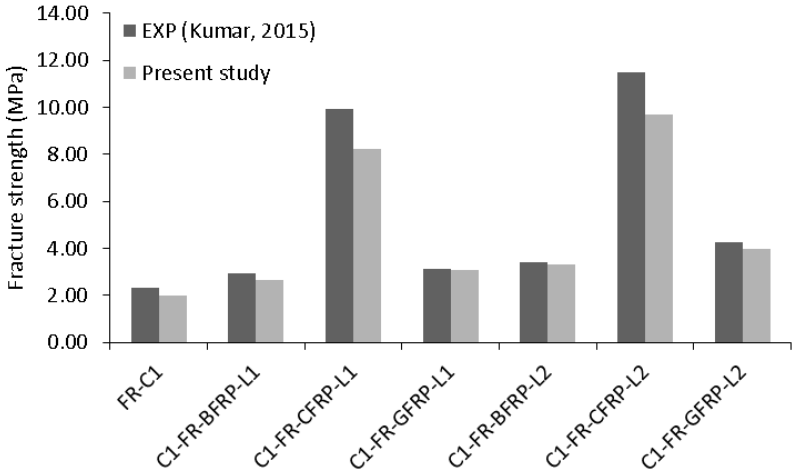


Figure 4.23 Comparison of fracture strength for concrete strength C1 with experimental data

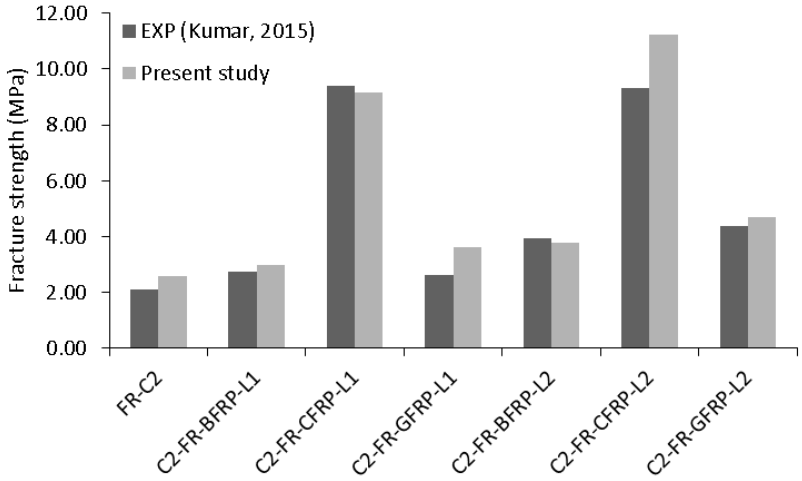


Figure 4.24 Comparison of fracture strength for concrete strength C2 with experimental data

## 4.6 REMARKS

Concrete element confine with different types of FRP modelled analytically to understand its behaviour in compression, flexural and fracture using two different types of concrete strength C1 and C2. The reliability of the finite element model was check with the experimental data and predicted models.

# CHAPTER 5

# FE MODELING OF STRENGTHENED RC BEAMS

## 5.1 GENERAL

SOLID65, LINK8 and SOLID46 were used to model concrete, reinforcement steel and FRP composite respectively by most of the researchers[69,81,85,95–98]. SHELL99 element was used to model FRP by the researcher Hawileh et al., 2013[81]. Mohammad et al., 2013[97] used SHELL41 element to model FRP and same SOLID65 and LINK8 element was used to model the concrete and rebar respectively. Sasmal et al., 2013[98] used tension only SHELL41 element to model single layered FRP considering the isotropic property of the FRP. Ronagh and Baji, 2014[83] considered two option for the modeling FRP, tension only membrane SHELL41 and membrane only SHELL181 both reinforced with REINF265 element. Researcher uses SOLID45 element for support and load steel plates.

In present study SOLID65 and LINK180 element is used to model the concrete and reinforcing steel. SHELL181 element with membrane only option is used to model the FRP composite. It is reasonable to use isotropic material data to model FRP sheet as FRP material are only subjected to tensile forces. The loading and support cylinder modeled with SOLID185 element. The contact between the beam surface and loading cylinder created with CONTA174 and TARGET170 element. The details of the material data used in the modeling the concrete, reinforcing bar and FRP composite are described in chapter 3.

## 5.2 GEOMETRY OF RC BEAMS

The 20 beams are divided into two different groups depending upon the concrete strength. One group have a concrete strength of C1=25.52 MPa and other having concrete strength of C2=39.11 MPa. Three types of FRP (BFRP, CFRP and GFRP) used for comparative study in strength enhancement of RC beam in shear and flexure. The Table 5.1 and Table 5.2 shows all beam assess in the present study along with FRP strengthening arrangement.

Table 5.1 Designation of FRP strengthened RC beams with concrete strength C1

| Beam ID | Description |
|---|---|
| C1-B0 | Control beam with concrete strength C1=25.52 MPa |
| C1-BFRP-B11 | Strengthened using BFRP sheet in flexure and shear |
| C1-CFRP-B12 | Strengthened using CFRP sheet in flexure and shear |
| C1-GFRP-B13 | Strengthened using GFRP sheet in flexure and shear |
| C1-BFRP-B21 | Strengthened using BFRP sheet only in shear |
| C1-CFRP-B22 | Strengthened using CFRP sheet only in shear |
| C1-GFRP-B23 | Strengthened using GFRP sheet only in shear |
| C1-BFRP-B31 | Strengthened using stripped BFRP sheet only in shear with 70 mm at 115 mm c/c |
| C1-CFRP-B32 | Strengthened using stripped CFRP sheet only in shear with 70 mm at 115 mm c/c |
| C1-GFRP-B33 | Strengthened using stripped GFRP sheet only in shear with 70 mm at 115 mm c/c |

Table 5.2 Designation of FRP strengthened RC beams with concrete strength C2

| Beam ID | Description |
|---|---|
| C2-B0 | Control beam with concrete strength C2=39.11 MPa |
| C2-BFRP-B11 | Strengthened using fully wrapped BFRP sheet in three part |
| C2-CFRP-B12 | Strengthened using fully wrapped CFRP sheet in three part |
| C2-GFRP-B13 | Strengthened using fully wrapped GFRP sheet in three part |
| C2-BFRP-B21 | Strengthened using BFRP sheet in flexure and shear |
| C2-CFRP-B22 | Strengthened using CFRP sheet in flexure and shear |
| C2-GFRP-B23 | Strengthened using GFRP sheet in flexure and shear |
| C2-BFRP-B31 | Strengthened using BFRP sheet in flexure and shear zone with 70 mm strip at 115 mm c/c |
| C2-CFRP-B32 | Strengthened using CFRP sheet in flexure and shear zone with 70 mm strip at 115 mm c/c |
| C2-GFRP-B33 | Strengthened using GFRP sheet in flexure and shear zone with 70 mm strip at 115 mm c/c |

The RC beam strengthened with CFRP and GFRP have one layer of CFRP and GFRP sheet. Due to less thickness as comparison to CFRP and GFRP, two layer of BFRP used in the model [2,3].

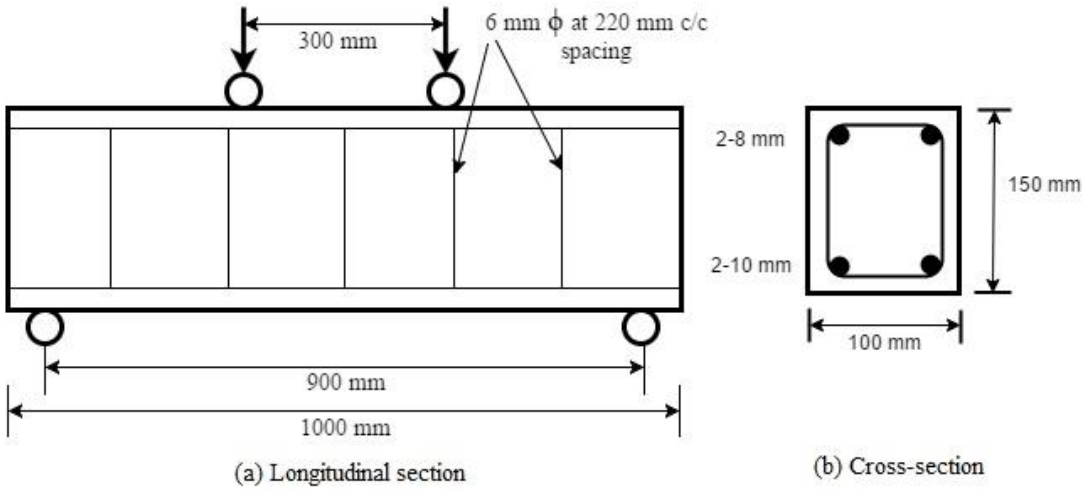


Figure 5.1 Geometry of RC beam considered for the study (Kumar, 2015)

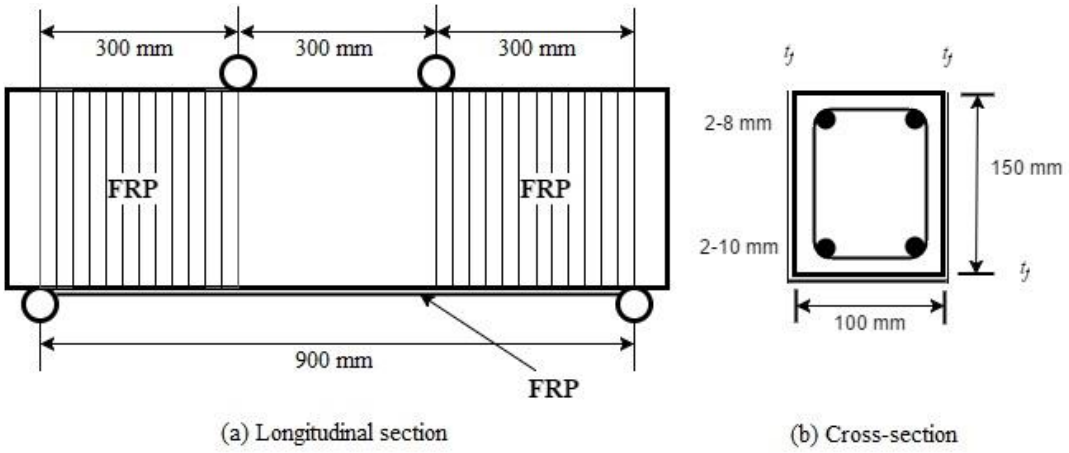


Figure 5.2 FRP strengthening detail for C1-BFRP-B11, C1-CFRP-B12, C1-GFRP-B13, C2-BFRP-B21, C2-CFRP-B22 and C2-GFRP-B23

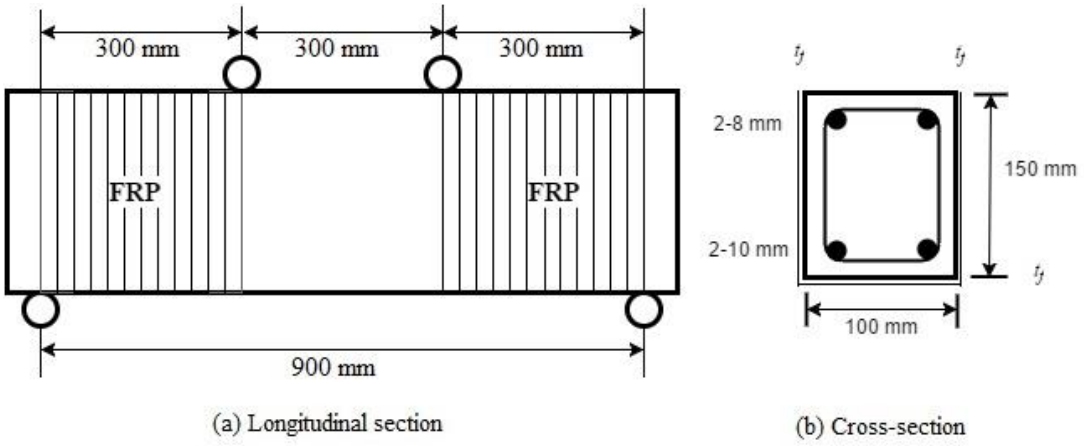


Figure 5.3 FRP strengthening detail for C1-BFRP-B21, C1-CFRP-B22 and C1-GFRP-B23

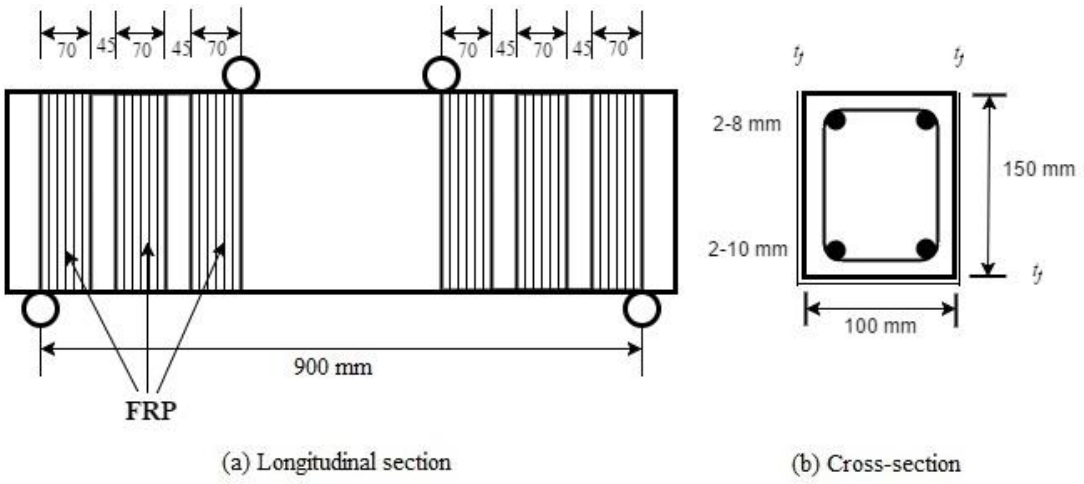


Figure 5.4 FRP strengthening detail for C1-BFRP-B31, C1-CFRP-B32 and C1-GFRP-B33

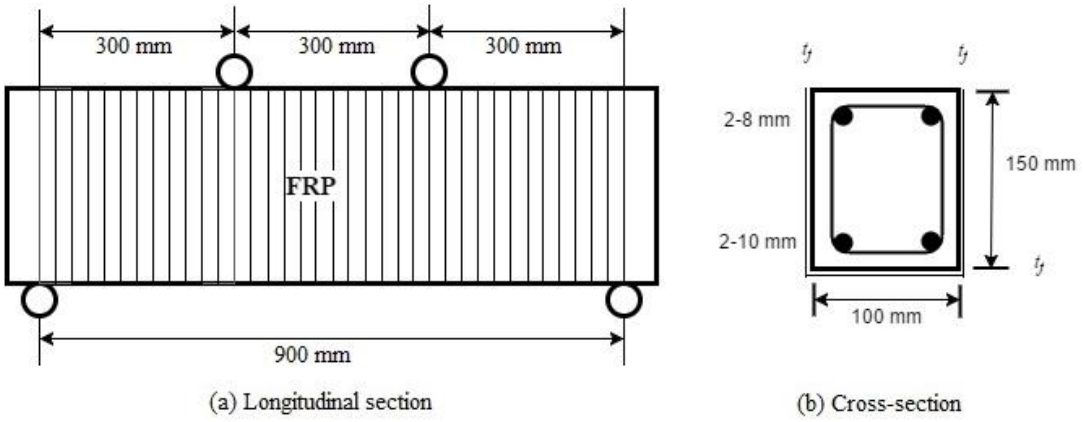


Figure 5.5 FRP strengthening detail for C2-BFRP-B11, C2-CFRP-B12 and C2-GFRP-B13

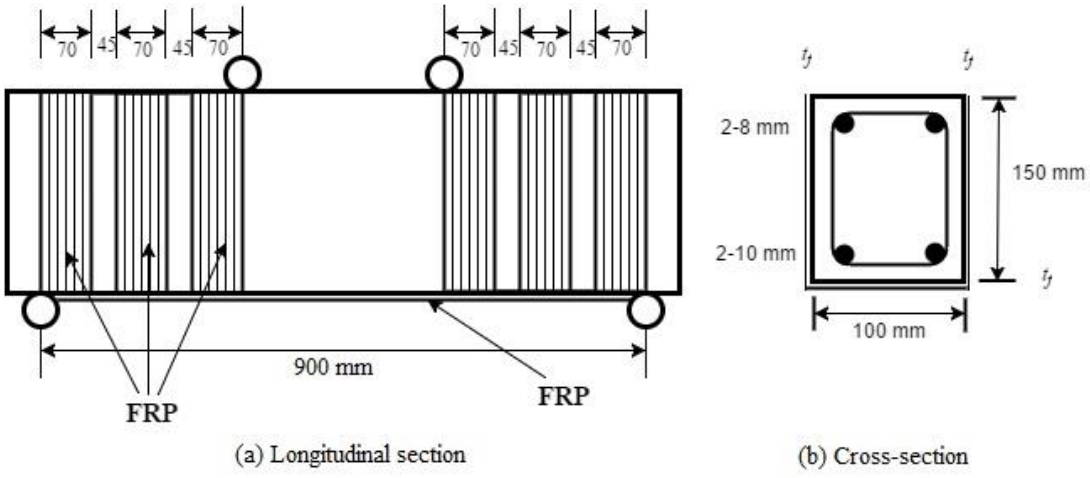


Figure 5.6 FRP strengthening detail for C2-BFRP-B31, C2-CFRP-B32 and C2-GFRP-B33

The geometry of the RC beam under investigation is the experimental beam as reported earlier (Kumar, 2015) carry dimension of 1000 mm X 150 mm X 100 mm with effective span of 900 mm. Figure 5.1 shows the RC beam with reinforcement detail considered for the present study. The FRP strengthening details with different pattern are shown in Figure 5.2, Figure 5.3, Figure 5.4, Figure 5.5 and Figure 5.6 for both groups of RC beams.

## 5.3 MODELING OF RC BEAM

A quarter of beam modeled due to symmetry of section, loads and supports. The volume modeled with dimension of 500 mm length and cross section of 50 mm X 150 mm. Two cylinder volumes also modeled to act as support and loading to prevent the stress concentration at the loading point. It facilitates the behavior as in case of the full experimental step up. The concrete volume modeled with SOLID65 element. And the reinforcement of beam modeled with LINK180 element. Three real constant defined for rebar dimension of the bottom reinforcement, top reinforcement and stirrups. The loading system modeled with SOLID185 they have given rigid property so that they will not deform during the load application. Figure 5.7 shows the volumes generated in ANSYS 14.0 and Figure 5.8 shows the reinforcement configuration used in the model.

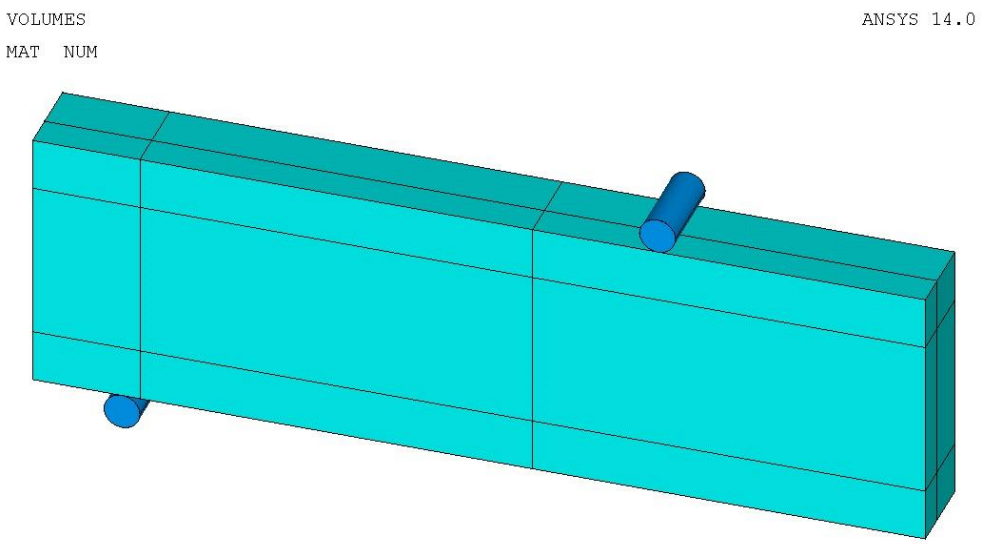


Figure 5.7 Volume generated in ANSYS 14.0

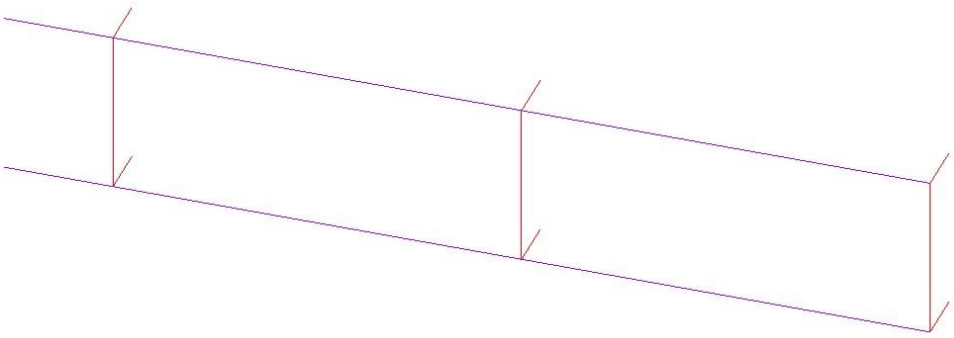

Figure 5.8 Reinforcement configuration model in ANSYS 14.0

The initial stage of finite element analysis is element discretization in which the whole model meshed into number of elements. Once the load is applied, the stress, strain and displacement calculated at the integration point of these elements[99]. It is an important step in finite element modeling to select an appropriate mesh density as the convergence of result obtain when a decent number of element used for the modeling. This is well known that increase in the mesh density gives negligible error in the results[100]. Thus, a convergence study was first carried in order to determine element size in ANSYS 14.0.

For the convergence study, quarter of RC control beam modeled considering the symmetry with concrete strength C2=39.11. To evaluate the convergence of result different element size were used starting form 25 mm. Three different parameters at the mid-span of the beam but at different location (deflection at center of bottom face, compressive stress in concrete at center of top face, tensile stress in bottom steel reinforcement) were checked to see the convergence of the results. For an appropriate convergence study, the output recorded at same applied load for different element size. Figure 5.9 shows the results obtained from the convergence study for the three different parameters.

Based on the convergence study shown in Figure 5.9, it is found out that the difference in the result were negligible for element size below 10 mm. So, the element size of 10 mm or below was selected for meshing the control RC beam which served as basis for modeling the FRP strengthened RC beams as well. The FRP modeled as area and meshed with SHELL181 element which takes the thickness, orientation, number of layers and material data of the FRP as section data.

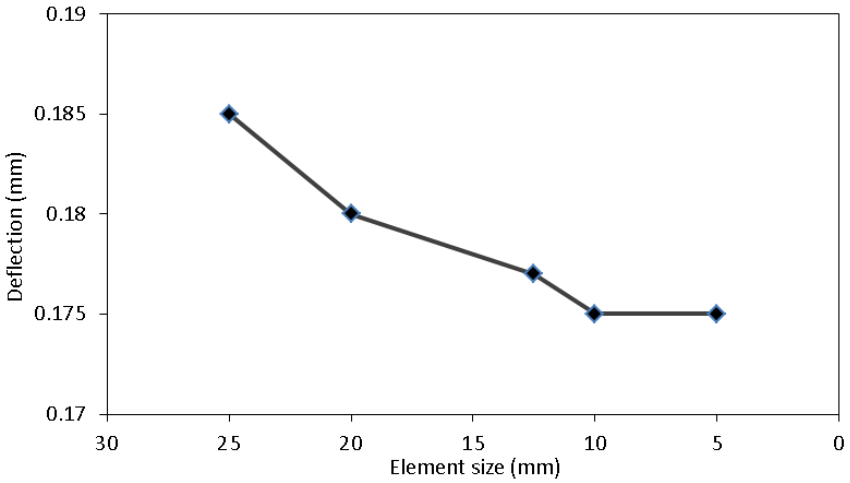


(a) Deflection at center of bottom face

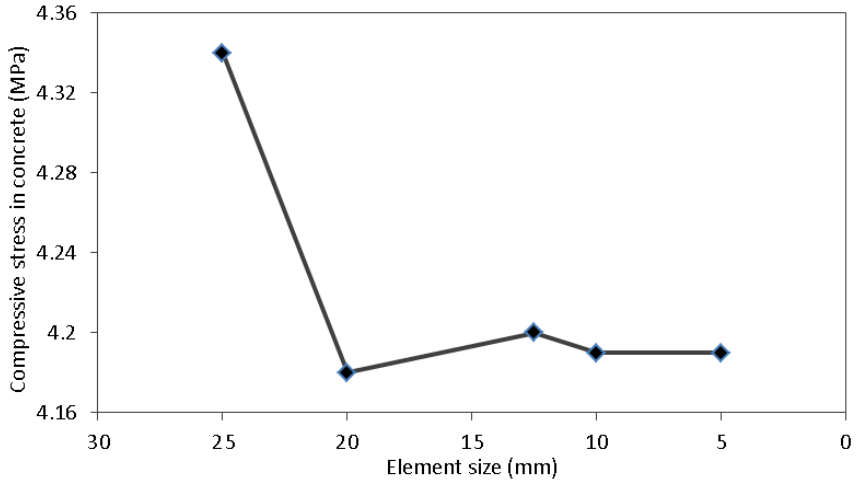


(b) Compressive stress in concrete at center of top face

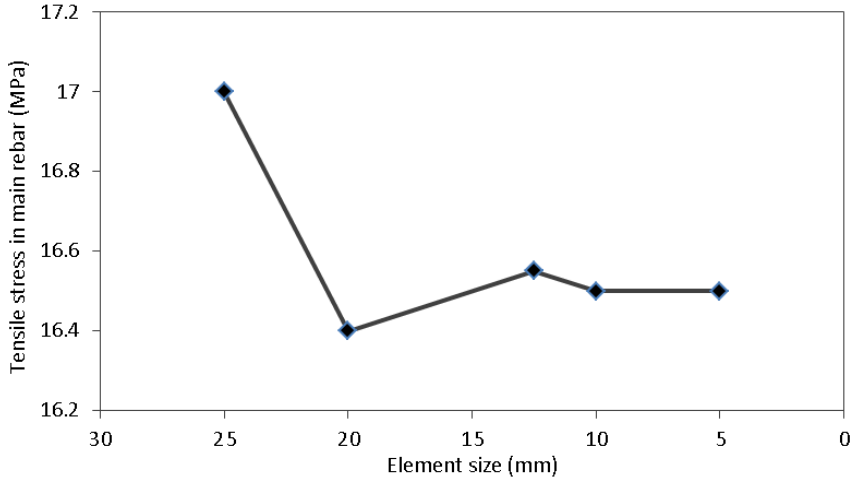


(c) Tensile stress in bottom reinforcement at mid span

Figure 5.9 Outcomes of convergence study

Figure 5.10 shows the meshed control reinforced concrete beam along with support and loading cylinder in ANSYS 14.0. After the material and meshing of all the elements, surface to surface contact created between the loading cylinder and beam surfaces using CONTA174 and TARGET170 element to transfer the load and reduce the stress concentration at the loading point.

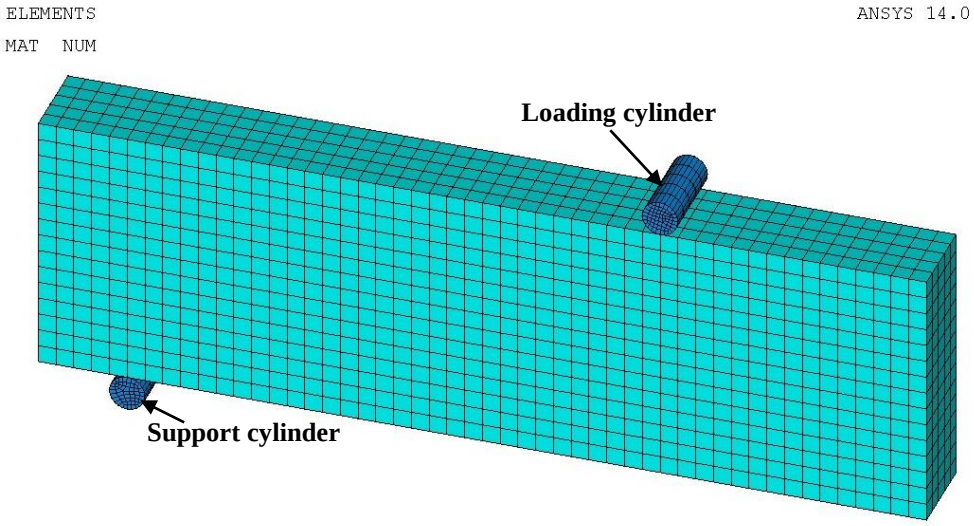


Figure 5.10 FEM discretization of RC beam, loading and support cylinder

Figure shows the finite element model generated in ANSYS 14.0 for strengthened beam with FRP sheet in complete shear zone, strip FRP sheet and beam wrapped with complete FRP in three parts respectively.

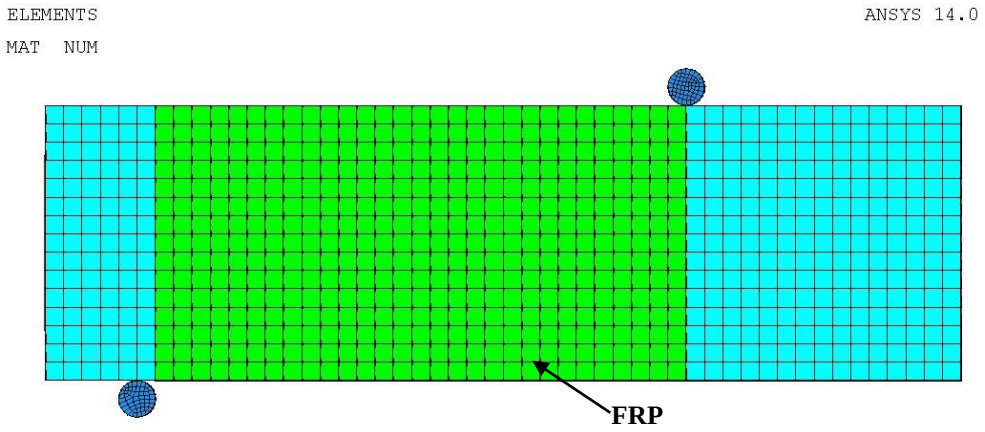


Figure 5.11 Finite element modeling of strengthened beam with FRP in shear zone

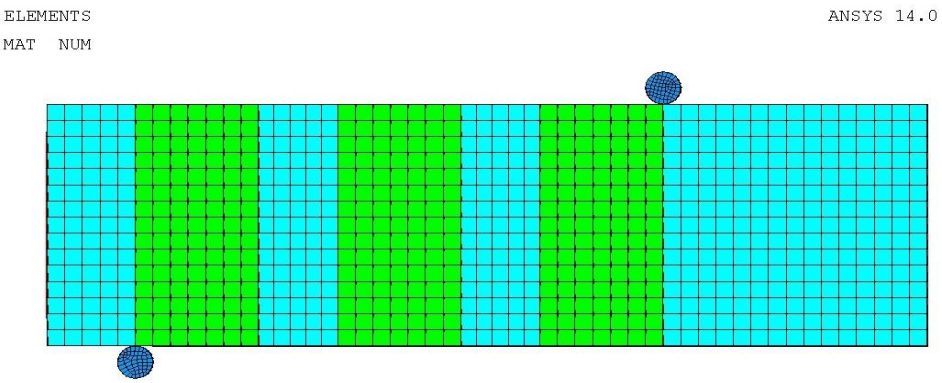


Figure 5.12 Finite element modeling of strengthened beam with strip FRP

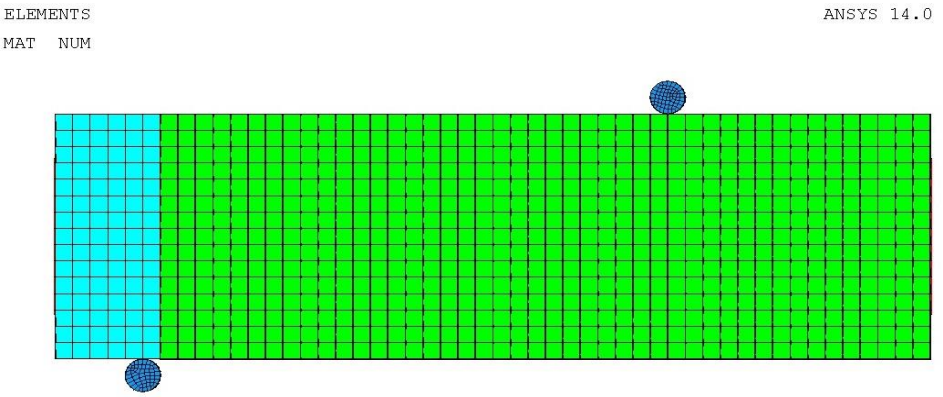


Figure 5.13 Finite element modeling of strengthened beam with fully wrapped FRP

## 5.4 LOADING AND BOUNDARY CONDITIONS

As quarter of beam used for the modeling symmetry boundary condition was applied at internal faces. The direction perpendicular to plane constrained for symmetry boundary condition. Figure 5.14 shows the symmetry boundary condition provided at the internal plane. At the centerline of the support cylinder constraint provided in y-direction to create a roller support. The load applied at the centerline of the loading cylinder. Figure 5.15 shows the loading and boundary conditions used in the model.

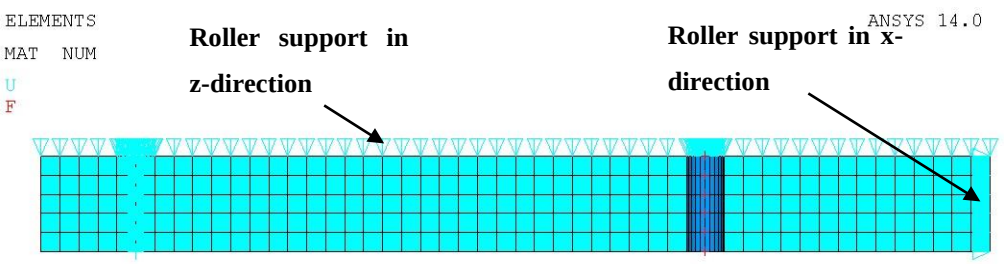


Figure 5.14 Symmetry boundary conditions

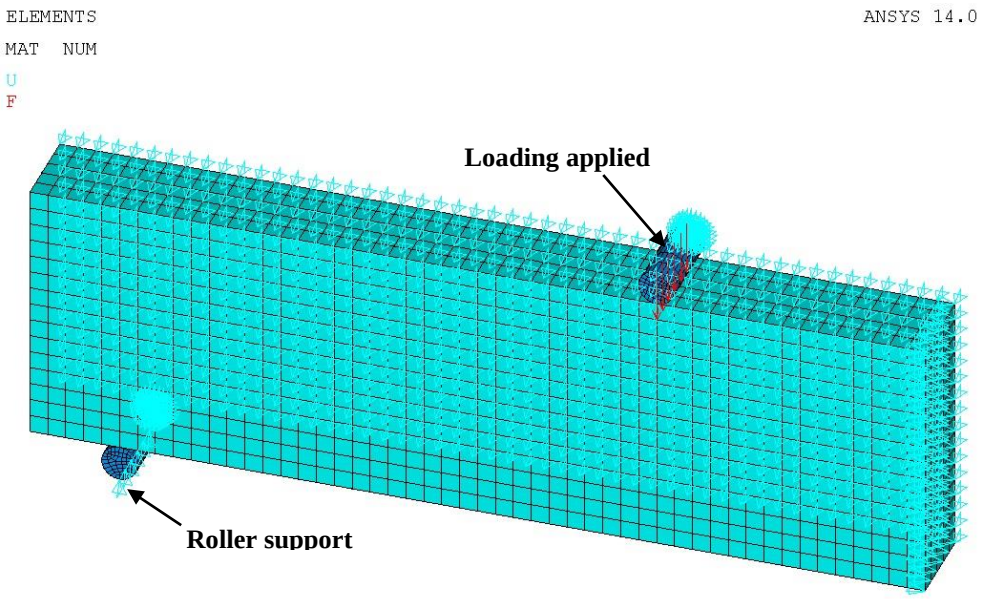


Figure 5.15 Loading and boundary condition applied

## 5.5 ANALYSIS PROCESS AND OUTPUTS

The present study is based on the analysis of FRP strengthened RC beam for which static analysis was opt. The ANSYS 14.0 utilize Newton-Raphson iteration method for nonlinear analysis. The convergence tolerance level of displacement and force increased by five times the default value for the convergence of the solution as difficulties in convergence observed for the nonlinear response and as suggested by previous researchers[69].

The total load was divided into number load-steps which further divided into sub-steps. The automatic time stepping option in ANSYS 14.0 helps in convergence and bisects load sub-step to minimum load step size when convergence problem occur for the given load step. The load applied gradually till the failure of beam. The size of each load step depends upon the behavior of the RC beam. For linear range, more loads can be applied at a time so the load step size in this case should not be small. The load step size gradually decreases with increment in the loads as the behavior of the RC beam changes from linear to nonlinear, yielding of the steel and severe cracking of the concrete at the constant moment region. The failure of the RC beam occurs when the solution does not converge for the load applied smaller than 1 N and large deflection error encountered. The strain in FRP checked for limiting values in FRP strengthened beams.

### 5.5.1 Effect of load application

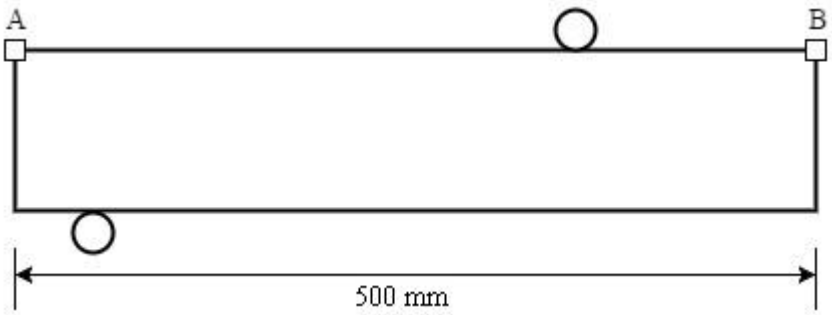


(a) Length AB considered for the path plot

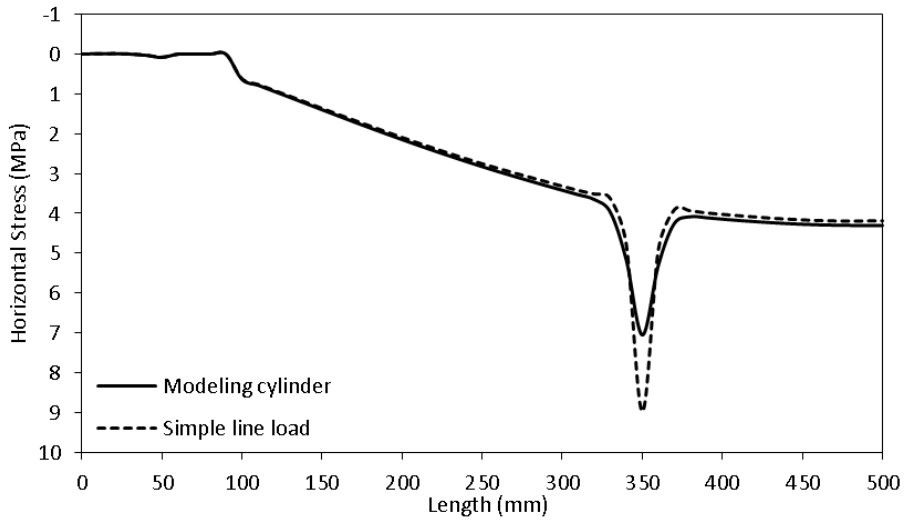


(b) Horizontal stress in control RC beam along path AB

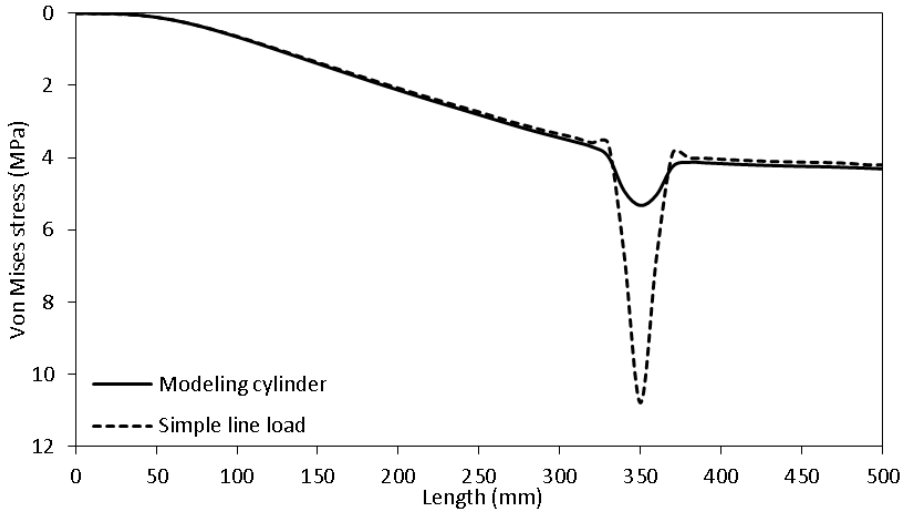


(c) Von Mises stress in control RC beam along path AB

Figure 5.16 Stress comparison of load applied using simple line load and modeling cylinder

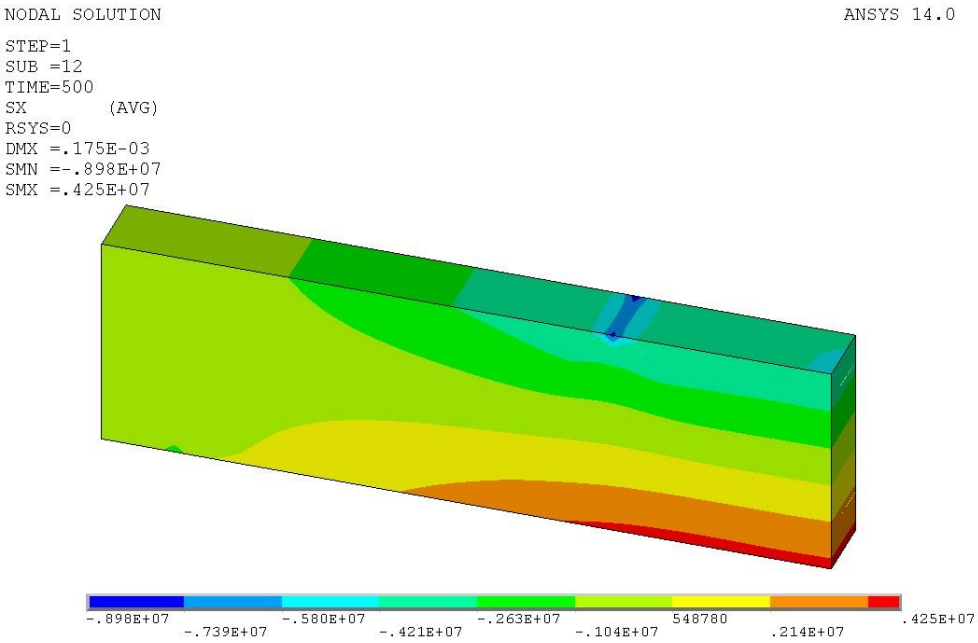


(a)

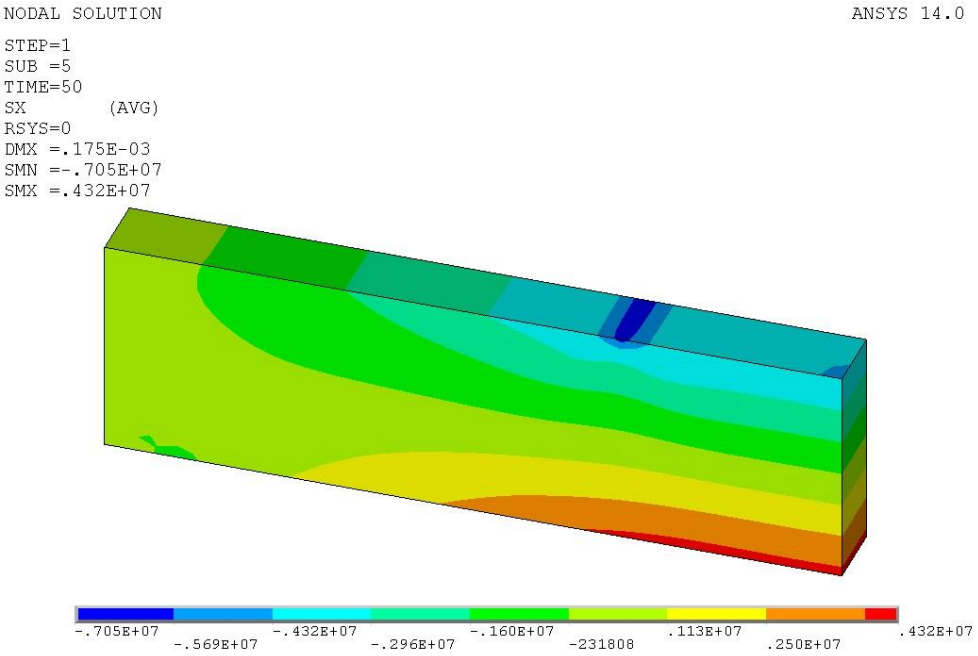


(b)

Figure 5.17 Horizontal stress contour comparison of load applied using (a) Simple line load and (b) Modeling cylinder and contact

The load transferred to the beam by modeling the cylinder and creating contact between the beam surface and the loading cylinder help in reducing stress concentration at loading point. The reduction in stress concentration due to load applied using the

cylinder can be explained by comparing the horizontal stress and Von Mises stress developed in the beam at the same load applied (up to linear range) with simple line load. Figure 5.16 shows the comparison of horizontal stress and Von Mises stress due to same load applied using simple line load and modeling cylinder. It is observed that the sharp stress concentration obtained due to simple line load is reduced significantly when load is applied using modeling cylinder and contact.

Figure 5.17 shows the comparison of horizontal stress obtained from finite element analysis for load applied up to elastic limit using simple line load and modeling cylinder. A smooth distribution of stress can be observed in the reason of load application when the load applied at the center line of the modeled cylinder. Table 5.3 compare the maximum horizontal and Von Mises stress at the point of loading.

Table 5.3 Comparison of maximum stress at loading point

| **Types** | **Simple line load** | **Modeling cylinder** | **Difference (%)** |
|---|---|---|---|
| Horizontal Stress | 8.98 MPa | 7.05 MPa | 21.50 |
| Von Mises Stress | 10.79 MPa | 5.32 MPa | 50.69 |

From the above table, it is observed that 21.5 percent reduction in horizontal stress and about 50 percent reduction in Von Mises stress concentration at the point of the loading can be achieved when the load is applied by modeling cylinder and creating contact between the beam surface and cylinder.

### 5.5.2 Effect of concrete cover

As the main rebar concrete cover detail was not available from experiment. A parametric study conducted to fix the concrete cover to main reinforcement bar of strengthened RC beam with complete BFRP wrapping in shear zone of beam (C1-BFRP-B21). For this, the load deflection plot obtained for BFRP strengthened RC beam modeled with different concrete cover to main reinforcement steel is compared with experimental load deflection plot[2]. Figure 5.18 shows the load deflection plot for effect of concrete cover to main steel reinforcement.

From the Figure 5.18, it is observed that with decrease in the concrete cover the stiffness increase but the ductility decreases. The yielding of steel takes place at higher load applied when lesser concrete cover is provided.

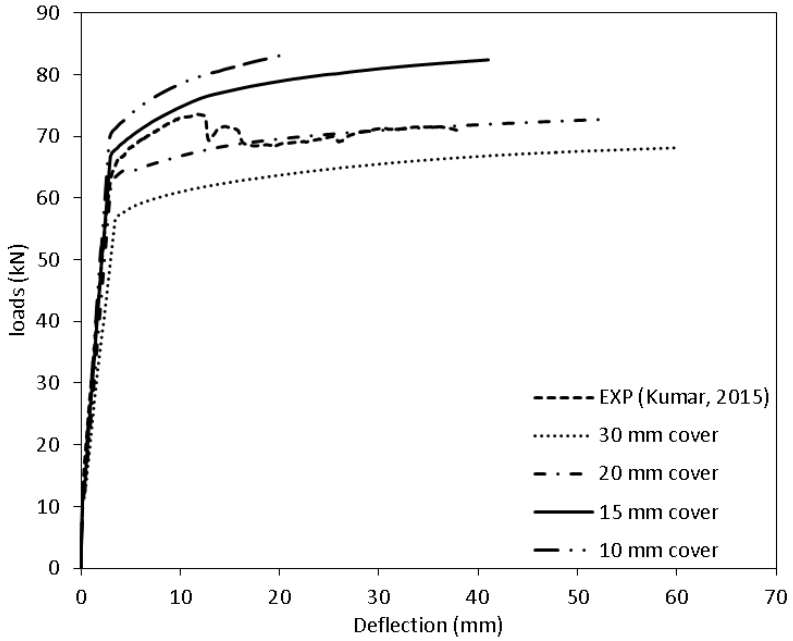


Figure 5.18 Load deflection plot for effect of concrete cover using beam C1-BFRP-B21

The Table 5.4 shows the load at which steel yields for strengthened RC beam with different concrete cover to main steel reinforcement.

Table 5.4 Comparison of steel yielding loads for effect of concrete cover

| **Concrete cover** | **Steel Yield load (kN)** | **Displacement at yielding (mm)** | **Stiffness (kN/mm)** |
|---|---|---|---|
| 30 mm | 56.31 | 3.44 | 16.37 |
| 20 mm | 63.21 | 3.35 | 18.87 |
| 15 mm | 66.83 | 3.00 | 22.28 |
| 10 mm | 69.31 | 2.85 | 24.50 |

From above table, it can be observed that with increase in the concrete cover the load at which the steel yields decreases. The stiffness at the steel yield for different concrete cover shows increase in stiffness with less concrete cover provided to strengthened RC beam. The steel yielding load and defection value for concrete cover 15 mm found to be close with experimental values at steel yielding i.e. load of 63.06 kN and deflection of 3.01 mm. So, a concrete cover of 15 mm is provided in all the FRP strengthened beams during the analytical analysis. The result obtained from the FEA is discussed in the next section.

## 5.6 RESULTS AND DISCUSSION

In this section the result obtained from finite element analysis is compared with experimental data of the full scale test conducted by Kumar, 2015[2]. The comparisons are made for the following topics: load deflection plots; crack pattern at failure; loads at steel yielding and failure. Also, the development of crack pattern for specific beam type is discussed. The failure loads obtained analytically is also compared with models given by different researchers.

### 5.6.1 Load-deflection plots

The deflections were measured using LVDT at the bottom face of the beam for the experimental beams. In finite element analysis, the deflection measured at the center of each beam for the comparison. Figure 5.19 to Figure 5.38 shows the load deflection plots of all beam compared with experimental results [2].

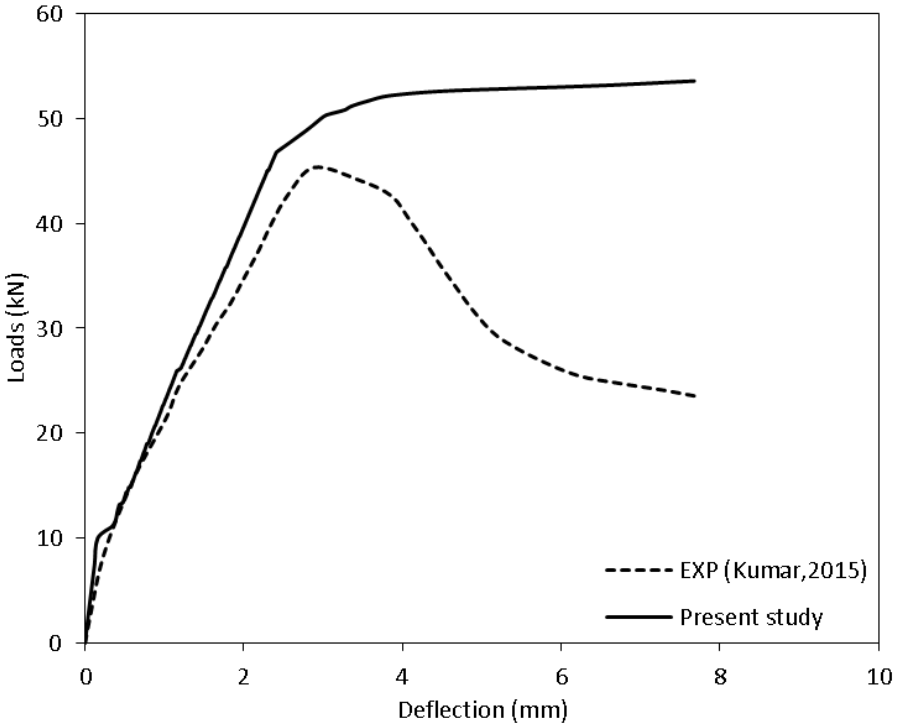


Figure 5.19 Load deflection plot for control beam C1-B0

Figure 5.19 and Figure 5.20 shows the load deflection plot obtained from finite element analysis for control beam C1-B0 and C2-B0 respectively shows reasonably good agreement with the experimental plots. The load deflection plot from FEA in the linear space is stiffer than the experimental plot in both cases. At steel yielding, the finite

element model is stiffer than control beam C1-B0 and C2-B0 by 22.5% and 29% respectively. The ultimate load in the beam C1-B0 and C2-B0 from finite element model found to be 53.60 kN and 63.72 kN which is higher than the ultimate load of 45.83 kN and 52.34 kN respectively from the experimental data.

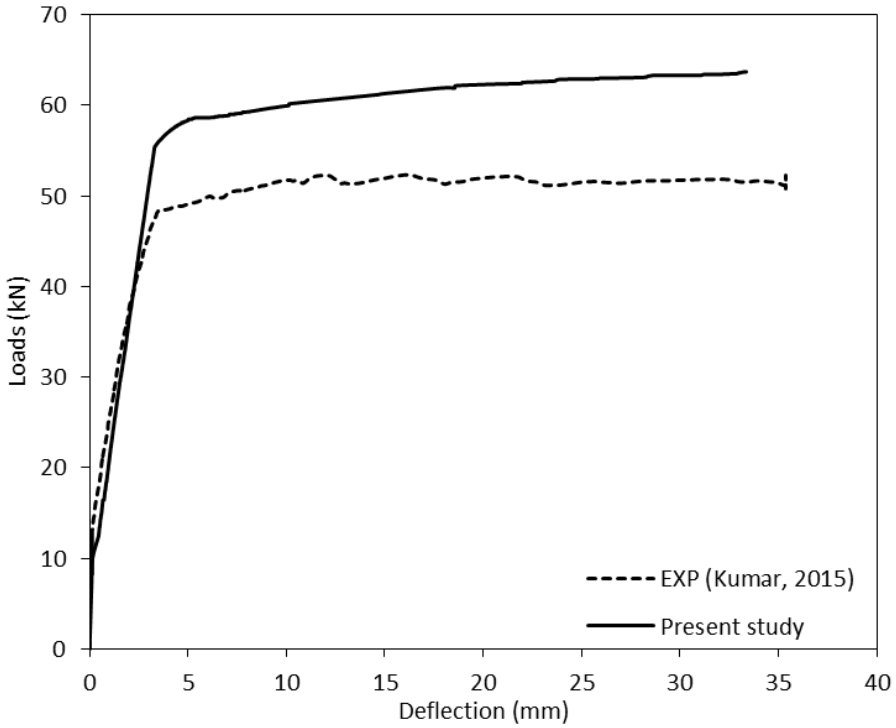


Figure 5.20 Load deflection plot for control beam C2-B0

Figure 5.21, Figure 5.22 and Figure 5.23 shows the comparison of load deflection plot for flexural shear strengthening of RC beam with BFRP , CFRP and GFRP respectively having concrete strength of C1=25.52 MPa. The all three plot from FEA correlate well with the experimental plots. The curve from FEA for beam C1-BFRP-B11, C1-CFRP-B12 and C1-GFRP-B13 produces higher stiffer till first crack in the beam. For beam C1-BFRP-B11, at steel yielding the finite element model found to be approximately 21% stiffer than actual beam. From FEA, the ultimate load in the beam is found to be 89.56 kN which is higher than 77.80 kN in the tested beam. For beam C1-CFRP-B12, after the first cracking have almost same stiffness as compared to the experimental beams. But the load at the ultimate in FEA is found to be 114.60 kN which is much higher compared to 95.12 kN in case of actual beam. Now for beam C1-GFRP-B13, the finite element model found to be stiffer at the steel yielding point by 27% from the

experimental results. The ultimate load from the FEA of 87.36 kN is close to the experimental ultimate load of 86.52 kN.

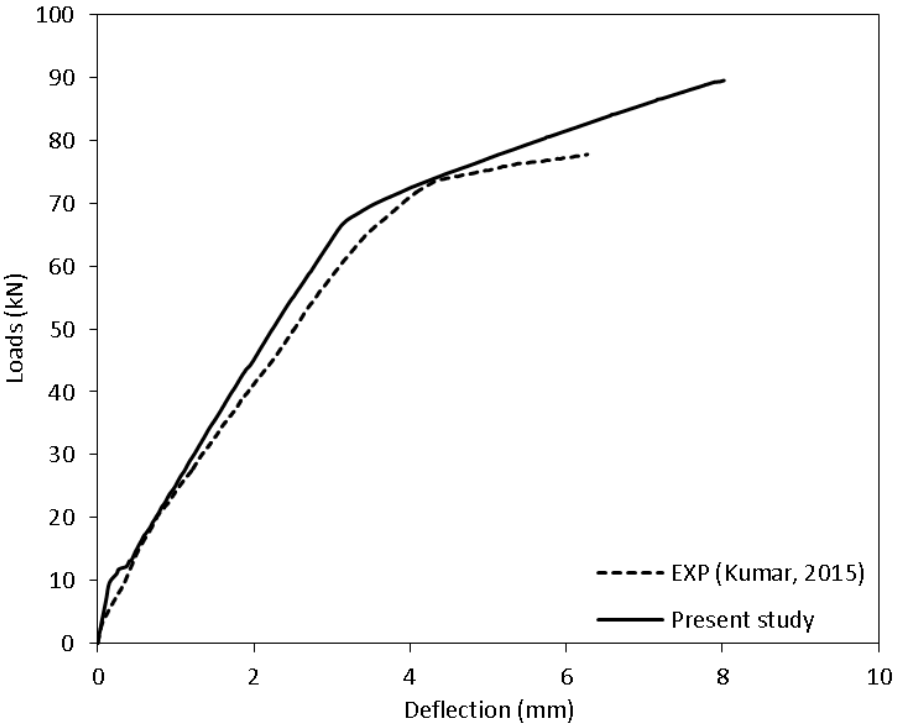


Figure 5.21 Load deflection plot for C1-BFRP-B11

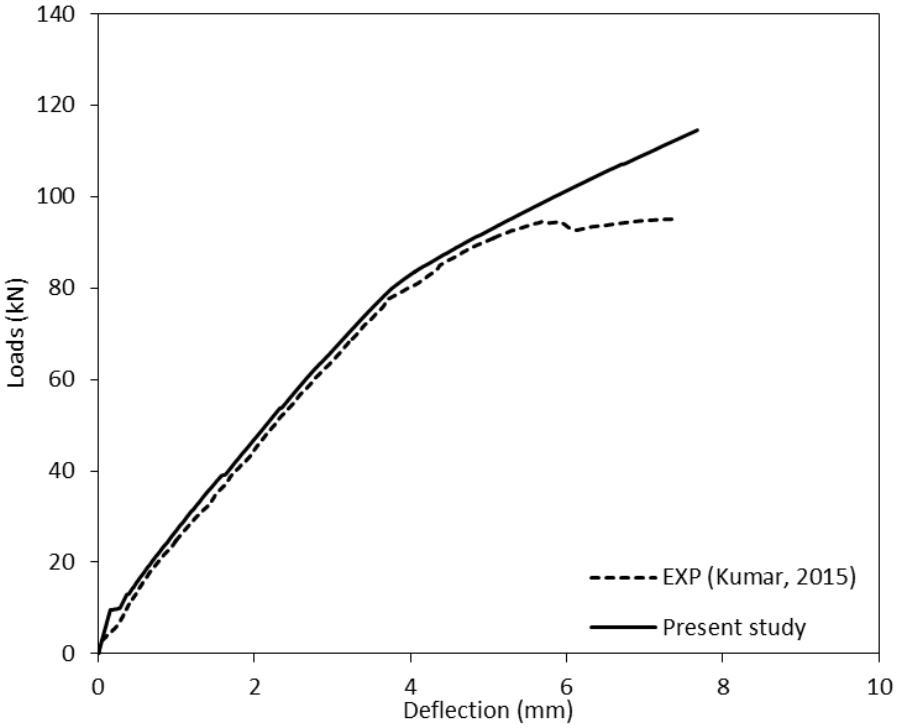


Figure 5.22 Load deflection plot for C1-CFRP-B12

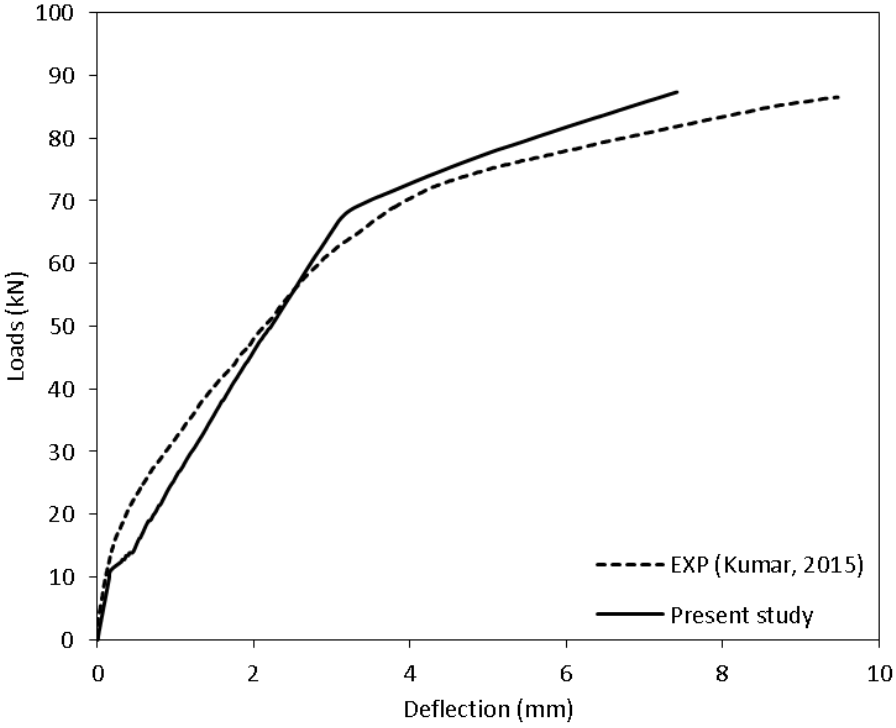


Figure 5.23 Load deflection plot for C1-GFRP-B13

Figure 5.24, Figure 5.25 and Figure 5.26 shows the comparison of load deflection plot for shear strengthening of RC beam with FRP in complete shear zone. The FEA plots of beam C1-BFRP-B21, C1-CFRP-B22 and C1-GFRP-B23 agree well with experimental results. For the entire three finite element model possess almost same stiffness till the steel yielding as compared to the experimental results. For finite element model beam C1-BFRP-B21, the stiffness at the steel yielding found to be slightly higher than the actual beam by 7%. The ultimate load from FEA is 82.40 kN which is higher than the experimental ultimate load of 73.57 kN. The finite element model (FEM) beam C1-CFRP-B22 is stiffer than the experimental than the experimental beam by 31% and also the ultimate load from FEA is 84.24 kN which is higher than the experimental ultimate load of 70.09 kN. The finite element model beam C1-GFRP-B23 is much stiffer than the experimental beam at steel yielding by 26% but have comparable ultimate loads of 81.60 kN from finite element analysis and 80.34 kN from experiment.

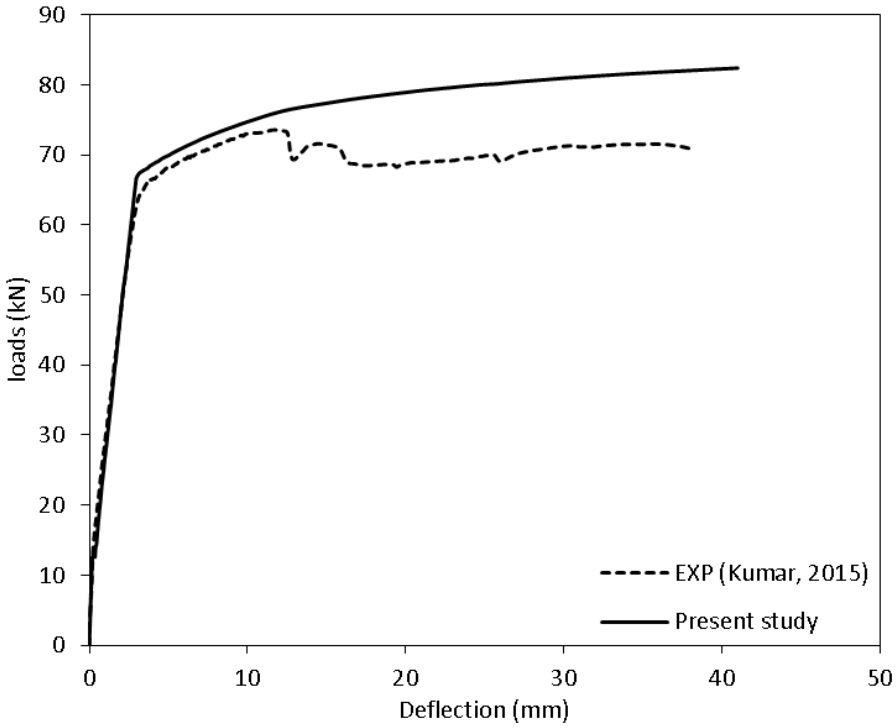


Figure 5.24 Load deflection plot for C1-BFRP-B21

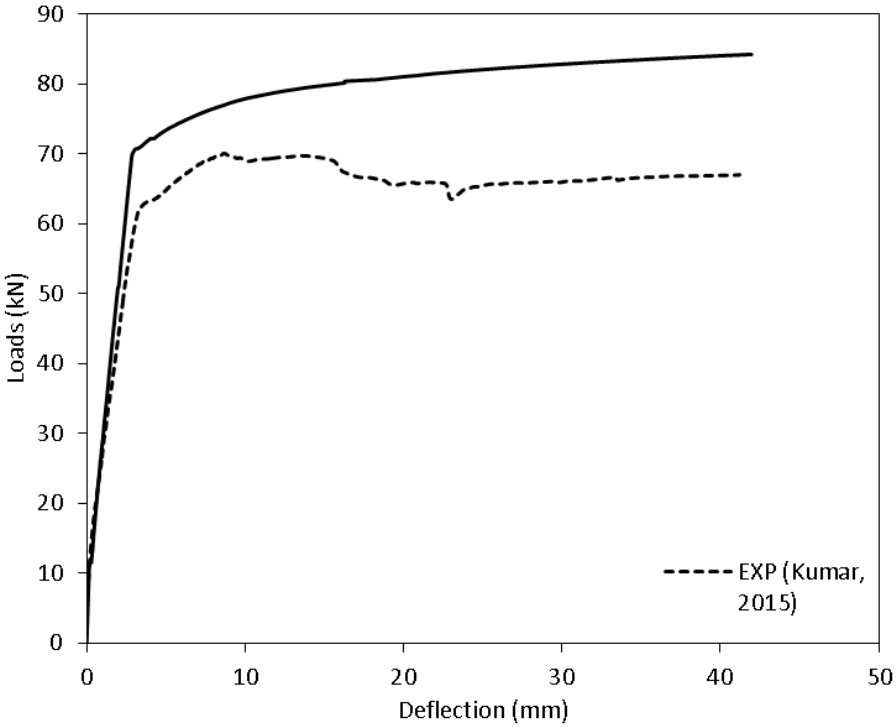


Figure 5.25 Load deflection plot for C1-CFRP-B22

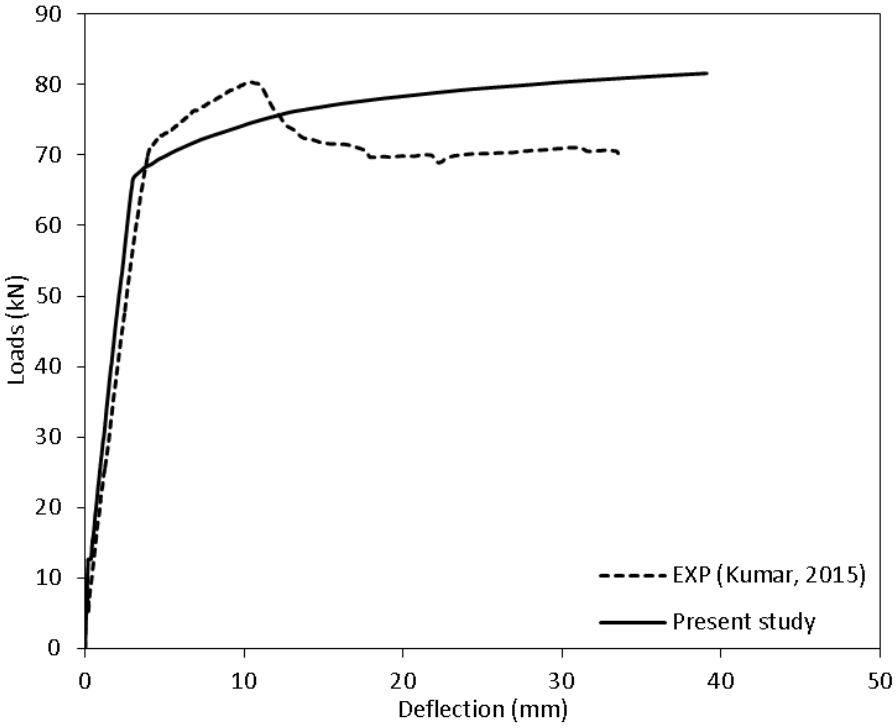


Figure 5.26 Load deflection plot for C1-GFRP-B23

Figure 5.27, Figure 5.28 and Figure 5.29 compares the two plots obtained from finite element analysis and experiment for shear strengthened beams with 70 mm strip BFRP, CFRP and GFRP respectively. The load deflection plot from finite element model reasonable agrees with the experimental results. The entire finite element model beam is stiffer in the linear range as compared to the experimental plots. Finite element model beam C1-BFRP-B31 shows same stiffness as compared with experimental beam till the steel yielding. At steel yield, the FEM beam is slightly stiffer than the experimental beam by 8%. After the yielding stiffness increases and finally, the ultimate load of finite element model beam is 79.08 kN which is higher the experimental ultimate load of 66.75 kN. Both finite element model beams C1-CFRP-B32 and C1-GFRP-B33 found to be stiffer than experimental results after the first crack. They are stiffer at the steel yielding by 64% and 37% respectively as compare to experimental results. The ultimate load of FEM beams C1-CFRP-B32 and C1-GFRP-B33 is 83.66 kN and 77.76 kN respectively which is higher from the experimental ultimate loads of 75.25 kN and 69.84 kN.

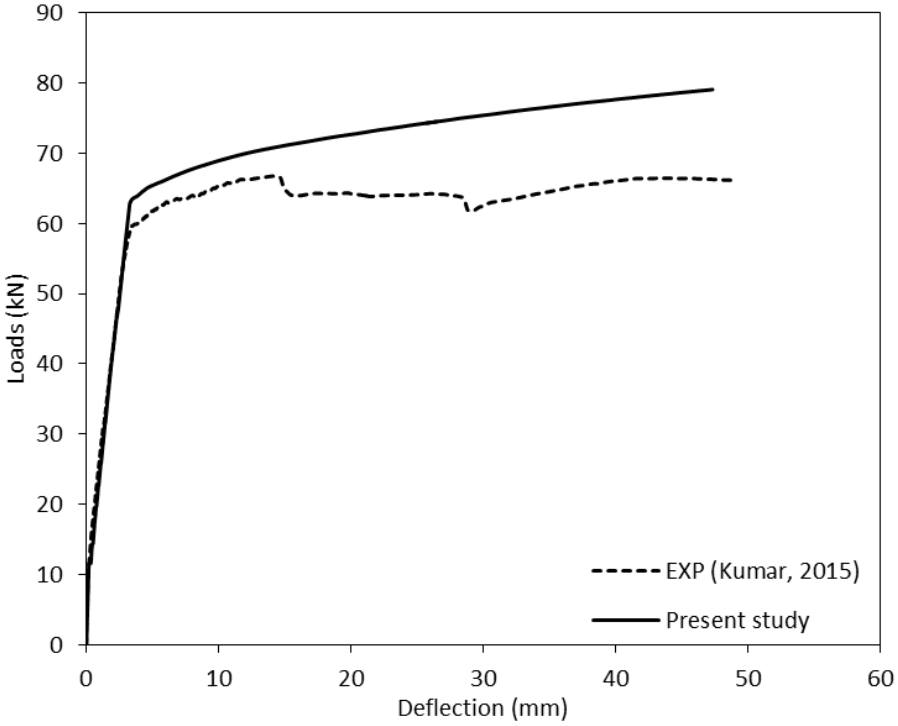


Figure 5.27 Load deflection plot for C1-BFRP-B31

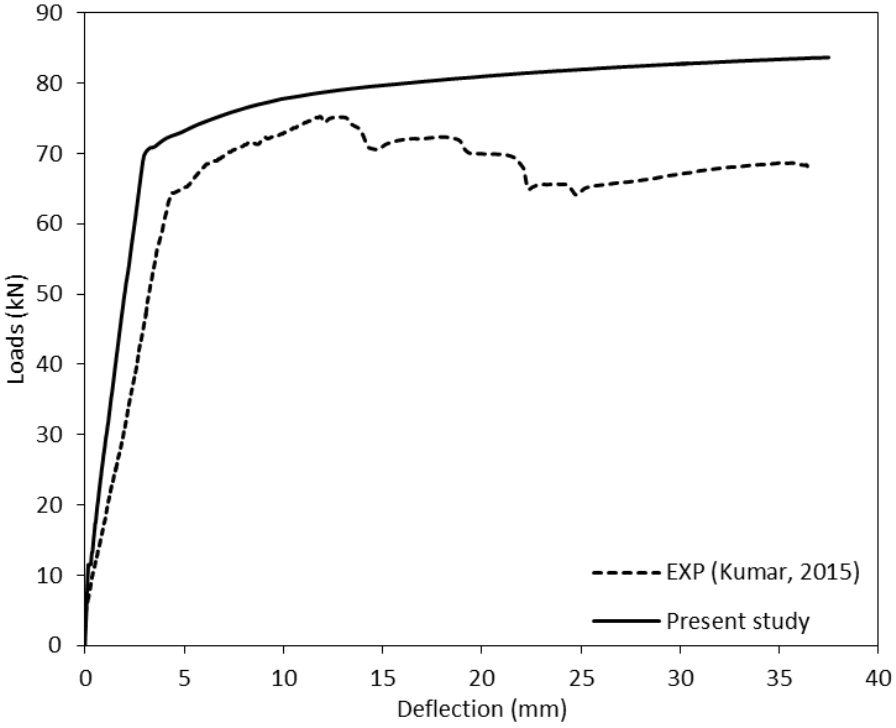


Figure 5.28 Load deflection plot for C1-CFRP-B32

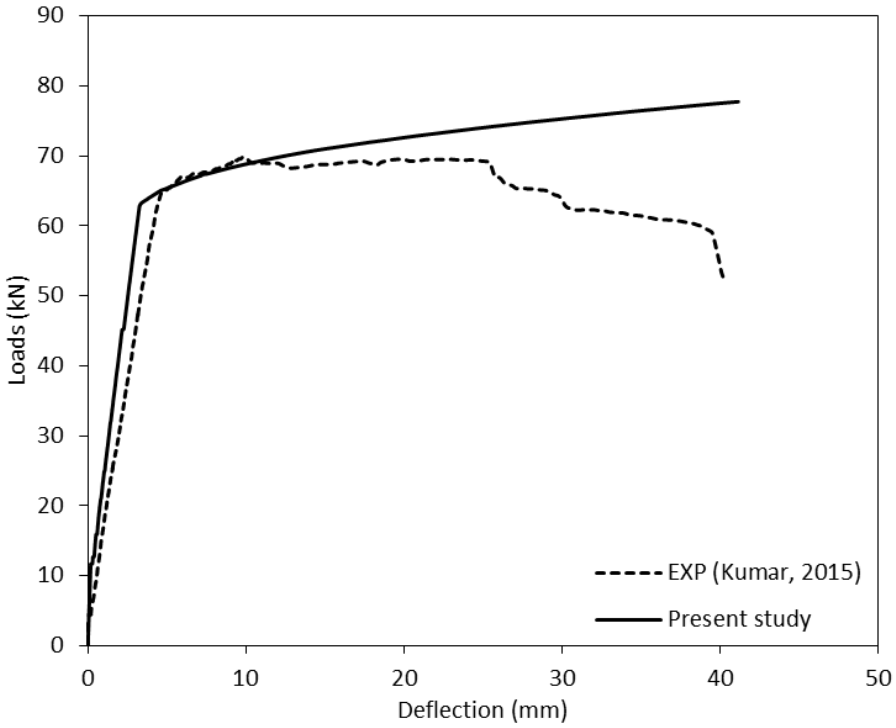


Figure 5.29 Load deflection plot for C1-GFRP-B33

Figure 5.30, Figure 5.31 and Figure 5.32 shows the load deflection plot for strengthened RC beam C2-BFRP-B11, C2-CFRP-B12 and C2-GFRP-B13 completely wrapped with FRP in three parts having concrete strength C2=39.11 MPa. The finite element model beam C2-BFRP-B11 is stiffer at the first crack of the beam. Then the stiffness decreases afterwards near the steel yielding the stiffness increases by 16% as compared to experimental results. The ultimate load of 102.27 kN is higher in the FEM beam then the experimental ultimate load of 89.68 kN. For the FEM beams C2-CFRP-B12 and C2-GFRP-B13, the stiffness is higher than corresponding experimental beams till the ultimate load. At the steel yielding point, the stiffness of FEM beam C2-CFRP-B12 and C2-GFRP-B13 is higher than the actual beam by 26% and 39% respectively. The ultimate loads in finite element model beam are also higher than the experimental beams. The ultimate load for FEM beam C2-CFRP-B12 is 107.5 kN and beam C2-GFRP-B13 is 99.77 kN that from experiment was 71.08 MPa and 71.69 MPa respectively.

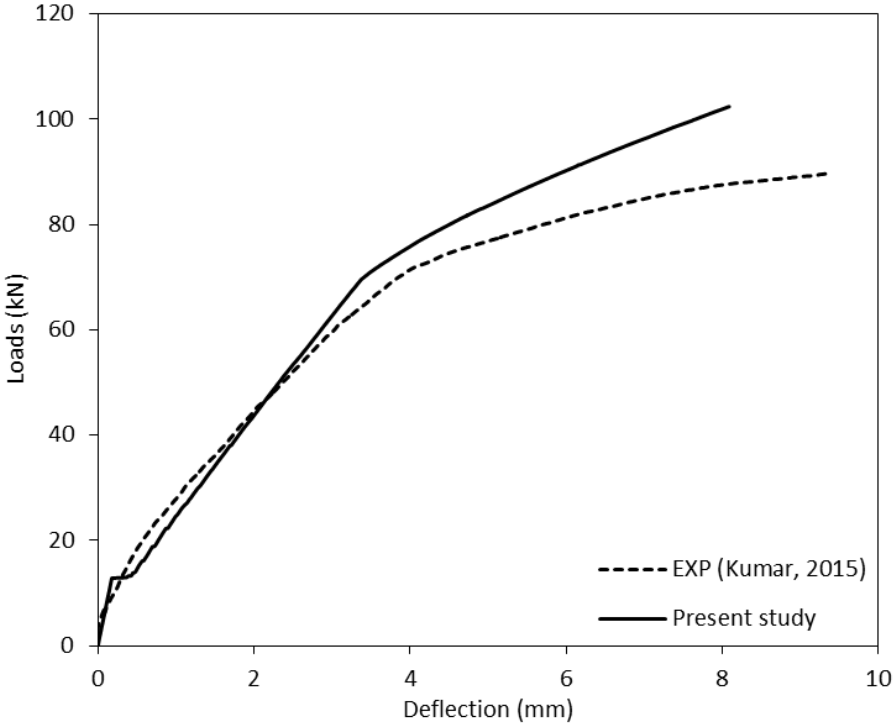


Figure 5.30 Load deflection plot for C2-BFRP-B11

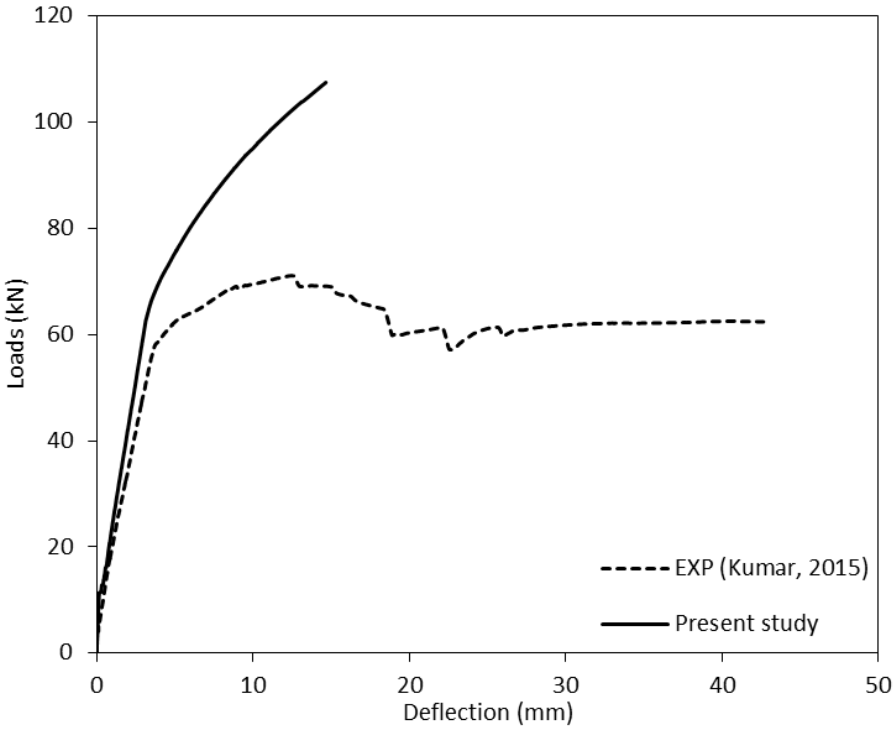


Figure 5.31 Load deflection plot for C2-CFRP-B12

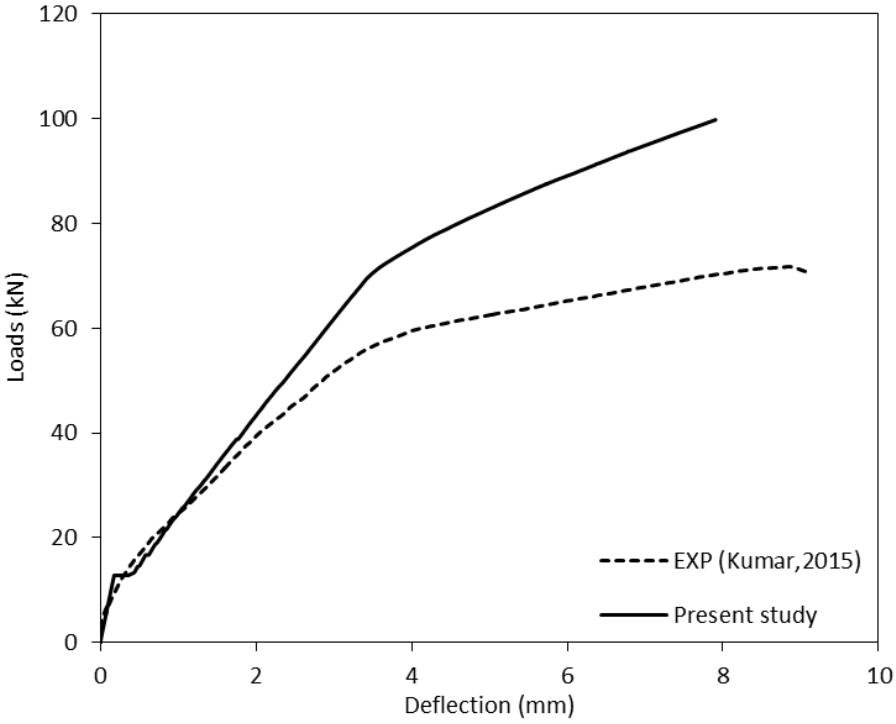


Figure 5.32 Load deflection plot for C2-GFRP-B13

Figure 5.33, Figure 5.34 and Figure 5.35 shows the analytical load deflection curve for flexural shear strengthening of reinforced concrete compared with experimental curves for beam type C2-BFRP-B21, C2-CFRP-B22 and C2-GFRP-B23 respectively. The compared curves demonstrate a good agreement. In the linear range, the finite element model load deflection curve is stiffer than the experimental results. For FEM beams C2-BFRP-B21 and C2-CFRP-B22, at steel yielding load deflection plot is stiffer than experimental plots by 18% and 28% respectively. For FEM beam C2-GFRP-B23 have almost stiffness as that of the actual beam at the steel yielding. The finite element model ultimate load for all cases found to higher compare to experimental ultimate loads. From finite element the ultimate load for beam types C2-BFRP-B21, C2-CFRP-B22 and C2-GFRP-B23 are 91.01 kN, 120.56 kN and 88.85 kN respectively corresponding ultimate load from experiment was 68.79 kN, 99.95 kN and 67.99 kN.

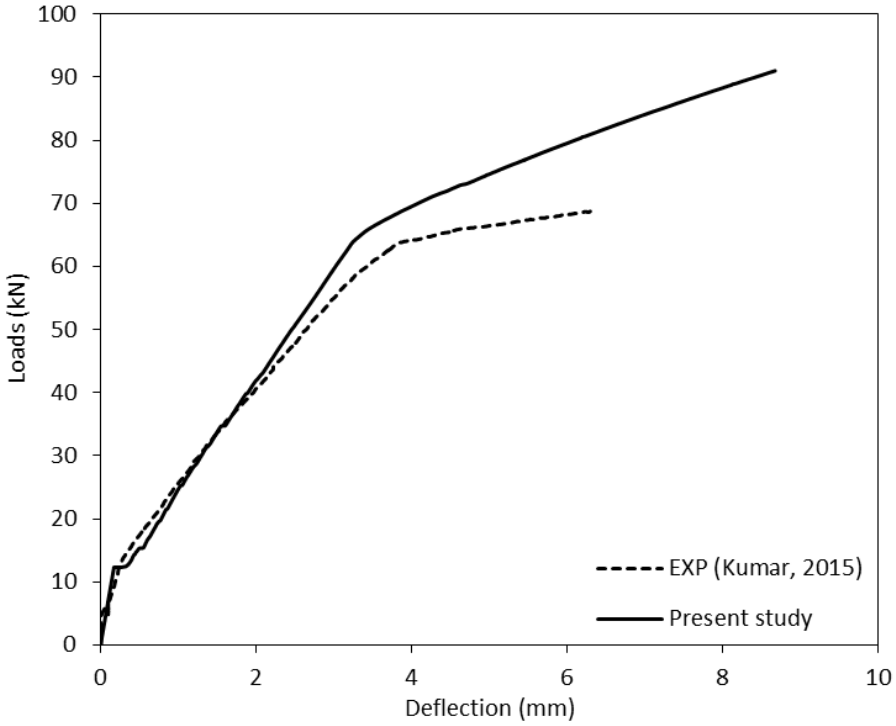


Figure 5.33 Load deflection plot for C2-BFRP-B21

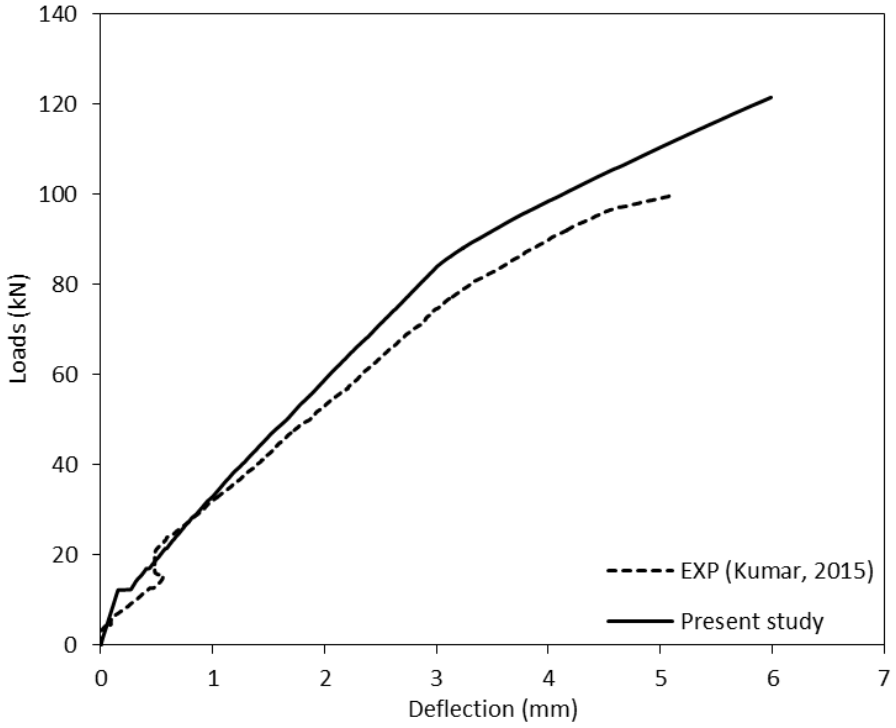


Figure 5.34 Load deflection plot for C2-CFRP-B22

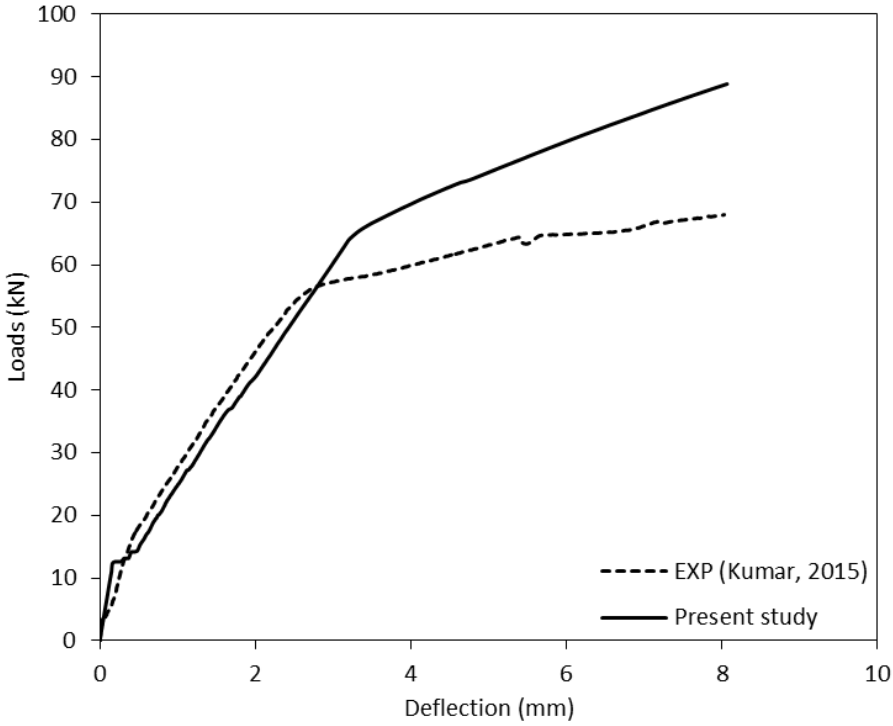


Figure 5.35 Load deflection plot for C2-GFRP-B23

As shown in Figure 5.36, Figure 5.37 and Figure 5.38, analytical load deflection plot correlates well with the experiment plots from beam strengthened in flexural and in shear with strip of 70 mm at 115 center to center spacing for beam types C2-BFRP-B31, C2-CFRP-B32 and C2-GFRP-B33 respectively. For beam type C2-BFRP-B31, experimental load deflection plot is stiffer than the finite element model plot by 17% at point of steel yielding but the ultimate load obtained from FEA gives higher value of 87.84 kN than the experimental ultimate load of 73.08 kN. For beam type C2-CFRP-B32, the finite element model load deflection plot shows almost similar stiffness in the linear range. At the point of steel yielding the FEM beam is stiffer than actual beam by 26%. This beam also shows a higher value of ultimate load of 109.16 kN compared to experimental ultimate load of 83.07 kN. For beam type C2-GFRP-B33, FEM load deflection plot stiffer than the experimental results at the first crack. After that it shows almost same behaviour as compared to actual beam. Finite element model is about 8% stiffer than experimental plot when steel yields. The ultimate load obtained from FEA is about 86.28 MPa which is moderately higher than the experimental ultimate load of 77.21 MPa.

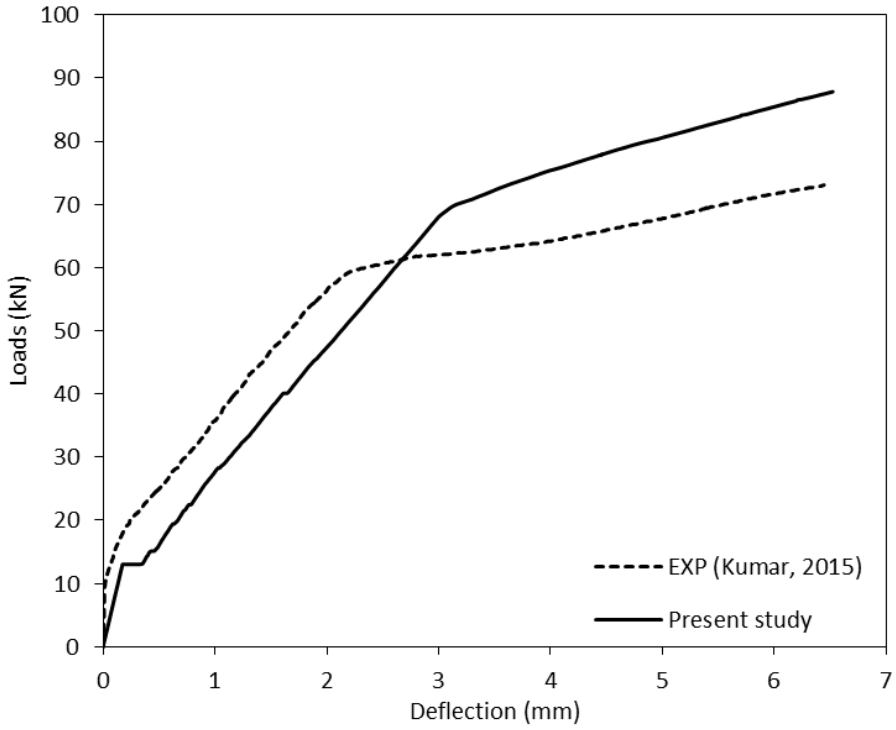


Figure 5.36 Load deflection plot for C2-BFRP-B31

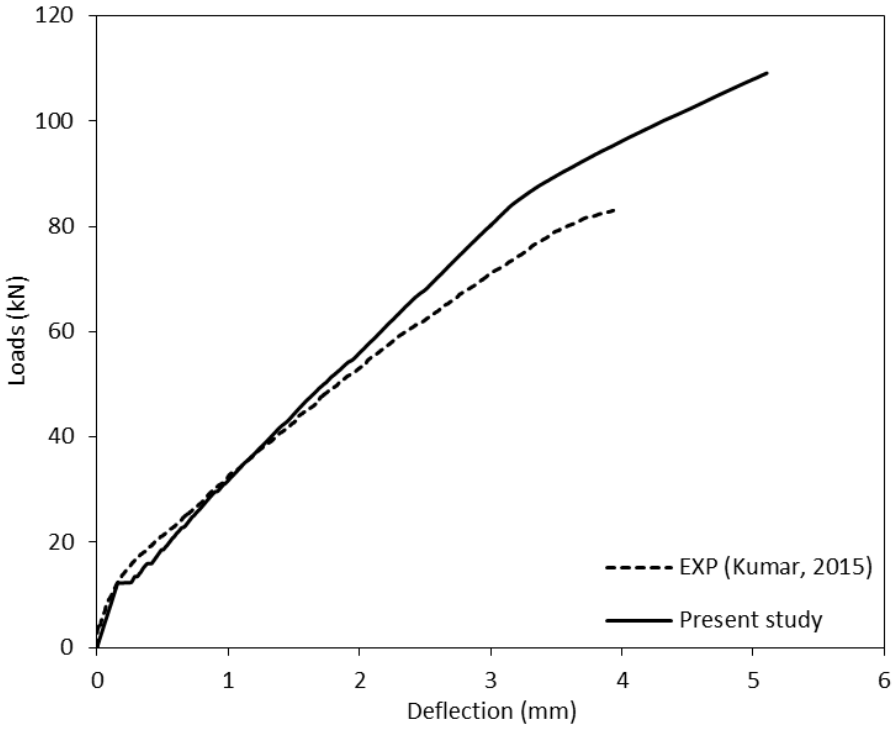


Figure 5.37 Load deflection plot for C2-CFRP-B32

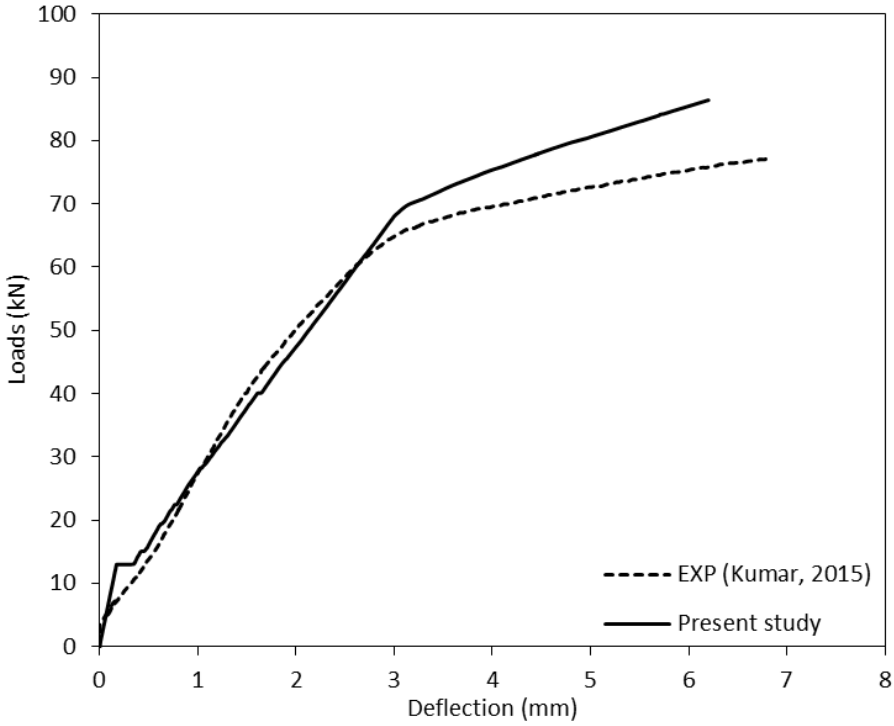


Figure 5.38 Load deflection plot for C2-GFRP-B33

Overall the load deflection plot obtained from finite element analysis for the all beams agrees reasonably well with the experimental curves. At the point of steel yielding, the FE load deflection curves are stiffer than the experimental load deflection curve by 0 to 64%. Also at the linear range and first cracking the finite element load deflection plot found to be stiffer. Finally the ultimate obtained from finite element analysis for all control and strengthened RC beam found to be higher than experimental ultimate loads.

The deviation or higher stiffness in the finite element results from experimental results could be due to various factors. Dry shrinkage micro cracks and deficiency during the experimental are present in the concrete to some extent. The bond between the concrete element and steel reinforcement element in FE model being assumed to be perfect with no slip, which is not true for the experimental beams. As in some beams slips may be occurred between the concrete and the reinforcement bars so that the composite action is lost. All the beams for a group C1 or C2 are modeled with a particular concrete strength and same concrete strength for all beams is not possible in case of experiment which may increase the stiffness in concrete model with higher concrete strength than actual concrete strength during experimental program. Also, the FRP is modeled with the ultimate strength of the FRP sheets assume to be linear elastic until failure that

shows the stress remains elastic. The data of the FRP sheets was taken from Kumar, 2015 and the FRP sheet test for the mechanical properties was not experimentally performed by Kumar, 2015 in laboratory. If the experimental true mechanical properties of the FRP sheets were available then the behaviour of the continuous failure of strengthened experimental beams could be arrested by the finite element model which subsequently reduces the ultimate load obtained from the finite element analysis. These are the factors which could increase the stiffness of the FEA over the experimental results.

### 5.6.2 Crack pattern

The crack pattern in different load steps for concrete element SOLID65 is recorded in ANSYS 14.0 software. The cracking appears at the integration point of the solid element once the tensile stress in concrete reaches ultimate stress or cracking stress. Circle outline in plane of crack show cracking and octahedron outline shows crushing. The first crack appears with red colour and the final crack or tertiary crack appears as blue colour which indicates the failure.

The progression in crack pattern is shown in Figure 5.39, Figure 5.40 and Figure 5.41 for control beam C2-B0, RC beam strengthened in flexural shear C1-CFRP-B12 and RC beam strengthened in only shear with strips C1-BFRP-B31. In all beams the first crack occurs at the mid span of the beam i.e. flexural crack. Beyond the first crack the cracking increases and began from mid span towards supports. At higher loads diagonals tension crack began to appear with more flexural cracks. Increase in loads induces additional diagonal tensile and flexural cracks. After the steel yielding, more cracks began to form near the constant moment region. At the end compressive crack appear below the loading system and severe crack at the constant moment region which causes the failure of the beam. In case of flexure shear beam significant occur near the top surface of the beam. For strip shear strengthened beam, crack appears in the concrete where the FRP confinement is not provided. The crack appeared in the considered beam at the ultimate load defines the failure of the member.

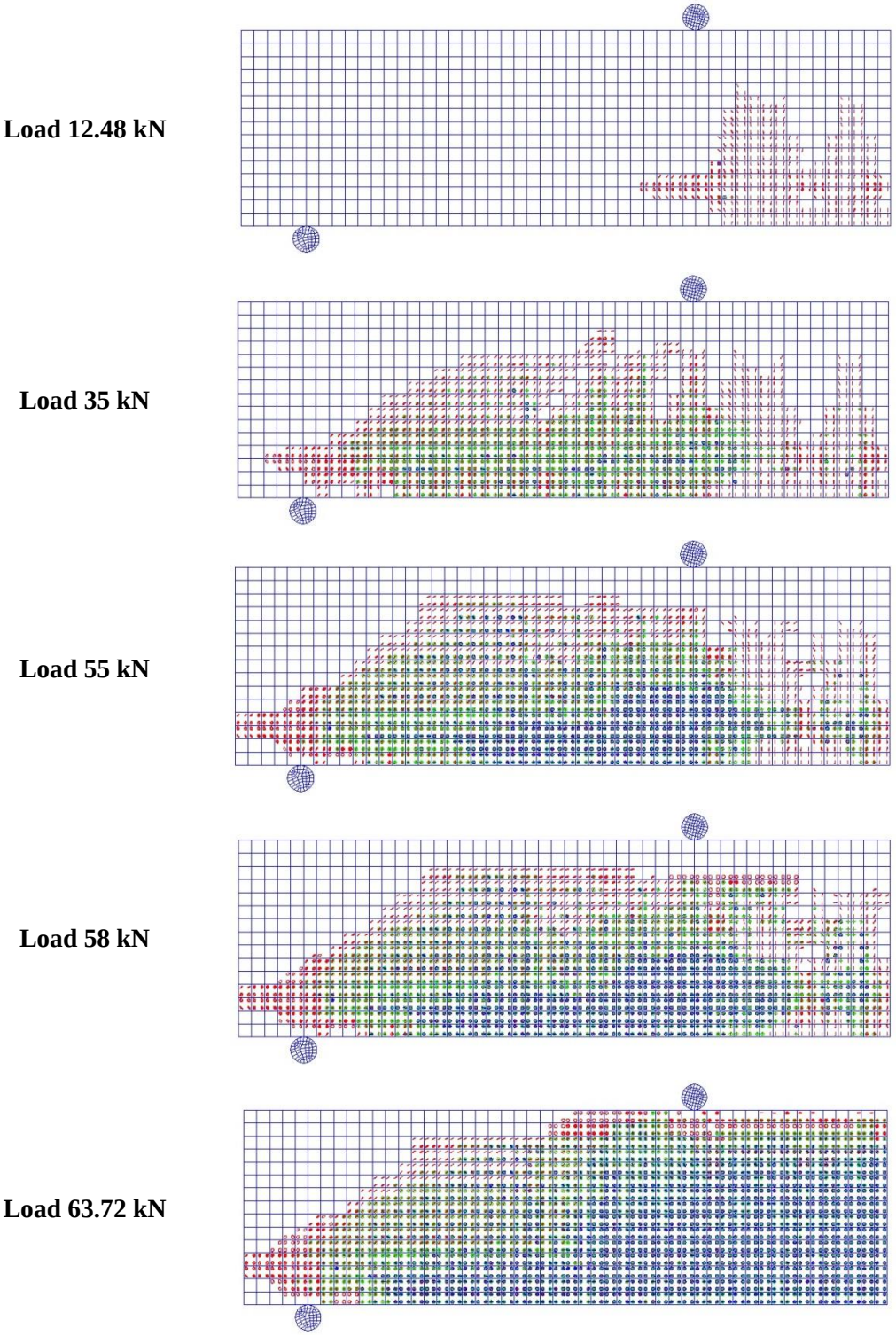


Figure 5.39 Progression of crack pattern for control beam C2-B0

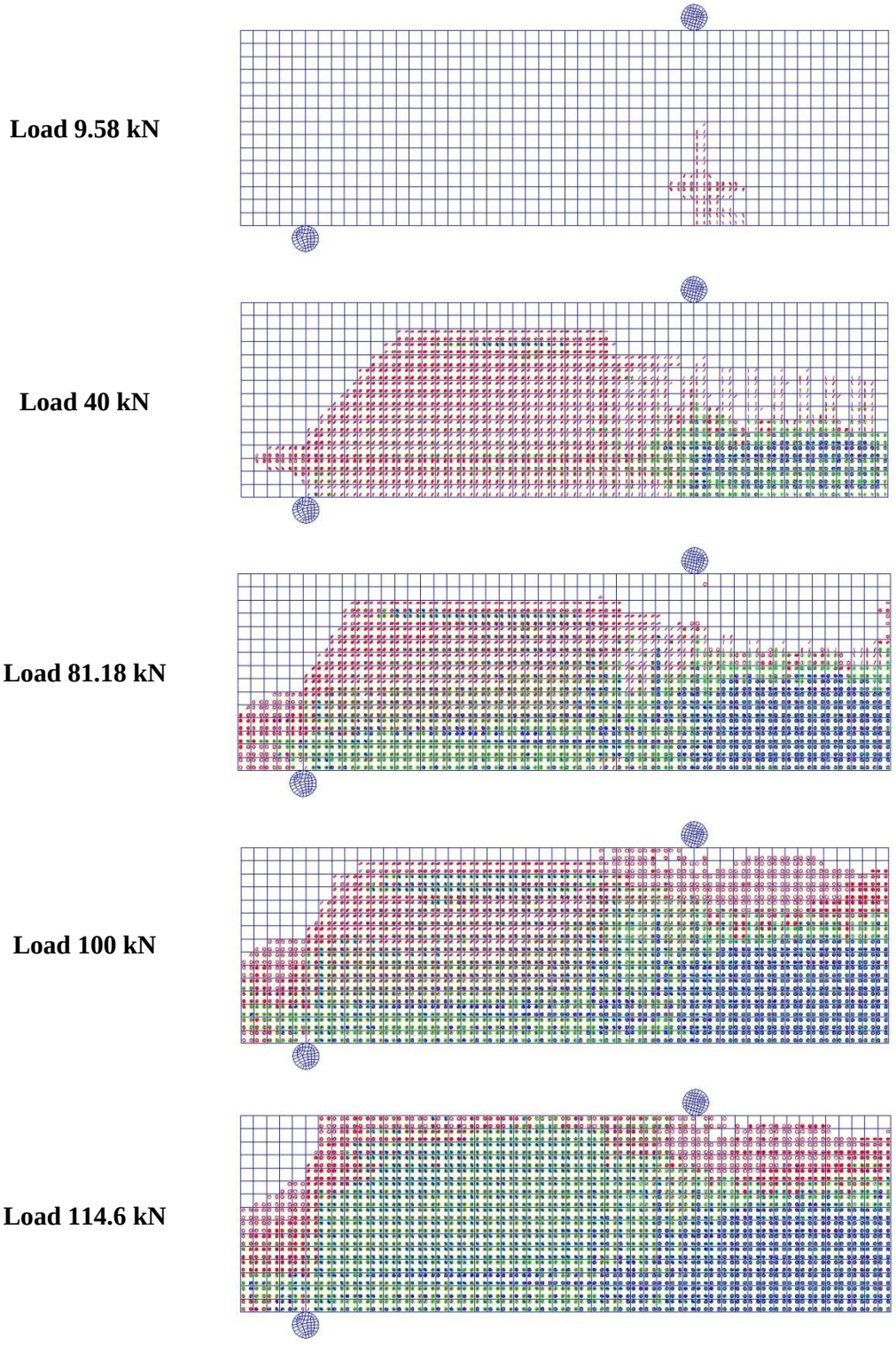


Figure 5.40 Progression of crack pattern for flexure shear beam C1-CFRP-B12

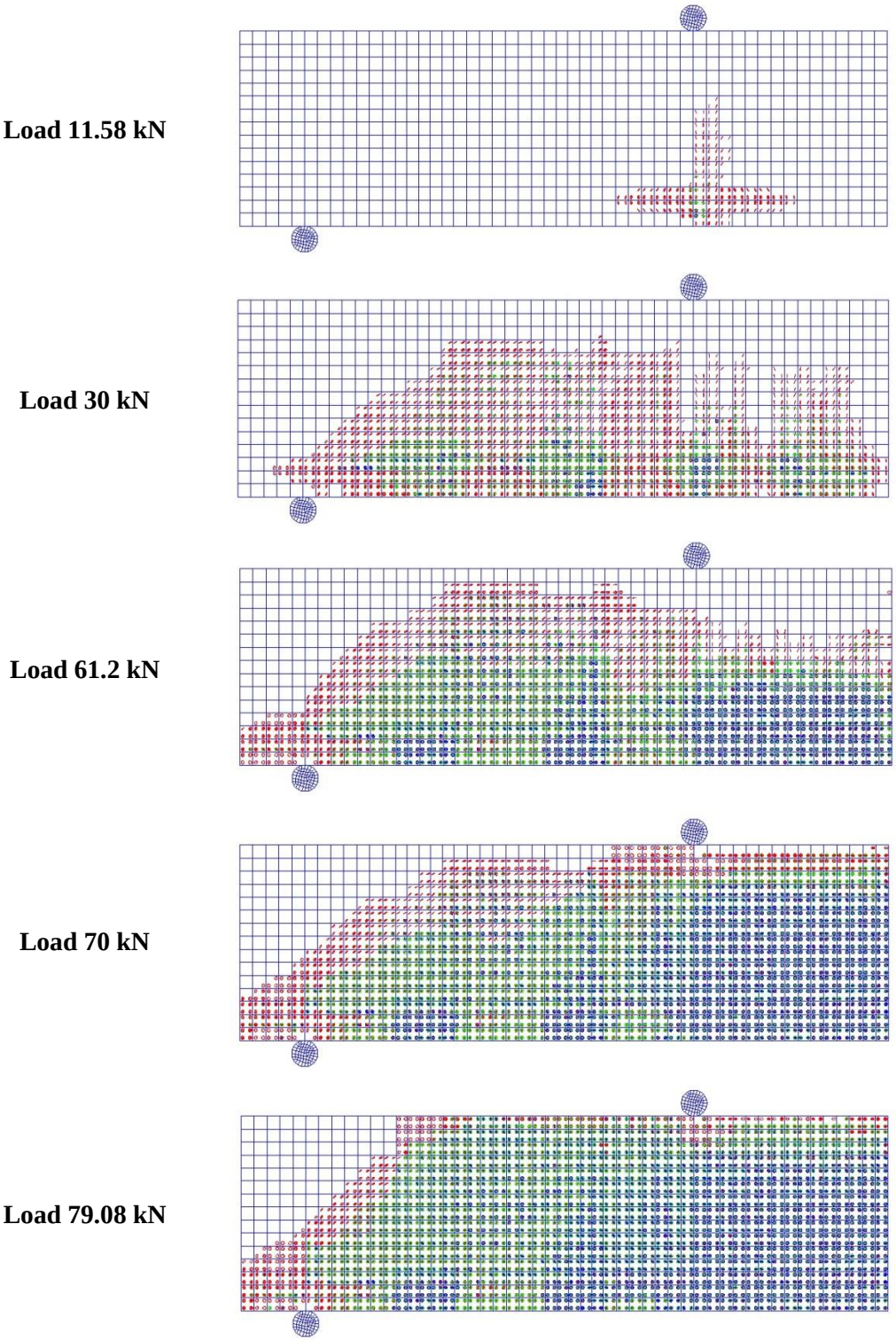


Figure 5.41 Progression of crack pattern for strip shear beam C1-BFRP-B31

Now, the crack pattern developed in ANSYS 14.0 software at integration point for all the beams at the failure load are compared with photograph of the experimental beams[2] at failure, shown in Figure 5.42 to Figure 5.61.

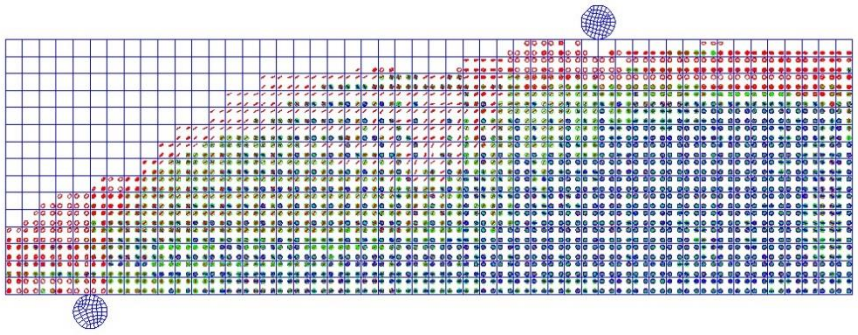

(a) Present study

(b) Experiment (Kumar, 2015)

Figure 5.42 Crack pattern at failure for control beam C1-B0

The failure of control reinforced concrete beam C1-B0 with concrete strength 25.52 MPa shown in Figure 5.42 agrees well with the experimental beam. The crack pattern of the finite element model shows that the diagonal tensile cracks propagate from the support to the loading.

Figure 5.43, Figure 5.44 and Figure 5.45 illustrate the crack pattern obtained at failure load in ANSYS 14.0 for RC beam strengthened in flexural shear with BFRP, CFRP and GFRP sheets. The crack pattern agrees well with experimental beam for beam type C1-BFRP-B11 and C1-GFRP-B13. In all three beams, several flexural cracks occur at the constant moment region of the beam and compressive cracks at the top face of the beam are observed which suggest that the beam would fail in flexure as observed in the experimental beams for C1-BFRP-B11 and C1-GFRP-B13. But in case of C1-CFRP-B22, during experiment failure occur due to delamination fiber in shear zone causing shear failure which is not observed in finite element model.

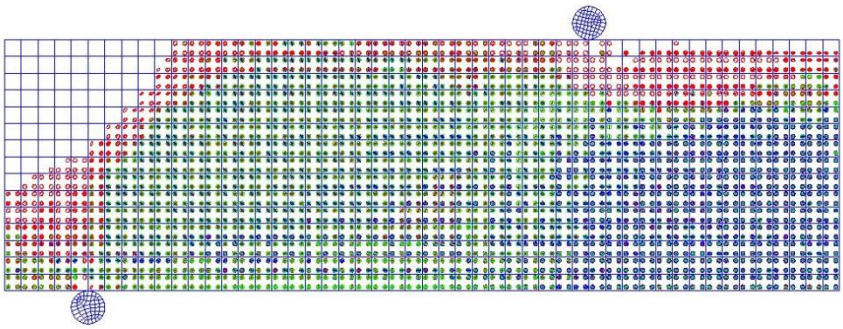

(a) Present study

(b) Experiment (Kumar, 2015)

Figure 5.43 Crack pattern at failure for C1-BFRP-B11

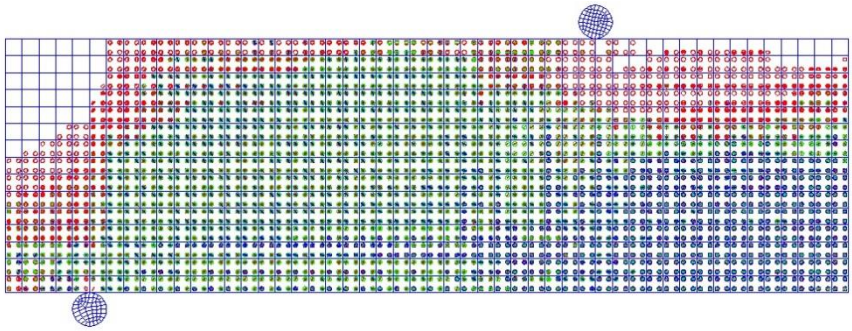

(a) Present study

(b) Experiment (Kumar, 2015)

Figure 5.44 Crack pattern at failure for C1-CFRP-B12

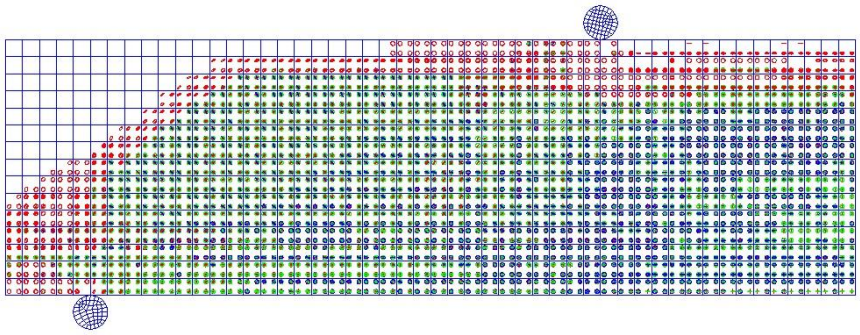

(a) Present study

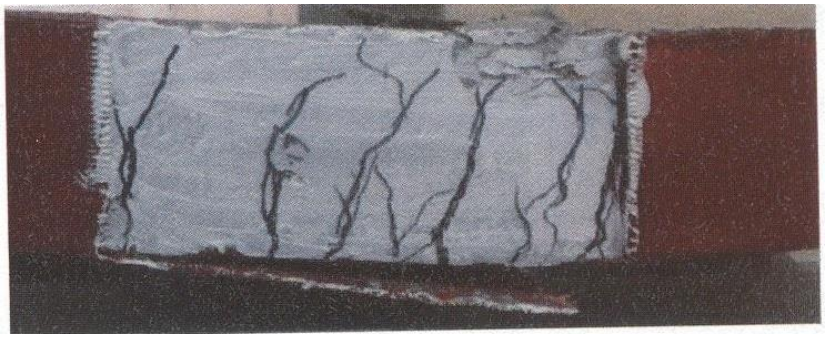

(b) Experiment (Kumar, 2015)

Figure 5.45 Crack pattern at failure for C1-GFRP-B13

Figure 5.46, Figure 5.47 and Figure 5.48 show the comparison of finite element model crack pattern at failure load for the shear strengthened beam in shear zone with experimental beam type C1-BFRP-B21, C1-CFRP-B22 and C1-GFRP-B23 respectively. The failure pattern obtained from ANSYS 14.0 agrees well the experimental beams. Many flexure cracks observed at the mid span of all three beams which correlates with the flexure mode of failure observed experimentally. As the crushing capability of the SOLID65 element was turn off due to convergence problem, so the crushing related cracks at the top of the beam is not visible. The failure of the C!-CFRP-B22 beam occur pre maturely due to its high modulus of elasticity which was also observed during the experimental program conducted by Kumar, 2015.

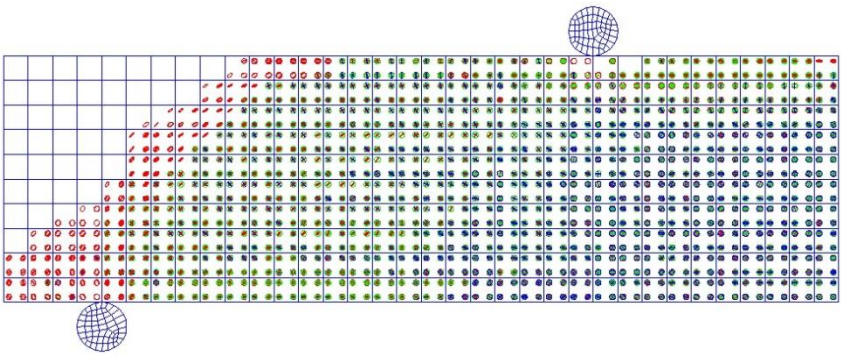

(a) Present study

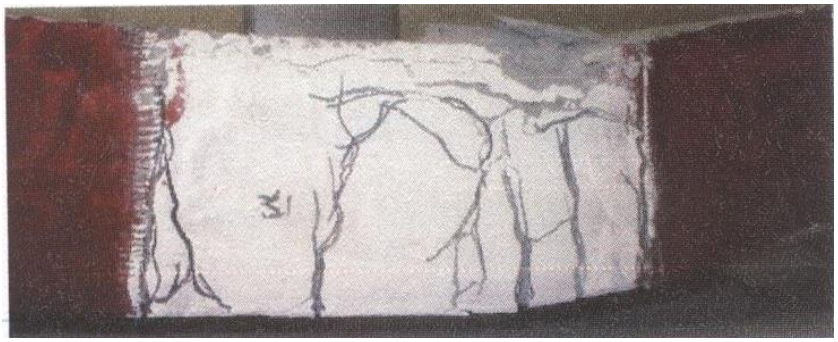

(b) Experiment (Kumar, 2015)

Figure 5.46 Crack pattern at failure for C1-BFRP-B21

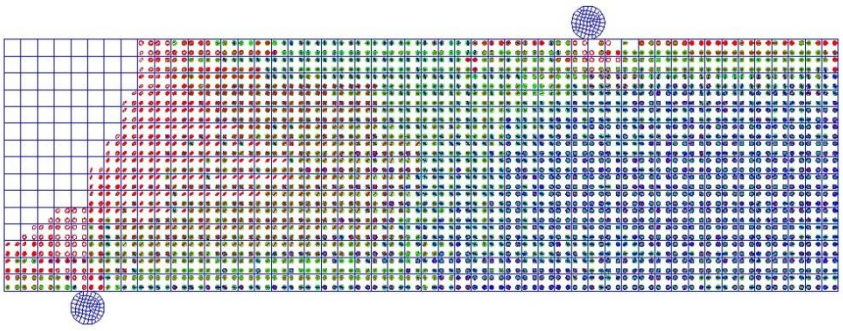

(a) Present study

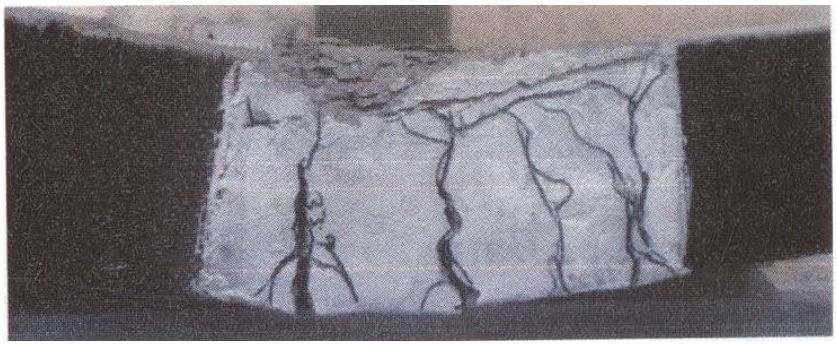

(b) Experiment (Kumar, 2015)

Figure 5.47 Crack pattern at failure for C1-CFRP-B22

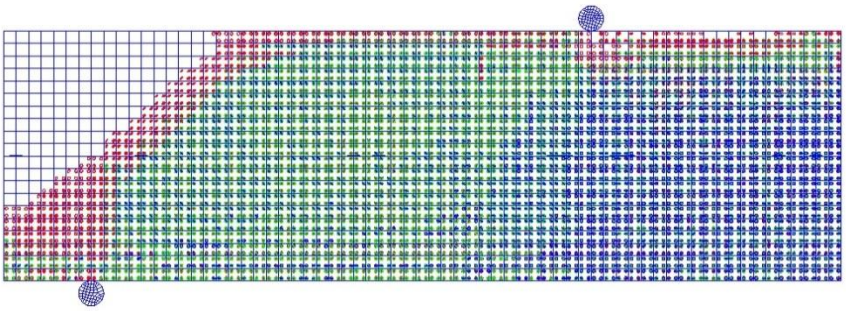

(a) Present study

(b) Experiment (Kumar, 2015)

Figure 5.48 Crack pattern at failure for C1-GFRP-B23

The crack pattern obtained at failure loads from FEA for the shear strengthened RC beam with strip FRP for beam type C1-BFRP-B31, C1-CFRP-B32 and C1-GFRP-B33 are shown in Figure 5.49, Figure 5.50 and Figure 5.51 respectively which demonstrate a good agreement when compare with the experimental crack pattern. As explained earlier for the shear strengthened beams. In this case also the failure is dominant by the flexure mode. Further some mild diagonal tensile cracks are observed between the spacing of the strip which was arrested by the FRP strips which was also observed during the experimental program.

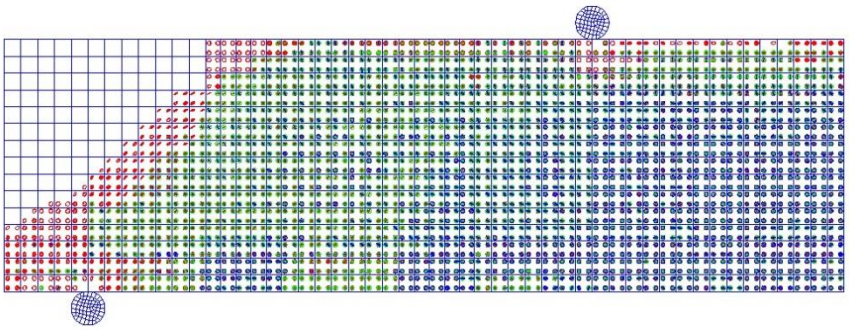

(a) Present study

(b) Experiment (Kumar, 2015)

Figure 5.49 Crack pattern at failure for C1-BFRP-B31

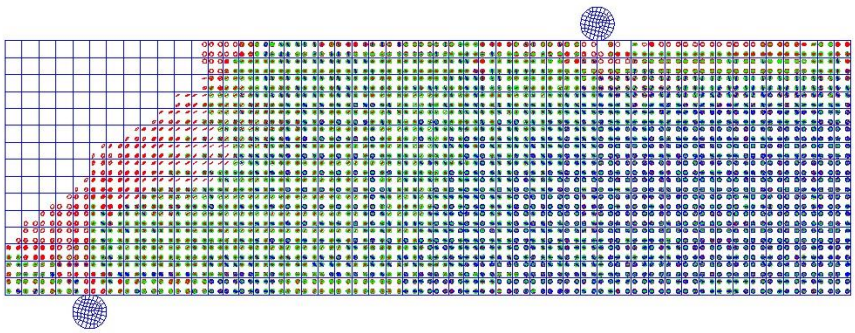

(a) Present study

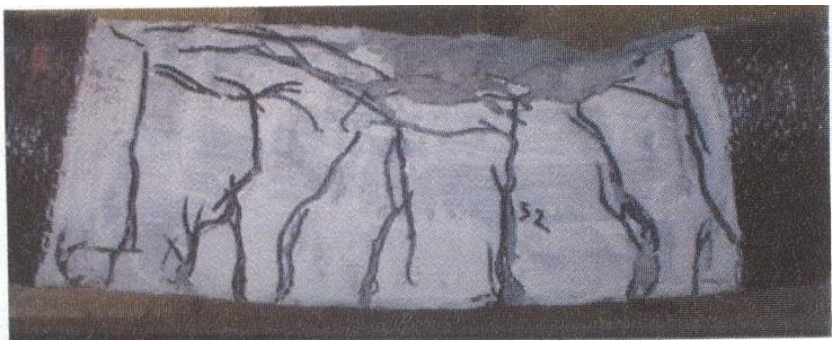

(b) Experiment (Kumar, 2015)

Figure 5.50 Crack pattern at failure for C1-CFRP-B32

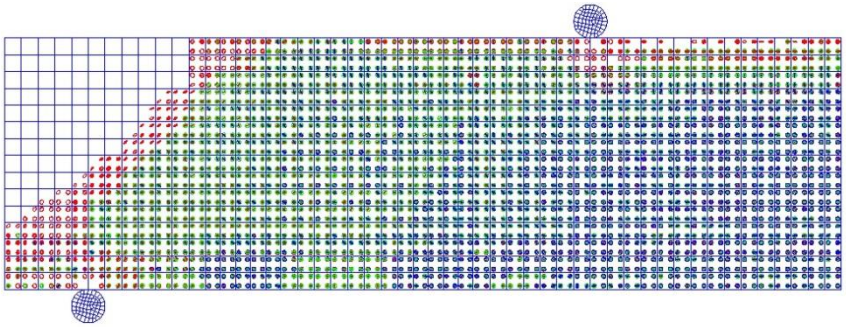

(a) Present study

(b) Experiment (Kumar, 2015)

Figure 5.51 Crack pattern at failure for C1-GFRP-B33

Figure 5.52 shows the crack pattern from analytical study and experimental study agrees very well for control reinforced concrete beam C2-B0 with concrete strength of 39.11 MPa. Several flexural cracks are observed at the constant moment region after the yielding of the tensile reinforcement which causes the failure of the beam in flexure. Again the crushing related crack is not seen at the top face of the FEM RC beam.

Figure 5.53, Figure 5.54 and Figure 5.55 illustrate the comparison of crack pattern at failure load obtained from finite element analysis with experimental beam for complete wrapping of RC beam with BFRP, CFRP and GFRP respectively which shows a good agreement. The failure mode of the all the three beams are due to flexural cracks occurring at the mid span. The failure in case experimental study was shown by rupture of FRP sheet. But in ANSYS 14.0 the failure of the FRP cannot be seen.

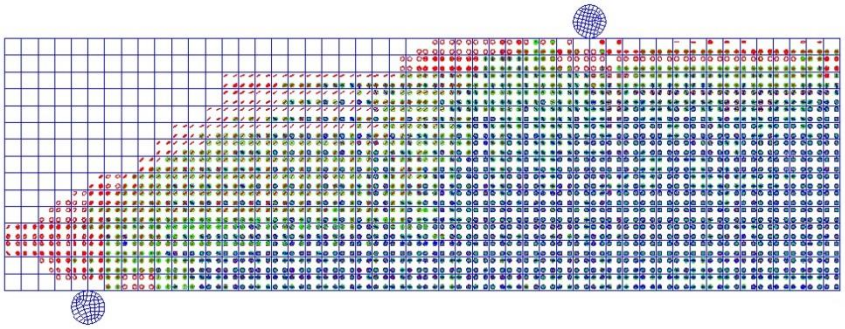

(a) Present study

(b) Experiment (Kumar, 2015)

Figure 5.52 Crack pattern at failure for control beam C2-B0

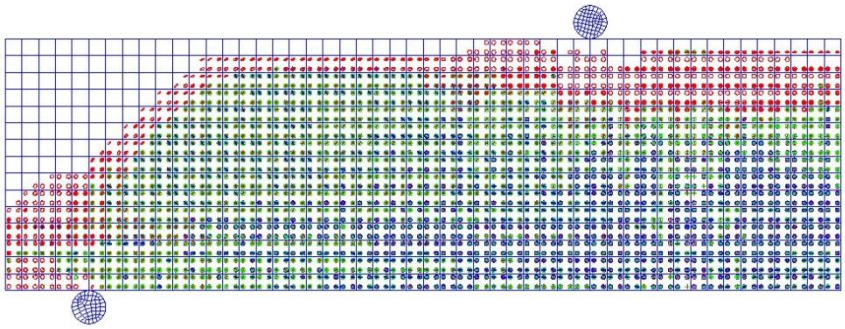

(a) Present study

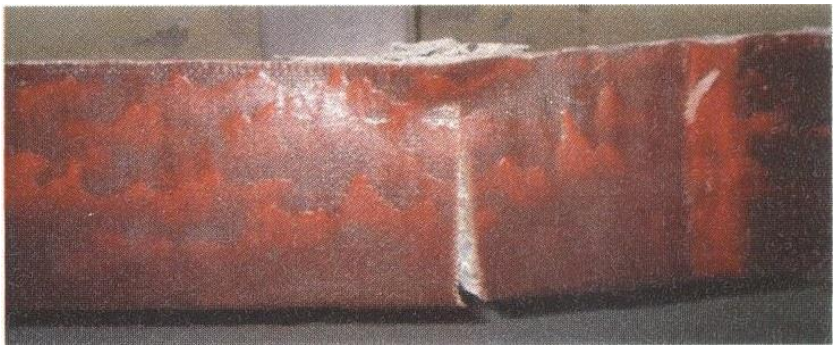

(b) Experiment (Kumar, 2015)

Figure 5.53 Crack pattern at failure for C2-BFRP-B11

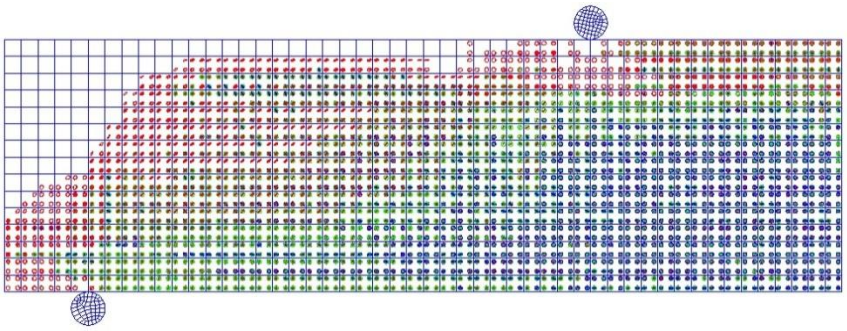

(a) Present study

(b) Experiment (Kumar, 2015)

Figure 5.54 Crack pattern at failure for C2-CFRP-B12

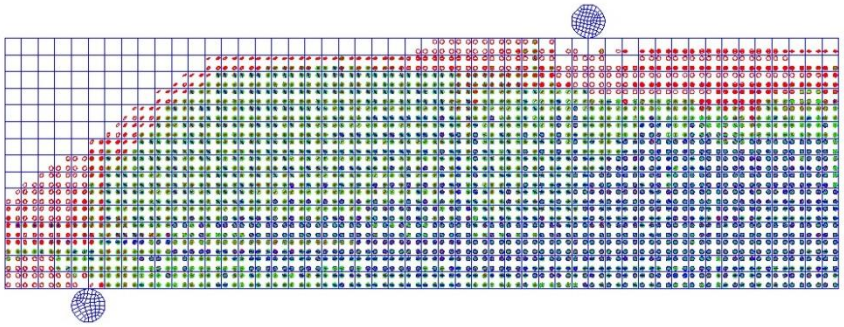

(a) Present study

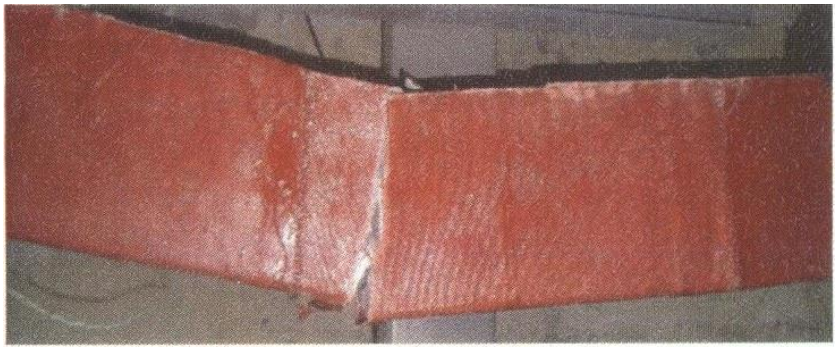

(b) Experiment (Kumar, 2015)

Figure 5.55 Crack pattern at failure for C2-GFRP-B13

Figure 5.56, Figure 5.57 and Figure 5.58 shows the crack pattern for flexure shear strengthened beam types C2-BFRP-B21, C2-CFRP-B22 and C2-GFRP-B23 respectively with concrete strength C2=39.11 MPa. The crack patterns observed are similar with flexural-shear strengthening of RC beam with concrete strength C1=25.52 MPa.

Figure 5.59, Figure 5.60 and Figure 5.61 demonstrate the crack pattern observed from analytical study correlate well with the experimental crack pattern for flexural shear strengthening of reinforced concrete beam with beam types C2-BFRP-B31, C2-CFRP-B32 and C2-GFRP-B33 respectively. Some minor cracks are observed in space between the FRP strips. The beam type C2-BFRP-B31 and C2-GFRP-B33 fails in flexure due to several flexural crack appear at the constant moment region. For C2-CFRP-B32, flexural crack appears at the mid span along with diagonal tensile crack at the shear zone.

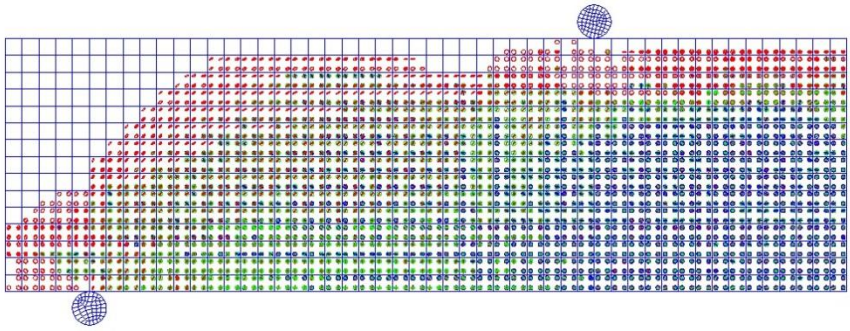

(a) Present study


(b) Experiment (Kumar, 2015)

Figure 5.56 Crack pattern at failure for C2-BFRP-B21

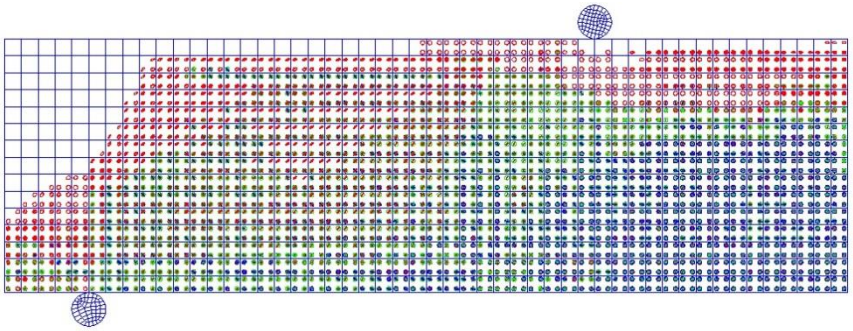

(a) Present study

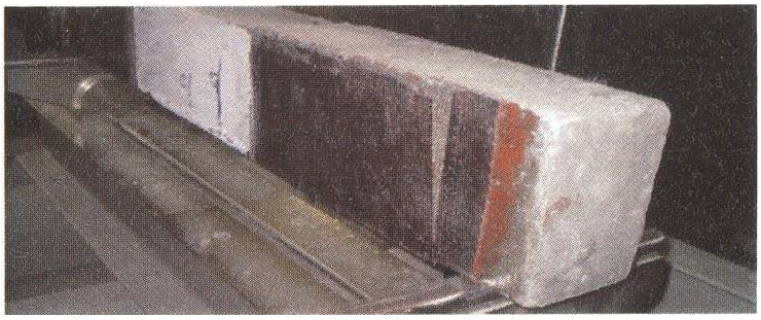

(b) Experiment (Kumar, 2015)

Figure 5.57 Crack pattern at failure for C2-CFRP-B22

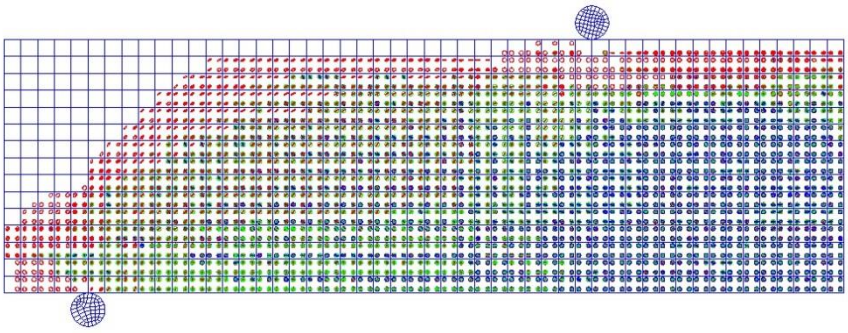

(a) Present study

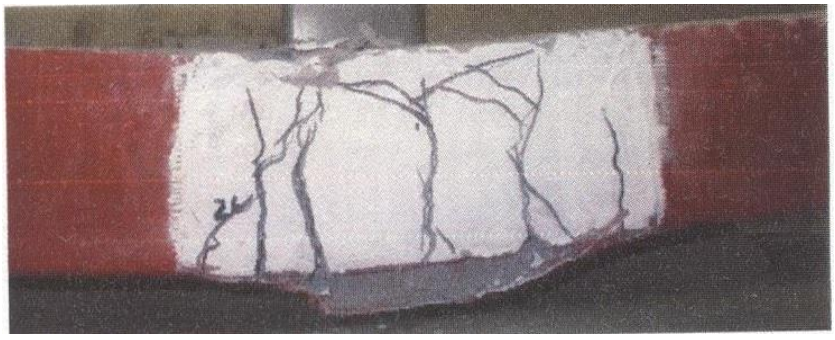

(b) Experiment (Kumar, 2015)

Figure 5.58 Crack pattern at failure for C2-GFRP-B23

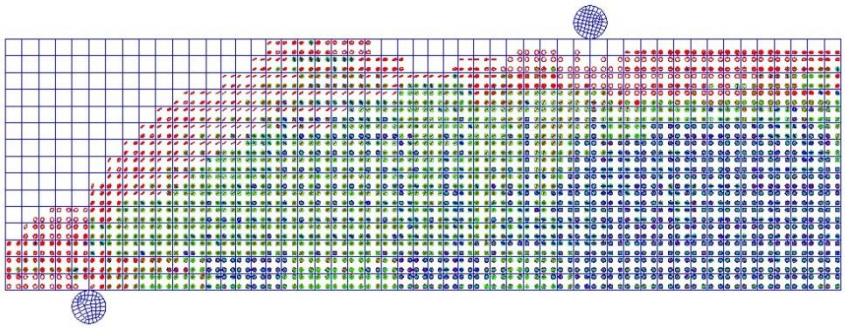

(a) Present study

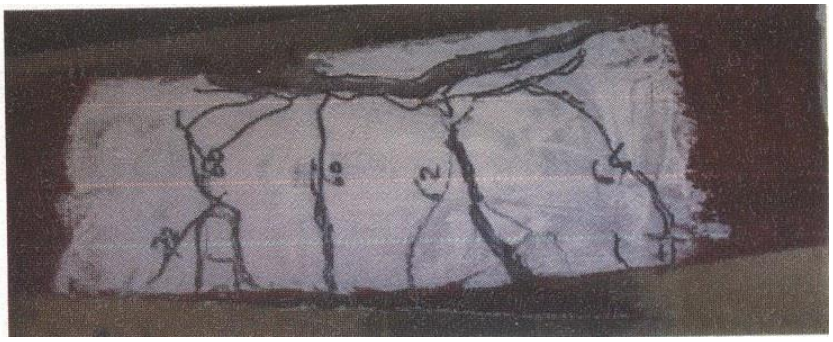

(b) Experiment (Kumar, 2015)

Figure 5.59 Crack pattern at failure for C2-BFRP-B31

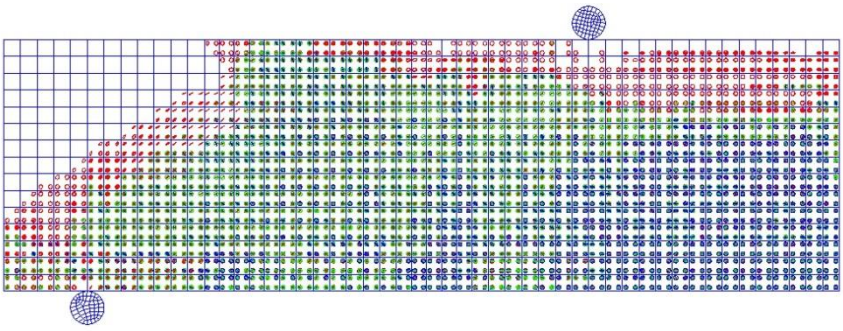

(a) Present study

(b) Experiment (Kumar, 2015)

Figure 5.60 Crack pattern at failure for C2-CFRP-B32

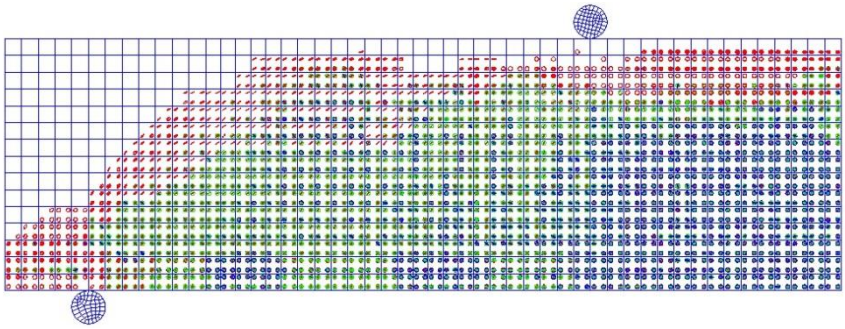

(a) Present study

(b) Experiment (Kumar, 2015)

Figure 5.61 Crack pattern at failure for C2-GFRP-B33

### 5.6.3 Failure loads

The load at which the yielding start in tensile reinforcement acquire from the finite element analysis is compared with experimental yield loads[2] for both concrete strength C1=25.52 MPa and C2=39.11 MPa in Table 5.5 and Table 5.6 respectively which is in between 0% to 16%.

The ultimate loads obtained from finite element analysis are compared with experimental ultimate loads in Table 5.7 and Table 5.8 for concrete strength C1 and C2 respectively. The table shows the increase in the ultimate load of FEM results over the experimental results.

The FRP reinforced RC beam flexural and shear strength can also be estimated using the design models proposed by different researchers. The design model proposed by Toutanji et al., 2006[101] to estimate the FRP strengthened beam in flexure by adding the contributions from steel reinforcement[102] and FRP.

$$P_1 = 6A_s f_y d/l - 3.54\left(A_s f_y\right)^2 \Big/ \left(f_{ck} bl\right) + 6A_f E_f R\varepsilon_{fu}\left(h-x\right)/l \qquad (5.1)$$

Barros et al., 2007[73] also proposed a Eqn. (5.2) for flexural strength adopted from ACI 440.2R-08[48].

$$P_2 = 6A_s f_y \left(d - 0.4x\right)/l + 5.1A_f E_f R\varepsilon_{fu} \left(h - 0.4x\right)/l \quad (5.2)$$

Where, $R$ is the reduction factor which is general taken to account for pre cracking equal to 0.5 for both models.

Table 5.5 Comparison of experimental and FEA yield loads for C1 group

| Beam ID | EXP yield load (kN) | FEA yield load (kN) | Differences (%) |
|---|---|---|---|
| C1-B0 | 45.83 | 45.84 | -0.02 |
| C1-BFRP-B11 | 72.95 | 66.624 | 8.67 |
| C1-CFRP-B12 | 76.63 | 81.18 | -5.94 |
| C1-GFRP-B13 | 71.82 | 67.362 | 6.21 |
| C1-BFRP-B21 | 63.06 | 65.66 | -4.12 |
| C1-CFRP-B22 | 62.09 | 68.91 | -10.98 |
| C1-GFRP-B23 | 70.21 | 65.26 | 7.05 |
| C1-BFRP-B31 | 59.06 | 61.2 | -3.62 |
| C1-CFRP-B32 | 64.35 | 68.59 | -6.59 |
| C1-GFRP-B33 | 64.25 | 61.8 | 3.81 |

Table 5.6 Comparison of experimental and FEA yield loads for C2 group

| Beam ID | EXP yield load (kN) | FEA yield load (kN) | Differences (%) |
|---|---|---|---|
| C2-B0 | 48.46 | 55.05 | -13.60 |
| C2-BFRP-B11 | 71.81 | 69.36 | 3.41 |
| C2-CFRP-B12 | 57.86 | 63.98 | -10.58 |
| C2-GFRP-B13 | 59.62 | 68.90 | -15.57 |
| C2-BFRP-B21 | 63.93 | 63.68 | 0.38 |
| C2-CFRP-B22 | 96.26 | 86.04 | 10.62 |
| C2-GFRP-B23 | 56.02 | 64.32 | -14.82 |
| C2-BFRP-B31 | 58.85 | 67.97 | -15.49 |
| C2-CFRP-B32 | 83.07 | 84.00 | -1.12 |
| C2-GFRP-B33 | 64.46 | 67.03 | -3.99 |

Table 5.7 Comparison of experimental and FEA ultimate loads for C1 group

| Beam ID | EXP ultimate load (kN) | FEA ultimate load (kN) | Differences (%) | Increased in ultimate load |
|---|---|---|---|---|
| C1-B0 | 45.83 | 53.60 | -16.95 | 1.00 |
| C1-BFRP-B11 | 77.80 | 89.56 | -15.12 | 1.67 |
| C1-CFRP-B12 | 95.12 | 114.60 | -20.47 | 2.14 |
| C1-GFRP-B13 | 86.52 | 87.36 | -0.97 | 1.63 |
| C1-BFRP-B21 | 73.57 | 82.40 | -12.00 | 1.54 |
| C1-CFRP-B22 | 70.09 | 84.24 | -20.19 | 1.57 |
| C1-GFRP-B23 | 80.34 | 81.60 | -1.57 | 1.52 |
| C1-BFRP-B31 | 66.75 | 79.08 | -18.47 | 1.48 |
| C1-CFRP-B32 | 75.25 | 83.66 | -11.18 | 1.56 |
| C1-GFRP-B33 | 69.84 | 77.76 | -11.34 | 1.45 |

Table 5.8 Comparison of experimental and FEA ultimate loads for C2 group

| Beam ID | EXP ultimate load (kN) | FEA ultimate load (kN) | Differences (%) | Increased in ultimate load |
|---|---|---|---|---|
| C2-B0 | 52.34 | 63.72 | -21.74 | 1.00 |
| C2-BFRP-B11 | 89.68 | 102.27 | -14.04 | 1.60 |
| C2-CFRP-B12 | 71.08 | 107.50 | -51.24 | 1.69 |
| C2-GFRP-B13 | 71.69 | 99.77 | -39.17 | 1.57 |
| C2-BFRP-B21 | 68.79 | 91.01 | -32.30 | 1.43 |
| C2-CFRP-B22 | 99.95 | 120.56 | -20.62 | 1.89 |
| C2-GFRP-B23 | 67.99 | 88.85 | -30.68 | 1.39 |
| C2-BFRP-B31 | 73.08 | 87.84 | -20.20 | 1.38 |
| C2-CFRP-B32 | 83.07 | 109.16 | -31.41 | 1.71 |
| C2-GFRP-B33 | 77.21 | 86.28 | -11.75 | 1.35 |

For calculating the shear capacity of FRP reinforced RC beam, can be evaluated by taking the contribution from concrete [103], transverse steel reinforcement [104,105] and FRP expressed as below

$$V_T = 0.44\left(1-0.35\,a_v/d\right)\sqrt{f_{ck}}bd + \left(A_v f_y/s\right)d\cot\theta + V_f \tag{5.3}$$

Where $V_f$ is the FRP contribution in shear.

The FRP contribution suggested by the researchers Lee et al., 2011[103] (Eqn. (5.4)) adopted from the ACI 440.2R-08[48].

$$V_f = 2\left(t_f/b\right)\left(w_f/s_f\right)R(\sin\beta+\cos\beta)d_f bf_{fu} \tag{5.4}$$

Where $R$ is the reduction factor can be estimated with the maximum value of $0.004/\varepsilon_{fu}$ as suggested by Jayaprakash et al., 2008[106] and El-Ghandour, 2011[107].

The combine flexural shear strength design models are not available. So, the flexural strength obtained from Eqn. (5.2) is combined individually with the Eqn. (5.3) to obtain the ultimate load for the flexural shear strengthens. The shear strength values for complete wrap beam consider being same as that of RC beam strengthened in shear zone only. The shear strength is calculated by adding the shear strength with the flexural strength of control RC beam. Table 5.9 and Table 5.10 show the comparison of FEA ultimate load with design models for flexural-shear and shear strengthens. From the table it is found that the FEA ultimate load gives comparative values for BFRP and GFRP strengthened RC beams.

Table 5.9 Comparison of FEA ultimate loads for flexural shear strengthening

| **Beam ID** | **FEA ultimate load (kN)** | **$P_{theo}$ (kN)** | **$P_{theo}/P_{fea}$** |
|---|---|---|---|
| C1-B0 | 53.60 | 54.72 | 1.02 |
| C2-B0 | 63.72 | 59.36 | 0.93 |
| C1-BFRP-B11 | 89.56 | 98.61 | 1.10 |
| C1-CFRP-B12 | 114.60 | 142.30 | 1.24 |
| C1-GFRP-B13 | 87.36 | 92.96 | 1.06 |
| C2-BFRP-B21 | 91.01 | 104.50 | 1.15 |
| C2-CFRP-B22 | 120.56 | 148.33 | 1.23 |
| C2-GFRP-B23 | 88.85 | 98.57 | 1.11 |
| C2-BFRP-B31 | 87.84 | 95.21 | 1.08 |
| C2-CFRP-B32 | 109.16 | 123.06 | 1.13 |
| C2-GFRP-B33 | 86.28 | 89.63 | 1.04 |

Table 5.10 Comparison of FEA ultimate loads for shear strengthening

| Beam ID | FEA ultimate load (kN) | $P_{theo}$ (kN) | $P_{theo}/P_{fea}$ |
|---|---|---|---|
| C1-BFRP-B21 | 82.40 | 88.12 | 1.07 |
| C1-CFRP-B22 | 84.24 | 119.18 | 1.41 |
| C1-GFRP-B23 | 81.60 | 87.01 | 1.07 |
| C1-BFRP-B31 | 79.08 | 78.83 | 1.00 |
| C1-CFRP-B32 | 83.66 | 93.92 | 1.12 |
| C1-GFRP-B33 | 77.76 | 78.07 | 1.00 |
| C2-BFRP-B11 | 102.27 | 94.09 | 0.92 |
| C2-CFRP-B12 | 107.50 | 134.85 | 1.25 |
| C2-GFRP-B13 | 99.77 | 92.98 | 0.93 |

## 5.7 REMARKS

The finite element model adopted for the modeling of reinforced concrete beam strengthened with externally bonded FRP sheet reasonable agree with the experimental results. Further the crack pattern at failure load agrees well with the crack pattern observed during the experimental. The element type and material data use for analysis of reinforced concrete portal discussed in next section.

# CHAPTER 6

# FE MODELING OF RC PORTAL

## 6.1 GENERAL

A simple 2D reinforced concrete portal is primarily design using SAP2000[108] for gravity and earthquake load (using response spectrum) is modeled analytical using finite element tool for lateral load analysis. From the analytical study of RC portal design with only gravity load, the failure of portal is studied. Then the RC portal is reinforced externally with different layer of CFRP sheets to increase its stiffness and performance during an earthquake.

The concrete, steel reinforcement and CFRP are modeled with SOLID65, LINK180 and membrane only option SHELL181 element. The compressive strength of concrete used in the study is C1=25.52 MPa, Fe500 grade of steel material property is used for the steel reinforcement and the material property of CFRP sheet is adopted from Niroomandi et al. (2010) shown in Table 3.2.

## 6.2 GEOMETRY AND NUMERICAL MODELING

The RC portal designed using SAP2000[108] with uniformly distributed dead load of 16 kN/m and live load of 6 kN/m. The length of beam is 5 m and column is 3 m high. The cross section of column and beam are 280 mm X 280 mm and 320 mm X 280 mm respectively. Figure 6.1 shows the geometry of RC portal design with gravity load only used for finite element analysis.

The second RC portal design in SAP2000[108] includes earthquake load in addition to the gravity load. The earthquake load given using response spectra of zone V, medium soil type and maximum considered earthquake from IS 1893 (part1):2002[109]. Figure 6.2 shows the response spectra used in design. The dimensions of the portal are identical, only longitudinal column reinforcement increase to 25 mm diameter bar instead of 20 mm diameter bar.

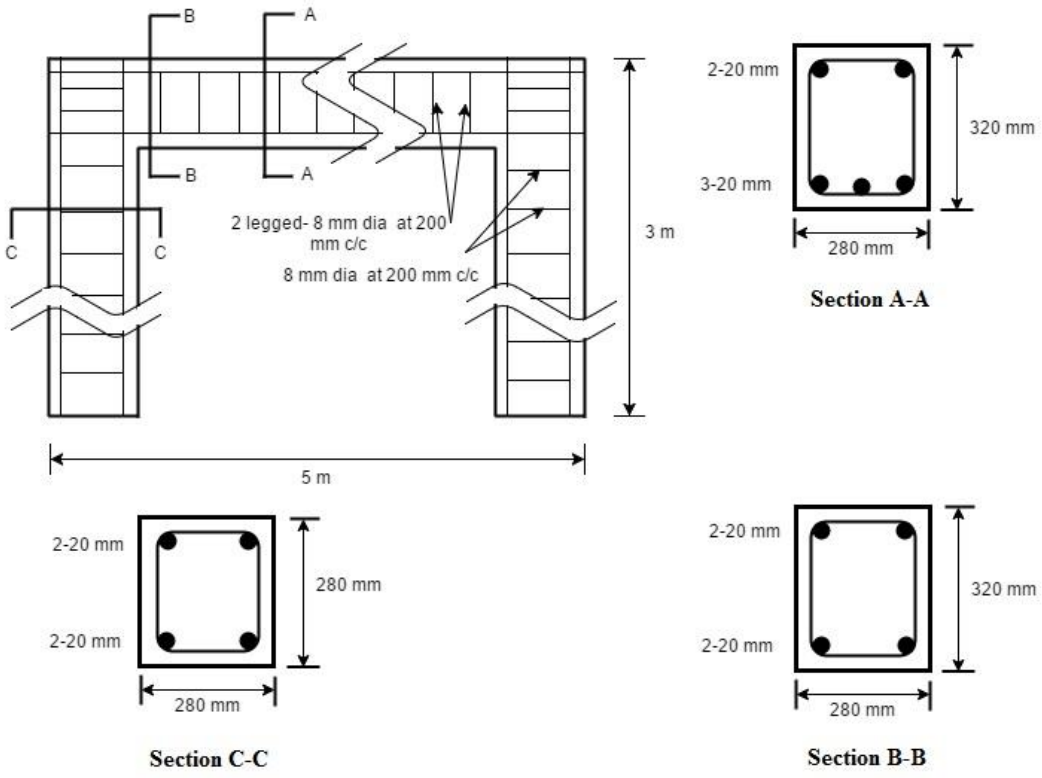


Figure 6.1 Details of RC portal design with only gravity load

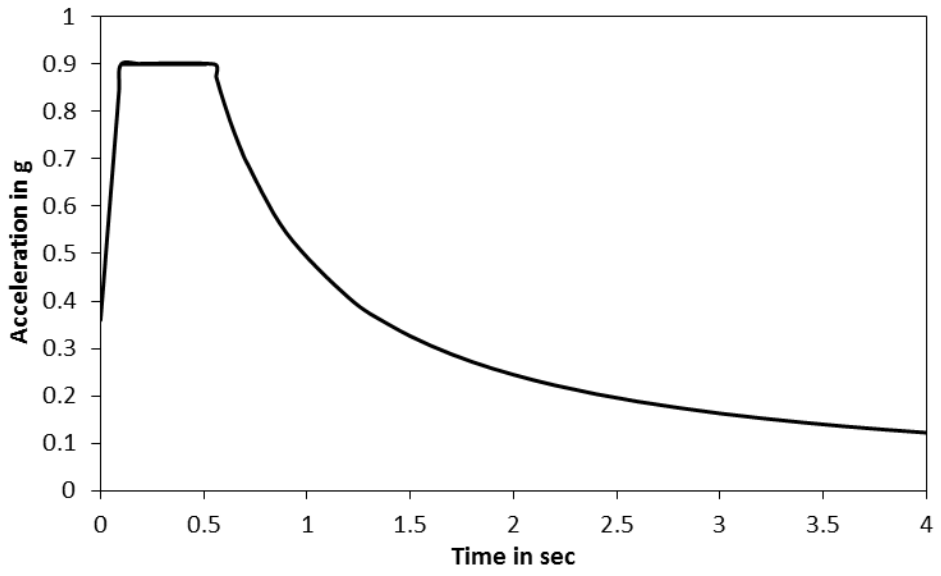


Figure 6.2 Response spectra used in the design[109]

Based on the crack condition of unreinforced or conventional RC portal, the different layer of CFRP sheet bonded around the top and bottom of both columns with fiber orientation along the column axes. The length of the CFRP sheet is one meter at both locations as shown in Figure 6.3 which is used for finite element analysis by

strengthening the column part only. There was no increase in the ductility in the RC portal when analyzed by only retrofitting the column. So, in addition to column, single layer CFRP affix to the top and bottom portion of the beam near the beam-column joint to a length of 1.2 m as shown in Figure 6.4 which is used for comparative study to check number of layers of CFRP required for continue use of portal during seismic event.

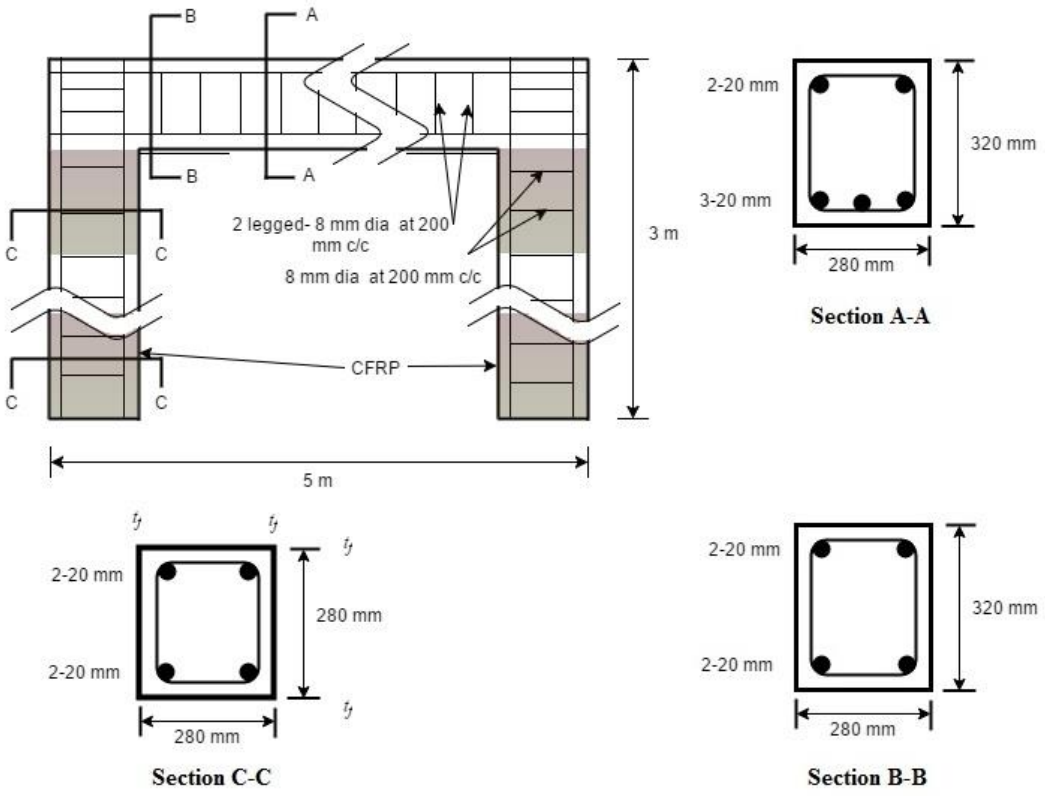


Figure 6.3 Details of strengthened portal: only column reinforced with CFRP

The 3D model of portal for lateral load analysis is modeled using finite element tool ANSYS 14.0. The numerical modeling of portal uses the same elements as described for the modeling of RC beam. Bottom of both column are fixed and a lateral load is applied gradually at the top of the column near the center the of the beam section for lateral load analysis. Figure shows the complete model of portal generated in ANSYS 14.0 with boundary condition and loading. The nonlinear process is same as adopted for the RC beam.

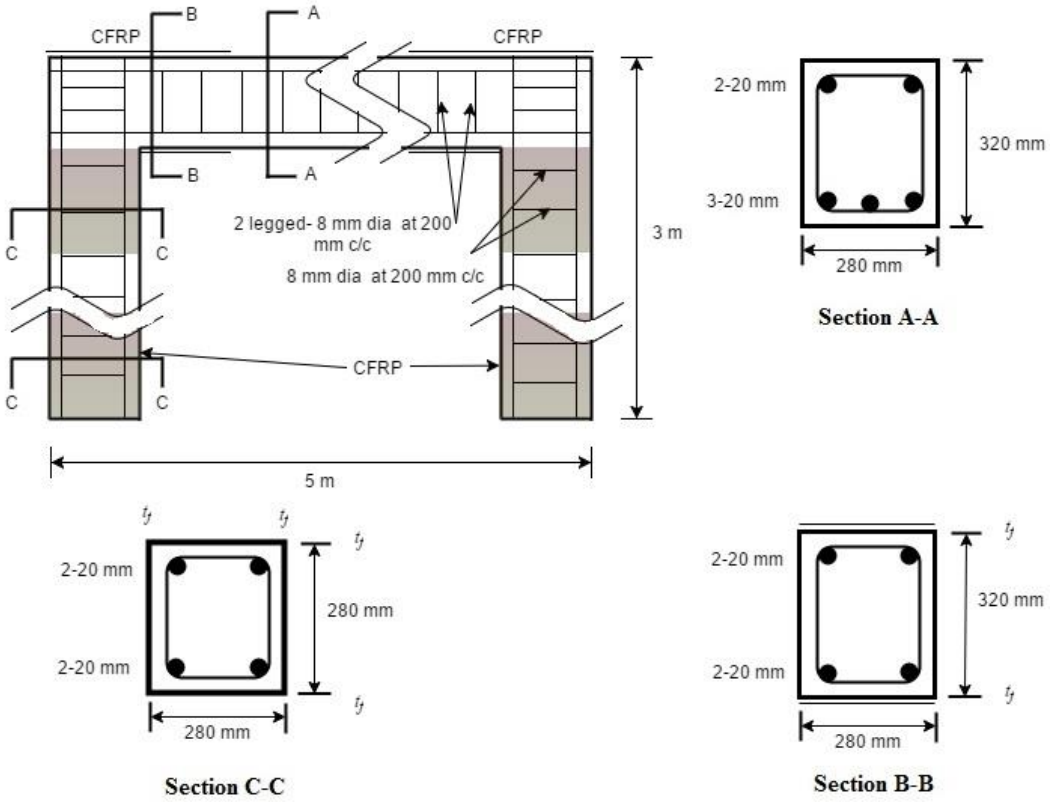


Figure 6.4 Details of strengthened portal: column and beam reinforced with CFRP

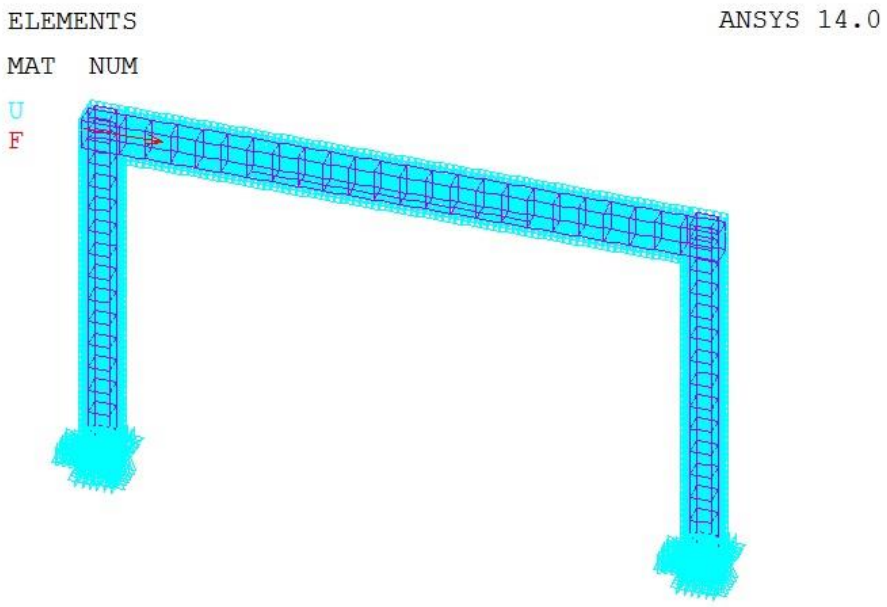


Figure 6.5 Finite element model of RC portal

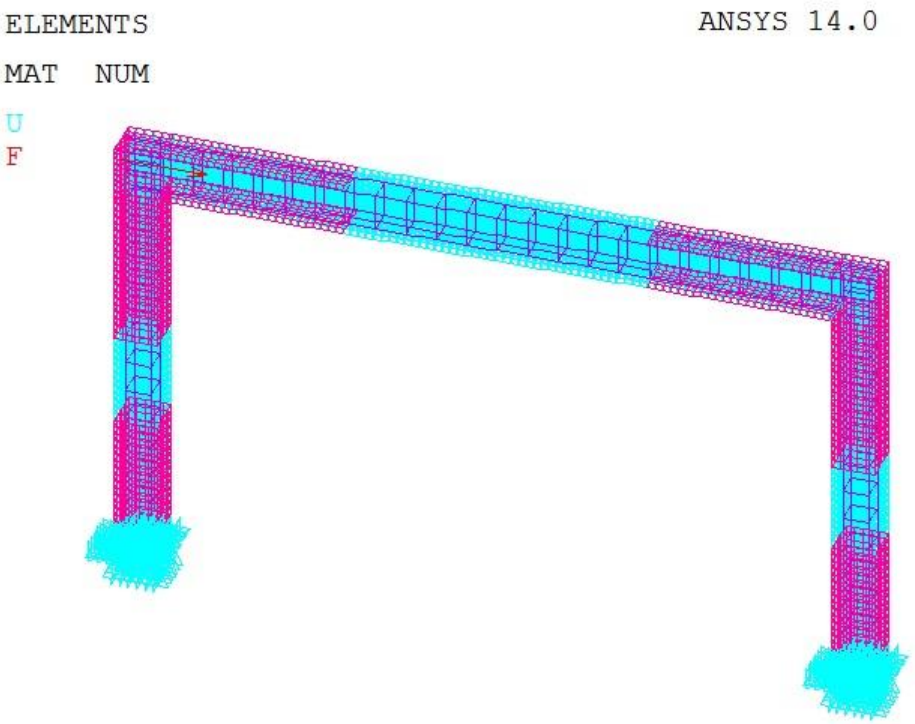


Figure 6.6 Finite element model of FRP reinforced portal

## 6.3 RESULT AND DISCUSSION

The finite element analysis of the RC portal design with gravity load carried out to understand its behavior under lateral load. The crack pattern from finite element analysis at the last converged step is shown in Figure 6.7.


Figure 6.7 Crack pattern for portal design with gravity load

As expected the behavior of RC portal under lateral loading is observed in the crack pattern obtained from finite element analysis. The first crack appears at the bottom right column. The portal fails due to several cracks occurring at the bottom right column. The maximum strain in concrete at the last converged load step found to be at the bottom right column near the fixed support which confirm the failure of RC portal.

Based on the results from lateral load analysis of RC portal, it is externally reinforced with different reinforcing scheme using single layer CFRP sheet of thickness 0.165 mm. The different reinforcing scheme summarized in Table 6.1. The load deflection plot obtained from finite element analysis is compared with unreinforced portal shown in Figure 6.8. From the load deflection plot, it is noticed that when only the column of portal is reinforced with CFRP (scheme R1 and R2), it enhance the strength of the portal but not the ductility.

Table 6.1 Reinforcing scheme used to strengthened RC portal

| **Designation** | **Details** |
|---|---|
| R0 | Unreinforced RC portal |
| R1 | Bottom part of column strengthened with 1 m length |
| R2 | Top and bottom of column strengthened with 1 m length |
| R3 | Both beam and column strengthened |

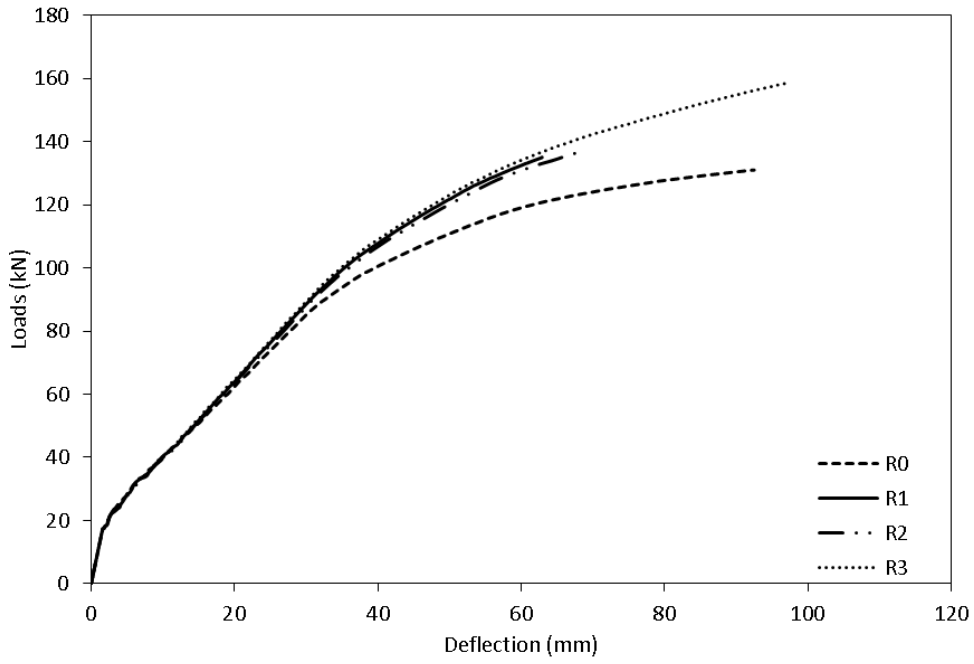


Figure 6.8 Load deflection plot for reinforcing scheme used for portal

When both beam and column of the portal reinforced with single layered CFRP. Load deflection plot shows that it significantly enhances the strength and ductility of the unreinforced RC portal.

Top and bottom part of column up to one meter length reinforced with one to three layers of CFRP and analyzed for lateral loads. The load deflection plot from finite element analysis compared with unreinforced portal as shown in Figure 6.9.

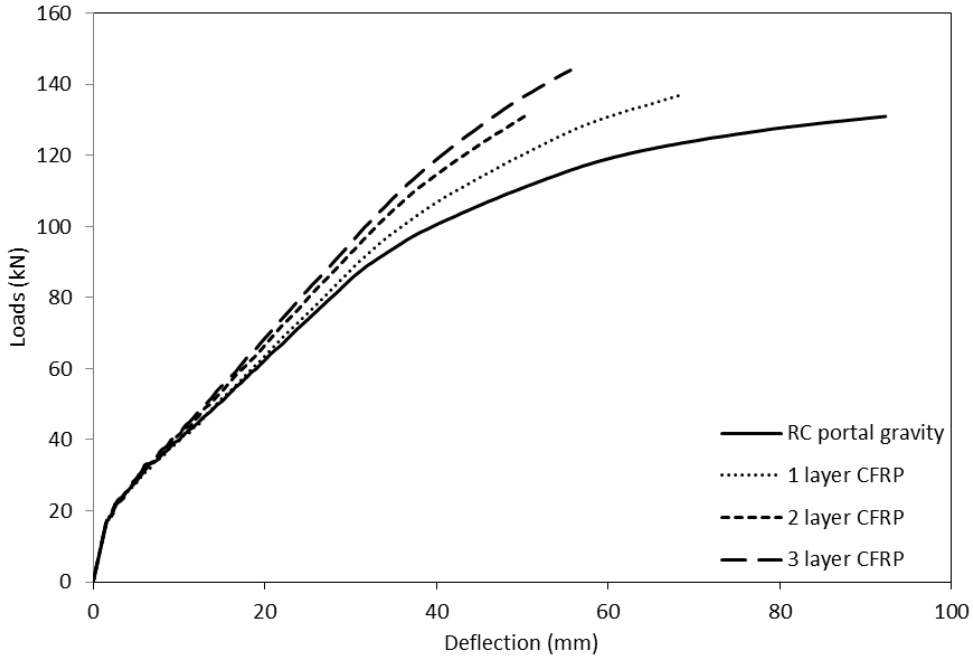


Figure 6.9 Load deflection plot for portal reinforced with different layers of CFRP

The Figure 6.9 shows the increase in the post crack strength of the reinforced concrete portal with increasing layer of CFRP sheets but no further increment is noticed in the strengthened portal due to attainment of limit strain in CFRP in the top section of the column. The present results corroborated with the research done by Coccia et al. (2005) for thickness of FRP ranging from 0.2 to 1.6 mm using ATENA program.

The reinforced concrete structures constructed over many years may be in need of strengthening due to introduction of seismic codes. Also, the RC portal which was design only for gravity load may not be able to sustain seismic loads. So, a comparative study is carried out to check the number of layers of CFRP required to strengthened the RC portal for their continue use. For this, RC portal is design with earthquake load (using response spectra) in addition to gravity loads for comparison with RC portal design with gravity load and retrofitted with different layers of CFRP. All the said

portals are modeled analytically for lateral loads analysis using finite element analysis. The beam and column of the portal is retrofitted as shown in Figure 6.4, in which only column is retrofitted with different layers of CFRP and the beam is retrofitted with single layer of CFRP for all cases. The load deflection plot obtained from finite element model for all portals are shown in Figure 6.10 for the comparison.

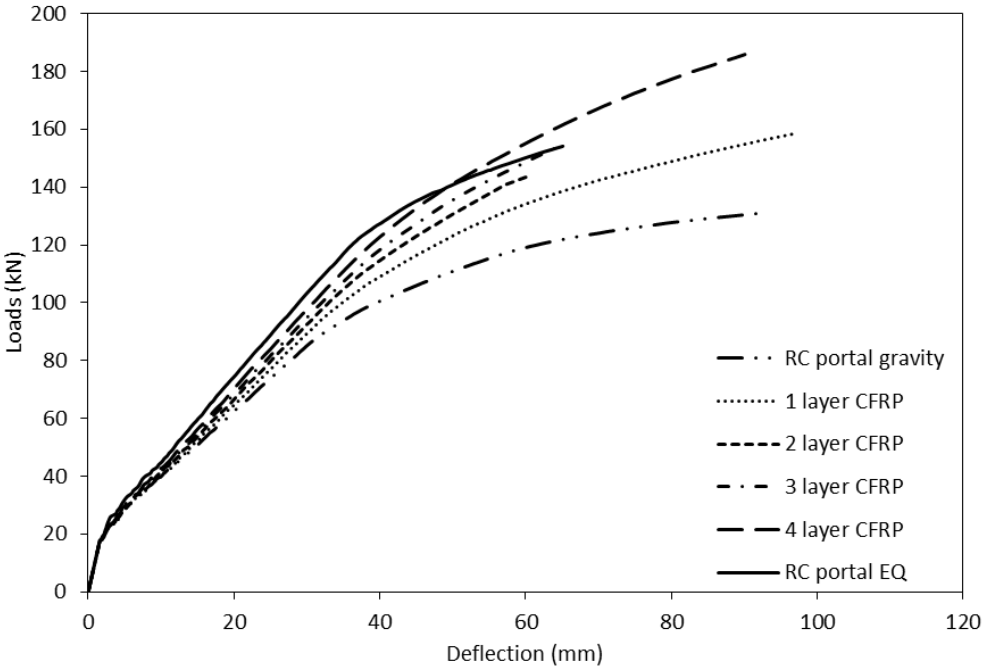


Figure 6.10 Load deflection plot for comparative study

Figure 6.10 shows that with increase in CFRP layer, both strength and ductility of the unreinforced portal increases. Three layer of CFRP is sufficient to increase the strength of the RC portal design with gravity load only but no further increase in the behaviour is noted. So, the four layer of CFRP can significantly improve both strength and ductility of the portal when subjected to seismic loading. The post cracking stiffness of the unreinforced gravity portal increases with increase in the number of layers. Table shows the comparison of strength enhancement of CFRP reinforced portal with unreinforced portal. From which it is found that using four layers of CFRP to retrofit column section increases the strength by 40% which is sufficient for the considered portal to resist during a MCE earthquake.

The load deflection plot observation corroborates with the work of the Coccia et al., 2005[4] on nonlinear analysis of FRP reinforced frames using ATENA program. The numerical analysis on simple RC portal was studied for FRP thickness 0.2 to 1.6 mm.

Table 6.2 Comparison of ultimate loads with unreinforced portal

| Portal | Ultimate load (kN) | Maximum deflection (mm) | Compared with unreinforced portal |
|---|---|---|---|
| RC portal gravity | 131.00 | 92.33 | 1.00 |
| 1 layer CFRP | 158.70 | 97.32 | 1.21 |
| 2 layer CFRP | 143.80 | 60.38 | 1.10 |
| 3 layer CFRP | 154.80 | 65.29 | 1.18 |
| 4 layer CFRP | 185.90 | 90.10 | 1.42 |
| RC portal EQ | 154.20 | 65.12 | 1.18 |

The CFRP layers relocate the failure of portal. For RC portal design with gravity, the maximum strain found at the bottom of the right column. After strengthening the bottom and top part of column with CFRP the strain developed at the top of the column. For 2 and 3 layers of CFRP, the portal fails due to attainment of effective strain in CFRP in the top section of column. Now, when the portal is reinforced with four layers of CFRP, the crack is distributed near the unreinforced section above one meter from the fixed end. The failure in the portal is due maximum strain develop at top and bottom section of the column.

Using CFRP layers for strengthening RC portal relocates the strain from the fixed end of the right column to the weaker section with decrease in the maximum strain. With increase in CFRP layer the location of the maximum strain changes to near weak section. In the four layers CFRP reinforced portal the strain relocates significantly.

## 6.4 REMARKS

The lateral load analysis using FEA conducted to check the behaviour of RC portal reinforced externally with CFRP laminates shows significant increase in strength and ductility with increase in the number of layers. Four layers of CFRP sheet found to be sufficient in enhancing the performance of portal design with gravity load to sustain earthquake loading. The next chapter concludes the dissertation with future scopes.

# CHAPTER 7

# CONCLUSIONS AND FUTURE SCOPE

## 7.1 CONCLUSIONS

### 7.1.1 Conclusions for FEM of confined concrete member

The present study focused on developing a nonlinear finite element model to predict the behaviour of the confined concrete cylinder under uniaxial compression. Also, the flexure and fracture behaviour of FRP affix concrete prism under four points and three point bending yields the following conclusions:

- The main aim of the study was to check the reliability and accuracy of simulation of concrete cylinder confined with BFRP, CFRP and GFRP sheets in ANSYS 14.0. The present FRP confined concrete finite element model was validated with experimental work from literature which shows that finite element model meticulously validates the model. So, the present model can be used to predict the FRP confined concrete strength for different material properties..
- The peak stress from finite element analysis was compared with various FRP confined concrete design models from literature. The comparison shows that the model proposed by ACI 440.2R-08 effectively predicts the peak confined concrete strength for all types of FRP used in the study.
- The analysis oriented models predict the axial stress-strain behaviour accurately for present CFRP confined concrete finite element model.
- The finite element model built to check accuracy and reliability of simulation of testing of flexural and fracture strength of concrete prism strengthened with FRP yields results which agrees well with experimental testing. Further the result confirms that the CFRP is more efficient than GFRP and BFRP in strengthening of concrete prism for flexural and fracture strength.

### 7.1.2 Conclusions for FEM of strengthened RC beam

The use of nonlinear finite element method to examine FRP strengthened RC beam was evaluated. The following conclusions were drawn from simulation of strengthened RC beam using ANSYS 14.0:

- The loading arrangement by creating contact between the beam surfaces and loading cylinder significantly reduces the stress concentration and contributes to distribution of stress at the loading surface of the beam.
- The minimum concrete cover to main steel reinforcement found to be effective for shear strengthened RC beams.
- The accepted performance of FE model for FRP strengthened reinforced concrete beam interpreted by load deflection plots shows a good agreement with the experimental data with slight deviations. The yield loads obtained from finite element analysis was accurately compared with experimental data. The ultimate loads from FE analysis show reasonable agreement.
- The FEM model adopted further corroborates that the BFRP, CFRP and GFRP effectively increases the strength of the conventional RC beam.
- The crack pattern emerging from finite element analysis at the failure indicates almost similar characteristics to those resulting from experiments. The failure mechanism of the strengthened RC beam was modeled quite well using the finite element analysis. The progress of crack pattern in strengthened beam can be clearly understood from the present finite element model.

### 7.1.3 Conclusions for FEM of RC portal

The nonlinear finite element analysis adopted to simulate the behaviour of RC portal with different layers of CFRP sheets corroborates with the work carried out previously in the literature. From obtained load deflection plots it confirm that the increasing the number of CFRP layer increase the structural strength. The strengthening of RC portal with CFRP effectively relocates the position of maximum strain and reduces the plastic spread along the elements. Four layers of CFRP sheets were found to be sufficient to strengthen the RC portal.

The study indicates that FEM modeling of FRP retrofitted systems can be effectively carried out provided that the elements are able to simulate prototype behaviour and boundary conditions are consistent with the existing physical conditions.

## 7.2 FUTURE SCOPE

The present study was limited to FRP strengthening of RC beam and RC portal. Many factors like strain reduction factor of FRP, dilation model of FRP and influence of type of FRP for ultimate condition of confined concrete need further research. Damages due to near field ground motion (NFGM) led to production of new fibers like Dyneema fiber (DFRP), Polyethylene Terephthalate Polyester (PET), Polyethylene Naphthlate (PEN) and others which have properties to absorb energy and large fracturing strain. These FRP needs new research for predicting its design model. The near field ground motion analysis of above FRP using finite element analysis will predicts it relative behaviour during seismic events.

# REFERENCES


[1] Hollaway L, Teng J-G. Strengthening and Rehabilitation of Civil Infrastructures Using Fibre-Reinforced Polymer (FRP) Composites. Woodhead Publishing limited; 2008.

[2] Kumar KVN. Effect of FRP wrapping on performance of RC Beam behaviour. M. Tech Dissertation, Indian Institute of Technology, Roorkee, 2015.

[3] Kumar KVN. Personal Communication 2015a.

[4] Coccia S, Ianniruberto U, Rinaldi Z. Non linear procedure for the analysis of FRP reinforced frames. Improv. Build. Struct. Qual. by New Technol. Proc. Final Conf. COST Action C12, Austria: Taylor & Francis; 2005, p. 207–12.

[5] Richart FE, Brandtzaeg A, Brown RL. A Study of The Failure of Concrete Under Combined Compressive Stresses. Univ Illinois Bulletin 1928;XXVI:110.

[6] Newman K, Newman JB. Failure theories and design criteria for plain concrete. int. civ. enf. mater. Conf. Struct., New York: Wiley interscience; 1969.

[7] Ahmad S, Shah S. Complete triaxial stress-strain curves for concrete. ACSE J Struct Div 1982;108(4):728–42.

[8] Mander JB, Preistley MJ., Park R, ASCE. Theoretical stress-strain model for confined concrete. J Struct Eng 1988;114:1804–26.

[9] Fardis M, Khalili H. FRP-encased concrete as a structural material. Mag Concr Res 1982;34(122):191–202.

[10] Ahmad S, Khaloo A, Irshid A. Behaviour of concrete spirally confined by fiberglass filaments. Mag Concr Res 1991;43(56):143–8.

[11] Saadatmanesh H, Ehsani M, Li M. Strength and ductility of concrete columns externally reinforced with fiber concrete straps. ACI Struct J 1994;91(4):434–47.

[12] Mirmiran A, Kargahi M, Samaan M, Shahawy M. Composite FRP-concrete column with bi-directional external reinforcement. Proc. 1st int. conf. Compos. Infrastruct., Tuscun, Arizona: University of Arizona: 1996.

[13] Miyauchi K, Nishibayashi S, Inoue S. Estimation of strengthening effects with concrete fiber sheet for concrete column. 3rd Int. Symp. non-metallic Reinf. Concr. Struct., 1997.

[14] Samaan M, Mirmiran A, Shahawy M. Model of Concrete Confined by Fiber Composites. J Struct Eng 1998;124:1025–31. doi:10.1061/(ASCE)0733-9445(1998)124:9(1025).

[15] Saafi M, Toutanji H, Li Z. Behavior of Concrete Columns Confined with Fiber Reinforced Polymer Tubes. ACI Mater Journals 1999;96:500–9.

[16] Spoelstra MR, Monti G. FRP-Confined concrete model. J Compos Constr 1999;3:143–50.

[17] Lam L, Teng JG. Design-oriented stress–strain model for FRP-confined concrete. Constr Build Mater 2003;17:471–89. doi:http://dx.doi.org/10.1016/S0950-0618(03)00045-X.

[18] De Lorenzis L, Tepfers R. Comparative Study of Models on Confinement of

Concrete Cylinders with Fiber-Reinforced Polymer Composites. J Compos Constr 2003;7:219–37.

[19] Bisby LA, Dent AJS, Green MF. Comparison of confinement models for fiber-reinforced polymer-wrapped concrete. ACI Struct J 2005;102(1):62–72.

[20] Ozbakkaloglu T, Lim JC, Vincent T. FRP-confined concrete in circular sections: Review and assessment of stress-strain models. Eng Struct 2013;49:1068–88.

[21] Wu H-L, Wang Y-F, Yu L, Li X-R. Experimental and Computational Studies on High-Strength Concrete Circular Columns Confined by Aramid Fiber-Reinforced Polymer Sheets. J Compos Constr 2009;13:125–34.

[22] Mirmiran A, Shahawy M, Samaan M, Echary H El, Mastrapa JC, Pico O. Effect of column parameter on FRP-confined concrete. J Compos Constr 1998;2:175–85.

[23] Matthys S, Taerwe L, Audenaert K. Tests on axially loaded concrete columns confined by fiber reinforced polymer. Proc. 4th Int. Symp. fiber Reinf. Polym. Reinf. Reinf. Concr. Struct., Detroit: 1999.

[24] Xiao Y, Wu H. Compressive behaviour of concrete confined by carbon fiber composite jackets. J Mater Civ Eng 2000;12(2):139–46.

[25] Pessiki S, Harries KA, Kestner J, Sause R, Ricles J. The axial behaviour of concrete confined with fiber reinforced composite jackets. ASCE J Compos Constr 2001;5(4):237–45.

[26] Harries KA, Carey A. Shape and "gap" effects on the behavior of variably confined concrete. Cem Concr Res 2002;33(6):873–80.

[27] Lam L, Teng J-G. Ultimate condition of FRP-confined concrete. ASCE J Compos Constr 2004;8(6):539–48.

[28] Ozbakkaloglu T, Oehlers DJ. Manufacturing and testing of a novel FRP tube confinement system. Eng Struct 2008;30:2448–59.

[29] Elwi AA, Murry DW. A 3D hypoelastic concrete constitutive relationship. ASCE J Eng Mech Div 1979;105(4):623–41.

[30] Willam K, Warnke E. Constitutive model for the triaxial behavior of concrete. Int Assoc Bridges and structures, 1975:1–30.

[31] Mirmiran A. Analytical and experimental investigation of reinforced concrete columns encased in fibre glass tubular jackets and use of fiber jacket for pile splicing. Contract no. B-9135, Florida Department of Transport: Tallahassee, FL: 1996.

[32] Karbhari VM, Gao Y. Composite Jacketed Concrete Under Uniaxial Compression-Verification of Simple Design Equations. J Mater Civ Eng 1997;9(4):185–93.

[33] Miyauchi K, Inoue S, Kuroda T, Kobayashi A. Strengthening effects with carbon fiber sheet for concrete column. Japan Concr Inst 1999.

[34] Toutanji H. Stress-Strain Characteristics of Concrete Columns Externally Confined with Advanced Fiber Composite Sheets. ACI Mater Journals 1999;96:397–404.

[35] Lin H-J, Chen C-T. Strength of Concrete Cylinder Confined by Composite Materials. J Reinf Plast Compos 2001;20:1577–600.

[36] Youssef MN, Feng MQ, Mosallam AS. Stress-strain model for concrete confined by FRP composites. Compos Part B Eng 2007;38:614–28.

[37] Girgin Z. Modified failure criterion to predict ultimate strength of circular columns confined by different materials. ACI Struct J 2009;106(6):800–9.

[38] Fahmy MFM, Wu Z. Evaluating and proposing models of circular concrete columns confined with different FRP composites. Compos Part B Eng 2010;41:199–213..

[39] Ilki A, Kumbasar N, Koc V. Low strength concrete members externally confined with FRP sheets. Struct Eng Mech 2004;18(2):167–94.

[40] Berthet JF, Ferrier E, Hamelin P. Compressive behavior of concrete externally confined by composite jackets: Part B: Modeling. Constr Build Mater 2006;20:338–47.

[41] Mathys S, Toutanji H, Audenaert K, Taerwe L. Axial load behavior of large-scale columns confined with fiber-reinforced polymer composites. ACI Struct J 2005;102(2):258–67.

[42] Jiang T, Teng J-G. Strengthening of short circular RC columns with FRP jackets: a design proposal. Proceeding 3rd Int. Conf. FRP Compos. Civ. Eng., Maimi, Florida, USA: 2006.

[43] Teng JG, Jiang T, Lam L, Luo YZ. Refinement of a Design-Oriented Stress – Strain Model for FRP-Confined Concrete. J Compos Constr 2009;13:269–78.

[44] Realfonzo R, Napoli A. Concrete confined by FRP systems: Confinement efficiency and design strength models. Compos Part B Eng 2011;42:736–55.

[45] Hognestad E. A Study of Combined Bending and Axial Load in Reinforced Concrete Members, Bulletin Series No. 399 1951:132.

[46] Richard RM, Abbott BJ. Versatile elastic-plastic stress-strain formula. ASCE J Eng Mech Div 1975;101(4):511–5.

[47] ACI Committee 318. Building Code Requirements for Structural Concrete (ACI 318-95) and commentary (ACI 318R-95)., Farmington Hills, Michigan(USA): American Concrete Institute, 1995.

[48] ACI 440.2R-08, ACI committee 440-02. Guide for the design and construction of externally bonded FRP systems for strengthening concrete structures. Farmington Hills, Michigan (USA): American Concrete Institute; 2008

[49] Sargin M. Stress-strain relationship for concrete and the analysis of structural concrete section. University of Waterloo: Ontario, Canada: 1971.

[50] Teng JG, Huang YL, Lam L, Ye LP. Theoretical Model for Fiber-Reinforced Polymer-Confined Concrete. J Compos Constr 2007;11:201–10.

[51] Xiao QG, Teng JG, Yu T. Behavior and Modeling of Confined High-Strength Concrete. Stress Int J Biol Stress 2010;14:249–59.

[52] Ozbakkaloglu T, Akin E. Behavior of FRP-Confined Normal- and High-Strength Concrete Under Cyclic Axial Compression. J Compos Constr 2012;16:451–63.

[53] Popovics S. A numerical approach to the complete stress-strain curve of concrete. Cem Concr Res 1973;3:583–99.

[54] Mirmiran A, Shahawy M. Dilation characteristics of confined concrete. Mech Cohesive-Frictional Mater 1997;2:237–49.

[55] Mirmiran A, Shahawy M. Behaviour of Concrete Columns Confined by Fiber Composites. ASCE J Struct Eng 1997;123:583–90.

[56] Fam AZ, Rizkalla SH. Confinement model for axially loaded concrete confined by circular fiber-reinforced polymer tubes. ACI Struct J 2001;98(4):451–61.

[57] Chun SS, Park HC. Load carrying capacity and ductility of RC columns confined by carbon fiber reinforced polymer. Proceeding 3rd Int. Conf. Compos. Infrastruct., 2002.

[58] Carreira DJ, Chu KH. Stress-strain relationship for plain concrete in compression. ACI J 1985;82(6):797–804.

[59] Mirmiran A, Zagers K, Yuan W. Nonlinear finite element modeling of concrete confined by fiber composites. Finite Elem Anal Des 2000;35:79–96.

[60] Rochette P, Labossiere P. A plasticity appraoch for concrete columns confined with composite materials. M. M. El-Badry (Ed.), Proc. Adv. Compos. Mater. Bridg. Struct. CSCE, 1996, p. 359–66.

[61] Shahawy M, Mirmiran A, Beitelman T. Tests and modeling of carbon-wrapped concrete columns. Compos Part B Eng 2000;31:471–80.

[62] Feng P, Lu XZ, Ye LP. Experimental research and finite element analysis of square concrete columns confined by FRP sheets under uniaxial compression. Engineering 2002:60–5.

[63] Li G, Kidane S, Pang SS, Helms JE, Stubblefield MA. Investigation into FRP repaired RC columns. Compos Struct 2003;62:83–9.

[64] Sadeghian P, Rahai a. R, Ehsani MR. Numerical Modeling of Concrete Cylinders Confined with CFRP Composites. J Reinf Plast Compos 2008;27:1309–21.

[65] Seffo M, Hamcho M. Strength of concrete cylinder confined by composite materials (CFRP). Energy Procedia 2012;19:276–85.

[66] Ritchie P, Thomas D, Lu L, Conneley G. External reinforcement of concrete beams using fiber reinforced plastics. ACI Struct J 1991;88:490–500.

[67] Saadatmanesh H, Ehsani MR. RC Beams Strengthened with GFRP Plates I: Experimental Study. J Struct Eng 1992;117:3417–33.

[68] Norris T, Saadatmanesh H, Ehsani MR. Shear and Flexural Strengthening of R/C Beams with Carbon Fiber Sheets. J Struct Eng 1997;123:903–11.

[69] Kachlakev D, Millar T, Yim S, Chansawat K, Potisuk T. Finite element modelling of Reinforced Concrete structures strengthened with FRP laminates. Oregen Department of Transportation-Research group, Salem or 97301-5192 and Federal Highway Administration, Washington DC, 20590, 2001.

[70] Kachlakev D, McCurry DD. Behavior of full-scale reinforced concrete beams retrofitted for shear and flexural with FRP laminates. Compos Part B-Engineering 2000;31:445–52.

[71] Wolanski AJ. Flexural Behavior of Reinforced and Prestressed Concrete Beams Using Finite Element Analysis 2004:87.

[72] Camata G, Spacone E, Zarnic R. Experimental and nonlinear finite element studies of RC beams strengthened with FRP plates. Compos Part B Eng 2007;38:277–88.

[73] Barros J a O, Dias SJE, Lima JLT. Efficacy of CFRP-based techniques for the flexural and shear strengthening of concrete beams. Cem Concr Compos 2007;29:203–17.

[74] Esfahani MR, Kianoush MR, Tajari a. R. Flexural behaviour of reinforced concrete beams strengthened by CFRP sheets. Eng Struct 2007;29:2428–44.

[75] Godat A, Neale KW, Labossière P. Numerical Modeling of FRP Shear-Strengthened Reinforced Concrete Beams. J Compos Constr 2007;11:640–9.

[76] Ibrahim AM, Mahmood MS. Finite element modeling of reinforced concrete beams strengthened with FRP laminates 2009.

[77] Godat A, Qu Z, Lu XZ, Labossiere P, Ye LP, Neale KW. Size effects for reinforced concrete beams strengthened in shear with CFRP strips. J Compos Constr 2010;14:260–71.

[78] López-González JC, Fernández-Gómez J, González-Valle E. Effect of Adhesive Thickness and Concrete Strength on FRP-Concrete Bonds. J Compos Constr 2012:245.

[79] Ouyang L, Lu Z, Chen W. Flexural experimental study on continuous reinforced concrete beams strengthened with basalt fiber reinforced polymer/plastic. J Shanghai Jiaotong Univ 2012;17:613–8.

[80] Dong J, Wang Q, Guan Z. Structural behaviour of RC beams with external flexural and flexural–shear strengthening by FRP sheets. Compos Part B Eng 2013;44:604–12.

[81] Hawileh RA, Naser MZ, Abdalla JA. Finite element simulation of reinforced concrete beams externally strengthened with short-length CFRP plates. Compos Part B Eng 2013;45:1722–30.

[82] Sasmal S, Kalidoss S, Srinivas V. Nonlinear Finite Element Analysis of FRP Strengthened Reinforced Concrete Beams. J Inst Eng Ser A 2013;93:241–9..

[83] Ronagh HR, Baji H. On the FE Modeling of FRP-Retrofitted Beam-Column Subassemblies. Int J Concr Struct Mater 2014;8:141–55.

[84] Tomlinson D, Fam A. Performance of Concrete Beams Reinforced with Basalt FRP for Flexure and Shear. DxDoiOrg 2014;04014036:4014036.

[85] Abu-Obeidah A, Hawileh RA, Abdalla JA. Finite element analysis of strengthened RC beams in shear with aluminum plates. Comput Struct 2015;147:36–46.

[86] ANSYS 14.0. ANSYS Mechanical APDL Element Reference. ANSYS Manual, ANSYS Inc., Canonsburg (PA 15317. USA): 2011.

[87] Niroomandi A, Maheri A, Maheri MR, Mahini SS. Seismic performance of ordinary RC frames retrofitted at joints by FRP sheets. Eng Struct 2010;32:2326–36.

[88] Teng JG, Smith ST, Yao J, Chen JF. Intermediate crack-induced debonding in RC beams and slabs. Constr Build Mater 2003;17:447–62. 6.

[89] IS 456:2000. Plain and Reinforced Concrete - Code of practice. Bur. Indian Stand., New Delhi, 2000.

[90] ANSYS 14.0. Theory Reference for the Mechanical APDL and Mechanical Applications. ANSYS Manual, ANSYS Inc., Canonsburg (PA 15317. USA):

2011.

[91] Kachlakev DI. Finite element analysis and model validation of shear deficient reinforced concrete beams strengthened with GFRP laminates. Third Int Conf Compos 2002:1–11.

[92] Mindess S, Young JF, Darwin D. Concrete. 2nd ed. Prenticce Hall, Pearson Education, Inc. Upper Saddle River, USA; 2003.

[93] Shah SP, Swartz SE, Ouyang C. Fracture Mechanics of Concrete. New York: John Wiley & Sons, Inc.; 1995.

[94] https://en.wikipedia.org/wiki/Saint-Venant%27s_Principle. 05/05/2016 n.d.

[95] Hawileh RA, Naser M, Zaidan W, Rasheed HA. Modeling of insulated CFRP-strengthened reinforced concrete T-beam exposed to fire. Eng Struct 2009;31:3072–9.

[96] Hawileh RA, El-Maaddawy TA, Naser MZ. Nonlinear finite element modeling of concrete deep beams with openings strengthened with externally-bonded composites. Mater Des 2012;42:378–87.

[97] Mohammed M, Elshafey AA, El-shami MM, Kandil KS. Strengthening of Concrete Beams in Shear 2013;4.

[98] Sasmal S, Kalidoss S, Srinivas V. Nonlinear Finite Element Analysis of FRP Strengthened Reinforced Concrete Beams. J Inst Eng Ser A 2013;93:241–9. doi:10.1007/s40030-013-0028-9.

[99] Bathe KJ. Finite Element Procedures. Prenticce Hall, Pearson Education, Inc. Upper Saddle River, USA; 2006.

[100] Adams V, Askenazi A. Building Better Products with Finite element analysis. OnWord Press, new Mexico; 1999.

[101] Toutanji H, Zhao L, Zhang Y. Flexural behavior of reinforced concrete beams externally strengthened with CFRP sheets bonded with an inorganic matrix. Eng Struct 2006;28:557–66.

[102] Rafi MM, Nadjai A, Ali F, Talamona D. Aspects of behaviour of CFRP reinforced concrete beams in bending. Constr Build Mater 2008;22:277–85..

[103] Lee HK, Cheong SH, Ha SK, Lee CG. Behavior and performance of RC T-section deep beams externally strengthened in shear with CFRP sheets. Compos Struct 2011;93:911–22.

[104] Kim G, Sim J, Oh H. Shear strength of strengthened RC beams with FRPs in shear. Constr Build Mater 2008;22:1261–70.

[105] Cladera A, Marí AR. Shear design procedure for reinforced normal and high-strength concrete beams using artificial neural networks. Part II: Beams with stirrups. Eng Struct 2004;26:927–36.

[106] Jayaprakash J, Abdul Samad AA, Anvar Abbasovich A, Abang Ali AA. Shear capacity of precracked and non-precracked reinforced concrete shear beams with externally bonded bi-directional CFRP strips. Constr Build Mater 2008;22:1148–65.

[107] El-Ghandour AA. Experimental and analytical investigation of CFRP flexural and shear strengthening efficiencies of RC beams. Constr Build Mater 2011;25:1419–29.

[108] SAP2000. nonlinear version 14.2.4, Analysis reference manual. Comput Struct Inc 2011.

[109] IS 1893 (Part 1) : 2002. Criteria for Earthquake Resistant Design of Structures (Part 1 General Provisions and Buildings). Bureau of Indian Standards; New Delhi, 2002.